

40434



National Library of Canada

Bibliothèque nationale du Canada

CANADIAN THESES ON MICROFICHE

THÈSES CANADIENNES SUR MICROFICHE

NAME OF AUTHOR/NOM DE L'AUTEUR

SU HO PUON

TITLE OF THESIS/TITRE DE LA THÈSE

Analytical studies with Amberlite XAD-2
PART I: POTENTIOMETRIC TITRATIONS
PART II: STUDIES OF ADSORPTION MECHANISM OF IONS

UNIVERSITY/UNIVERSITÉ

University of Alberta

DEGREE FOR WHICH THESIS WAS PRESENTED /
GRADE POUR LEQUEL CETTE THÈSE FUT PRÉSENTÉE

Ph.D

YEAR THIS DEGREE CONFERRED/ANNÉE D'OBTENTION DE CE GRADE

Spring 1979

NAME OF SUPERVISOR/NOM DU DIRECTEUR DE THÈSE

Dr. Cantwell

Permission is hereby granted to the NATIONAL LIBRARY OF CANADA to microfilm this thesis and to lend or sell copies of the film.

L'autorisation est, par la présente, accordée à la BIBLIOTHÈQUE NATIONALE DU CANADA de microfilmer cette thèse et de prêter ou de vendre des exemplaires du film.

The author reserves other publication rights, and neither the thesis nor extensive extracts from it may be printed or otherwise reproduced without the author's written permission.

L'auteur se réserve les autres droits de publication; ni la thèse ni de longs extraits de celle-ci ne doivent être imprimés ou autrement reproduits sans l'autorisation écrite de l'auteur.

DATED/DATE

Feb 27

SIGNED/SIGNÉ

Su Puon

PERMANENT ADDRESS/RÉSIDENCE FIXE

c/o Dept. of Chem.

U. of Alberta

Edmonton, Alberta T6G 2G2



National Library of Canada

Cataloguing Branch
Canadian Theses Division

Ottawa, Canada
K1A 0N4

Bibliothèque nationale du Canada

Direction du catalogage
Division des thèses canadiennes

NOTICE

The quality of this microfiche is heavily dependent upon the quality of the original thesis submitted for microfilming. Every effort has been made to ensure the highest quality of reproduction possible.

If pages are missing, contact the university which granted the degree.

Some pages may have indistinct print especially if the original pages were typed with a poor typewriter ribbon or if the university sent us a poor photocopy.

Previously copyrighted materials (journal articles, published tests, etc.) are not filmed.

Reproduction in full or in part of this film is governed by the Canadian Copyright Act, R.S.C. 1970, c. C-30. Please read the authorization forms which accompany this thesis.

**THIS DISSERTATION
HAS BEEN MICROFILMED
EXACTLY AS RECEIVED**

AVIS

La qualité de cette microfiche dépend grandement de la qualité de la thèse soumise au microfilmage. Nous avons tout fait pour assurer une qualité supérieure de reproduction.

S'il manque des pages, veuillez communiquer avec l'université qui a conféré le grade.

La qualité d'impression de certaines pages peut laisser à désirer, surtout si les pages originales ont été dactylographiées à l'aide d'un ruban usé ou si l'université nous a fait parvenir une photocopie de mauvaise qualité.

Les documents qui font déjà l'objet d'un droit d'auteur (articles de revue, examens publiés, etc.) ne sont pas microfilmés.

La reproduction, même partielle, de ce microfilm est soumise à la Loi canadienne sur le droit d'auteur, SRC 1970, c. C-30. Veuillez prendre connaissance des formules d'autorisation qui accompagnent cette thèse.

**LA THÈSE A ÉTÉ
MICROFILMÉE TELLE QUE
NOUS L'AVONS REÇUE**

THE UNIVERSITY OF ALBERTA

ANALYTICAL STUDIES WITH AMBERLITE XAD-2

PART I : POTENTIOMETRIC TITRATIONS

PART II: STUDIES OF ADSORPTION MECHANISM OF
IONS

BY



SU HO PUON

A THESIS

SUBMITTED TO THE FACULTY OF GRADUATE STUDIES AND
RESEARCH IN PARTIAL FULFILMENT OF THE REQUIREMENTS
FOR THE DEGREE OF DOCTOR OF PHILOSOPHY

IN

CHEMISTRY

EDMONTON, ALBERTA

SPRING 1979

THE UNIVERSITY OF ALBERTA
FACULTY OF GRADUATE STUDIES AND RESEARCH

The undersigned certify that they have read,
and recommend to the Faculty of Graduate Studies and
Research, for acceptance, a thesis entitled ANALYTICAL
STUDIES WITH AMBERLITE XAD-2, PART I: POTENTIOMETRIC
TITRATIONS; PART II: STUDIES OF ADSORPTION MECHANISMS
OF IONS submitted by Su H. Puon in partial fulfilment
of the requirements for the degree of Doctor of
Philosophy in Chemistry.

F.F. Cantwell

F.F. Cantwell, Supervisor

W.E. Harris

W.E. Harris

B. Kratochvil

B. Kratochvil

M.J. Robins

M.J. Robins

R. Moskalyk

R. Moskalyk (Pharmacy)

M.V. Novotny

M.V. Novotny, External Examiner

Date Feb 22, 1979

ABSTRACT

In Part I of this thesis, a novel heterogeneous potentiometric titration technique is reported in which acids of various charge types are titrated with sodium hydroxide in an aqueous slurry of the nonionic adsorbent Amberlite XAD-2. Major shifts are observed in the resulting titration curves compared to those obtained in the absence of adsorbent. Titration curve shapes are interpreted in terms of both acid-base and phase-distribution equilibria of the several conjugate species of the sample compound. Theoretical titration equations are derived for acids of the types: BH^+ , HA , H_2A^+ , and mixtures of BH^+ and HA . Validity of the titration equation for BH^+ was verified by comparing the predicted and experimentally observed titration curves for diphenylguanidine hydrochloride, for which quantitative agreement was observed. As examples of the other three charge type cases the following compounds were titrated: *m*-nitrophenol, naloxone hydrochloride and a mixture of *m*-nitrophenol and molindone hydrochloride.

The heterogeneous potentiometric titration technique makes possible the titration of cationic acids in water which are otherwise too weak to give accurate end points. It also permits the differential titration, in water, of mixtures of acids with similar ionization constants but different charge types.

In order to accurately describe the heterogeneous titration curves by appropriate equations it was found necessary to take into

account the sorption of the ionic conjugate species, (e.g. BH^+ , A^-) as well as the neutral species (e.g. B , HA). Also, the titration studies showed that while changes in concentration and type of inert electrolyte in the solution have little effect on the distribution coefficient of a neutral species between XAD-2 and the aqueous phase, they have a profound effect on the distribution coefficient of an adsorbed ionic species.

In order to elucidate the mechanism by which ions are adsorbed on a nonionic adsorbent in the manner described in Part I, a study of this phenomenon was undertaken in Part II of this thesis. Adsorption isotherms were measured for diphenylguanidinium and benzylammonium ions in the presence of various concentrations of inert electrolyte. In addition, the electrophoretic mobility of resin particles was measured in solutions containing diphenylguanidinium ion and various concentrations of inert electrolyte. The results of both the isotherm studies and the electrophoretic measurements are quantitatively consistent with the Stern-Gouy-Chapman (SGC) model of the charged interface.

An understanding of ionic adsorption in terms of the SGC model allows a prediction of the conditions under which linear adsorption isotherms may be obtained for ionic samples and also suggests ways in which chromatographic retention volumes of ions may be varied by changes in ionic strength and ionic composition of the mobile phase. Under conditions where the surface potential is made constant, the reciprocal of the adjusted retention volume is linearly dependent on the reciprocal of the square root of the mobile phase ionic strength.

ACKNOWLEDGEMENT

The author wishes to express his sincere gratitude to Dr. Frederick F. Cantwell of this institution for his guidance and encouragement during the course of his work.

The microelectrophoresis apparatus was kindly loaned to the author by Dr. Michael Kessick of the Alberta Research Council.

TABLE OF CONTENTS

	Page
PART I	
1. INTRODUCTION	2
2. PROPOSED MODEL	6
3. EXPERIMENTAL	
3.1. Apparatus	49
3.2. Chemicals	54
3.3. Reagents	57
3.4. Resins	58
3.5. Potentiometric Titrations	60
3.6. Distribution Isotherms	62
3.7. Solubility	64
4. RESULTS AND DISCUSSION	
4.1. Sorption of H_3O^+	65
4.2. Diphenylguanidine Hydrochloride	68
4.3. Diphenylguanidine Hydrochloride : Effect of the concentration of the TBABr on the titration curve.....	84
4.4. Diphenylguanidine Hydrochloride : Effect of various quaternary ammonium salt on the titration curve	88
4.5. Benzylammonium Chloride	90
4.6. Molindone Hydrochloride	94
4.7. Dextromethorphan Hydrobromide	97
4.8. <u>m</u> -Nitrophenol	100
4.9. Naloxone Hydrochloride	104

4.10 Mixture of Molindone Hydrochloride and <i>m</i> -nitro-phenol	107
5. CONCLUSION	110
6. FURTHER WORK	111
PART II	
1. INTRODUCTION	113
2. PROPOSED MODEL	
2.1 Stern-Gouy-Chapman Model	122
2.2 Microelectrophoresis	140
3. EXPERIMENTAL	
3.1 Chemicals	143
3.2 Reagents	144
3.3 Chromatographic Apparatus	145
3.4 Resins	146
3.5 Adsorption Isotherms	147
3.6 Chromatographic Studies	148
3.7 Microelectrophoresis	150
4. RESULTS AND DISCUSSION	
4.1 Adsorbent Properties	152
4.2 Distribution Isotherms of $DPGH^+$ and BZH^+ and the SGC Theory	
4.2.1 Diphenylguanidinium Ion ($DPGH^+$)	153
4.2.2 Benzylammonium Ion (BZH^+)	183
4.3 Microelectrophoresis	193
4.4 Effect of the Different Counterions on Chromatographic Behavior	198

4.5 Chromatographic Behavior and the Effect of TBA^+ on the Retention of Tonic Species	205
4.6 Chromatographic Behavior of a Neutral Species	220
5. CONCLUSION	226
6. FURTHER WORK	227
REFERENCES	228
APPENDIX I. Theoretical Derivation of the Titration Curve of BH^+ Type Acid in the Absence of XAD-2 Resin	239
APPENDIX II. Theoretical Derivation of the Titration Curve of BH^+ Type Acid in the Presence of XAD-2 Resin	243
APPENDIX III. Theoretical Derivation of the Titration Curve of HA Type Acid in the Presence of XAD-2 Resin	247
APPENDIX IV. Derivation of the pH difference at Half-Equivalent Point in the Titration of BH^+ and HA Acids	250
APPENDIX V. Theoretical Derivation of the Titration Curve of AH_2^+ Type Acid in the Presence of XAD-2 Resin	253
APPENDIX VI. Theoretical Derivation of the Titration Curve for the Mixed Type Acids BH^+ and HA in the Presence of XAD-2 Resin	261
APPENDIX VII. Calculation of the Titration Curve C, Figure 11 .	272

LIST OF TABLES

NUMBER	TITLE	PAGE
1	Equilibrium constant and distribution coefficient expressions for acids of the charge type BH^+ and HA.	10
2	Hypothetical titration data for Curve 1, Figure 1.	17
3	Hypothetical titration data for Curve 2, Figure 1.	18
4	Hypothetical titration data for Curve 3, Figure 1.	19
5	Hypothetical titration data for Curve 4, Figure 1.	20
6	Hypothetical titration data for Curve 5, Figure 1.	21
7	Hypothetical titration data for Curve 6, Figure 1.	22
8	Hypothetical titration data for Curve 1, Figure 2.	23
9	Hypothetical titration data for Curve 2, Figure 2.	24
10	Hypothetical titration data for Curve 3, Figure 2.	25
11	Hypothetical titration data for Curve 4, Figure 2.	26
12	Hypothetical titration data for Curve 5, Figure 2.	27
13	Hypothetical titration data for Curve 6, Figure 2.	28
14	Equilibrium constants and distribution coefficients for acid AH_2^+ and acid mixture BH^+ , HA.	32
15	Distribution coefficient of diphenylguanidine HCl (BH^+) in 0.10 M sodium chloride and aqueous phase (pH=3).	69
16	Distribution coefficient of diphenylguanidine HCl in 0.10 M TBABr and aqueous phase (pH=3).	73

17	Distribution coefficient of diphenylguanidine base form in 0.10 M TBABr and aqueous phase (pH=11).	78
18	Determination of K_B of diphenylguanidine base form (chromatographic method) using different percentages of methanol in the mobile phase (pH=11).	80
19	Dependence of $\Delta pH_{1/2}$ for diphenylguanidinium ion on concentration of TBABr.	87
20	Dependence of $\Delta pH_{1/2}$ for diphenylguanidinium ion on different quaternary ammonium bromide (0.1M).	89
21	Distribution coefficients of benzylamine/benzylammonium ion from batch equilibration.	91
22	Batch analysis data for obtaining the distribution coefficients of m-nitrophenol/m-nitrophenolate.	103
23	Data for the distribution isotherm of $DPGH^+$ on XAD-2 resin in 0.011 M NaCl.	156
24	Data for the distribution isotherm of $DPGH^+$ on XAD-2 resin in 0.05 M NaCl.	157
25	Data for the distribution isotherm of $DPGH^+$ on XAD-2 resin in 0.10 M NaCl.	158
26	Data for the distribution isotherm of $DPGH^+$ on XAD-2 resin in 0.25 M NaCl.	159
27	Data for the distribution isotherm of $DPGH^+$ on XAD-2 resin in 0.50 M NaCl.	160
28	Summary of the quantities used to prepare Figure 27. From the distribution isotherms at an activity of $DPGH^+$ of 3.0×10^{-4} .	171

29	Summary of the quantities used to prepare Figure 27. From the distribution isotherms at an activity of DPGH ⁺ of 5.0×10^{-4} .	172
30	Summary of the quantities used to prepare Figure 27. From the distribution isotherms at an activity of DPGH ⁺ of 1.0×10^{-3} .	173
31	Summary of the quantities used to prepare Figure 27. From the distribution isotherms at an activity of DPGH ⁺ of 3.0×10^{-3} .	174
32	Summary of the quantities used to prepare Figure 27. From the distribution isotherms at an activity of DPGH ⁺ of 5.0×10^{-3} .	175
33	Summary of the quantities used to prepare Figure 27. From the distribution isotherms at an activity of DPGH ⁺ of 1.0×10^{-2} .	176
34	Summary of the quantities used to prepare Figure 27. From the distribution isotherms at an activity of DPGH ⁺ of 2.0×10^{-2} .	177
35	Summary of the quantities used to prepare Figure 27. From the distribution isotherms at an activity of DPGH ⁺ of 3.0×10^{-2} .	178
36	Surface potentials and capacitances for the adsorption of DPGH ⁺ on Amberlite XAD-2.	179
37	Surface potentials and capacitances for the adsorption of BZH ⁺ on Amberlite XAD-2.	192

LIST OF FIGURES

NUMBER	TITLE	PAGE
1	Theoretical titration curves for acid BH^+ in a resin-solution medium. Effect of K_B .	13
2	Theoretical titration curves for acid BH^+ in a resin-solution medium. Effect of K_{BH} .	15
3	Theoretical titration curves for acid AH_2^+ in the presence of resin. Effect of K_{AH_2A} .	35
4	Plots of $-\log [AH]$ versus pH in the presence of resin. Effect of K_{AH_2A} .	38
5	Plots of $-\log [AH_2A]_R$ versus pH in the presence of resin. Effect of K_{AH_2A} .	40
6	Theoretical titration curves for acid mixture of BH^+ and HA in the presence of resin. Effect of K_{BHA} .	42
7	Plots of $-\log [B]$ versus pH in the presence of resin. Effect of K_{BHA} .	45
8	Plots of $-\log [BHA]_R$ versus pH in the presence of resin. Effect of K_{BHA} .	47
9	Diagram of the liquid chromatograph.	51
10	Distribution isotherms for H_3O^+ and OH^- between Amberlite XAD-2 resin and 0.10 M aqueous sodium bromide	66

11	Titration of diphenylguanidine hydrochloride with sodium hydroxide. Comparison of experimental with theoretical titration behavior.	71
12	Distribution isotherm for diphenylguanidine HCl between Amberlite XAD-2 and aqueous electrolytes.	74
13	Distribution isotherm for diphenylguanidine between Amberlite XAD-2 resin and 0.10 M TBABr aqueous phase at pH = 11.0.	76
14	Distribution coefficient of diphenylguanidine base form in 0.10 M NaCl and 10^{-3} M NaOH.	83
15	Dependence of $\Delta\text{pH}_{1/2}$ for diphenylguanidinium ion on concentration of tetra-n-butylammonium bromide.	85
16	Experimental titration curves of benzylamine hydrochloride with sodium hydroxide in 50 ml of 0.10 M sodium bromide in the presence and absence of 5.0 g of Amberlite XAD-2 resin.	92
17	Experimental titration curves of molindone hydrochloride with sodium hydroxide in 50 ml of 0.10 M TBABr in the presence and absence of 5.0 g of Amberlite XAD-2 resin.	95
18	Experimental titration curves of dextromethorphan hydrobromide with sodium hydroxide in 50 ml of 0.10 M TBABr - 30 percent methanol in the presence and absence of 2.5 g of Amberlite XAD-2 resin.	98
19	Experimental titration curves of <u>m</u> -nitrophenol with sodium hydroxide in 50 ml of 0.10 M sodium bromide in the presence and absence of 5.0 g of Amberlite XAD-2 resin.	101

- 20 Experimental titration curves of naloxone hydrochloride with sodium hydroxide in 50 ml of 0.10 M sodium bromide in the presence and absence of 5.0 g of Amberlite XAD-2 resin. 106
- 21 Experimental titration curves of a mixture of molindone hydrochloride and *m*-nitrophenol with sodium hydroxide in 50 ml of 0.10 M sodium bromide in the presence and absence of 5.0 g of Amberlite XAD-2 resin. 108
- 22 Schematic view of the interfacial region between Amberlite XAD-2 resin and aqueous electrolyte solution containing sodium chloride and diphenylguanidinium chloride. 125
- 23 Dependence of the electrical potential layer on distance from the charge surface for a fixed total concentration of uniunivalent electrolyte in the bulk solution ($c = 0.10$ M) and varying surface potential. 129
- 24 Dependence of the electrical potential in the double layer on distance from the charge surface for a fixed surface potential and varying total concentrations of uniunivalent electrolyte in the bulk solution. 132
- 25 Adsorption isotherms for diphenylguanidinium ion in the presence of various bulk solution concentrations of sodium chloride. 154

- 26 Langmuir adsorption isotherms for diphenylguanidinium ion in the presence of various bulk solution concentration of sodium chloride plotted according to equation 60. 161
- 27 Adsorption data for diphenylguanidinium ion according to the SGC equation 53 at eight surface potentials. 169
- 28 Dependence of surface potential (Ψ_0) on log of activity of potential-determining ion (DPGH⁺). 181
- 29 Adjusted retention volume for six different concentrations of benzylammonium ion at various total bromide concentrations on a 0.28 x 30-cm. column. 185
- 30 Dependence of the experimental surface charge on the concentration of benzylammonium ion in the aqueous phase at five different total bromide concentrations. 187
- 31 Adsorption data for benzylammonium ion according to the SGC equation 53 at four surface potentials. 190
- 32 Dependence of zeta potential of XAD-2 particles on surface charge due to adsorbed diphenylguanidinium ion plotted according to equation 58. 195
- 33 Effect of counterion type in the mobile phase on the adjusted retention volume of benzylammonium ion on a 0.28 x 30-cm column of XAD-2. 199

34	Adjusted retention volume of benzylammonium ion versus total electrolyte concentration in the mobile phase at three different concentrations of tetra-n-butylammonium bromide, on a 0.28 x 30-cm column of XAD-2.	208
35	Adjusted retention volume of codeinium ion versus total electrolyte concentration in the mobile phase at three different concentrations of tetra-n-butylammonium bromide, on a 0.28 x 30-cm column of XAD-2.	210
36	Adjusted retention volume of diphenyl-guanidinium ion versus total electrolyte concentration in the mobile phase at three different concentrations of tetra-n-butylammonium bromide, on a 0.28 x 30-cm column of XAD-2.	212
37	Dependence of adjusted retention volume of diphenyl-guanidinium ion on the concentration of tetra-n-butylammonium ion in the mobile phase at various total bromide concentrations on a 0.28 x 30-cm column of XAD-2.	214
38	Dependence of adjusted retention volume of diphenyl-guanidinium ion on the total electrolyte concentration in the mobile phase at three different concentrations of tetra-n-butylammonium bromide, on a 0.28 x 30-cm column of XAD-2.	218
39	Adsorption isotherms for acetaminophen in the presence of various bulk solution concentrations of sodium chloride.	221

40 Effect of counterion type in the mobile phase on the
adjusted retention volume of acetaminophen, on a
0.28 x 30-cm column of XAD-2.

224

LIST OF SYMBOLS

a_i	Activity of species i .
A	Cross-sectional area.
c	Electrolyte concentration.
C	Capacitance, farad cm^{-2} .
e	Electronic charge, 1.602×10^{-19} coulomb.
F	Faraday constant, $94,687$ coulomb mole^{-1} , or, 2.893×10^{14} $\text{cm}^{3/2} \text{g}^{1/2} \text{s}^{-1} \text{mol}^{-1}$.
ΔG	Free energy term.
ΔG_{elec}	Free energy term from the electrostatic force.
ΔG_{spec}	Free energy term from the chemical forces.
k	Boltzmann constant, 1.38×10^{-16} erg deg^{-1} .
k	Specific conductance, $\text{ohm}^{-1} \text{cm}^{-1}$.
K	Equilibrium constant.
L	Interelectrode distance, cm.
n_i	Number of moles (or number of ions) of species i .
$[i]_R$	Concentration of species i on the resin phase, moles/kg.
N	Avogadro constant, 6.023×10^{23} mol^{-1} .
r	Resistance, ohm.
R	Gas constant, 8.314×10^7 erg $\text{mol}^{-1} \text{deg}^{-1}$.
R	Ratio of the positive surface excess to the negative surface excess.
R'	Correction factor.
T	Absolute temperature, $^{\circ}\text{K}$.
T_i	Total number of moles of species i injected onto to chromatographic column.

U_E	Mobility, micrometer-cm volt ⁻¹ s ⁻¹ .
V_M	Void volume.
V_N	Adjusted retention volume.
V_R	Retention volume.
V	Volume of the aqueous phase.
W	Weight of the resin.
Z	Charge of the electrolyte.
α	Fraction of a cation.
κ	Reciprocal of the thickness of the double layer, cm ⁻¹ .
ϵ	Permittivity.
σ_0	Surface charge density, coulomb cm ⁻² .
σ_{DL}	Charge density in and beyond the OHP.
σ_0	Charge density.
ζ	Zeta potential, volt.
γ_i	Activity coefficient of species i .
η	Viscosity, poise.
δ	Thickness of the compact double layer capacitor, Å.
ψ_0	Potential at the surface.
ψ_{OHP}	Potential at the outer Helmholtz plane.
Γ_i	Experimental surface excess of the potential determining ion, i .
Γ_i^{AD}	Surface excess of the potential determining ion, i ; that is adsorbed on the surface.
Γ_i^{DL}	Surface excess of the potential determining ion i that has been expelled by electrostatic expulsion from the diffusion part of the double layer into the bulk solution.

Γ_{+}^{DL}

Surface excess of cations.

Γ_{-}^{DL}

Surface excess of anions.

$\Gamma_{i,MAX}$

Surface excess corresponding to monolayer coverage with species i .

LIST OF ABBREVIATIONS

TMABr	Tetramethylammonium Bromide.
TEABr	Tetraethylammonium Bromide.
TBABr	Tetra-n-butylammonium Bromide.
DPGH ⁺	Diphenylguanidinium Ion.
BZH ⁺	Benzylammonium Ion.
LC	Liquid Chromatography.
HPLC	High Performance Liquid Chromatography.
SGC	Stern-Gouy-Chapman Model.
IHP	Inner Helmholtz Plane.
OHP	Outer Helmholtz Plane.

PART I. POTENTOMETRIC TITRATIONS

1. INTRODUCTION

Acid-base titration which involves the use of a glass electrode, a saturated calomel electrode and pH meter has rendered potentiometric titration nearly as convenient to perform as indicator methods of volumetric analysis. A titration curve is plotted as the pH versus the amount of titrant added. For example, the inflection point of a titration curve is the equivalent point; and the half-equivalent point yields a pK value.

However, pH titration has its limitations: If the weak acid or base being titrated has a pK_a or pK_b value greater than 9 or, if the concentration used in the titration is less than 10^{-3} molar, then a titration curve will not give a sharp end point. This is because water, which is used as the medium, has a large autoprotolysis constant of $1.00 \cdot 10^{-14}$ at 25°C . Water would compete with the weak acid (weak base) as a proton donor (proton acceptor) at pH values above approximately 11. Usually, the analytically useful pH range is between 3 and 11. Those two pH extremes correspond to the pH of a 10^{-3} M strong acid solution and to the pH of a 10^{-3} M strong base solution.

In order to overcome the above difficulties, titration in a solvent other than water has been investigated. Nonaqueous solvents, with small autoprotolysis constants, or nonpolar solvents have been used widely (1,2). Titrations in mixed aqueous-organic solvents and aqueous solvents containing a high concentration of neutral electrolyte have also been investigated (3).

A different way to approach this problem is by using heterogeneous titration. In this titration, there is the presence of a second phase, other than the aqueous phase. This second phase removes from the aqueous phase one or more of the species in the acid-base equilibrium. The process involved can be precipitation, extraction or adsorption. This process can be expressed as a phase distribution. If the phase distribution favors the product of an acid-base titration, then, according to the principle of Le Chatelier, the acid-base equilibrium will shift to the right. The net effect in a titration is that the compound titrates as though it were a stronger acid or base. On the other hand, if the phase distribution involves a reactant in an acid-base equilibrium, the compound titrates as a weaker acid or base. This subject has been reviewed by several workers (4,5,6,7).

Only those previous studies which involve an organic solvent or a solid adsorbent as the second phase are analogous to the XAD-2 system reported here, and those studies are surveyed below. Christensen (8) studied the influence of an immiscible organic solvent on the titration behavior of acids and bases and has used the resulting potentiometric titration to evaluate distribution coefficients. Ratajewics and Ratajewicz (9) studied potentiometric titrations of sparingly soluble diprotic bases in a two liquid phase system and the result was used to determine the dissociation constants of the bases. Komer (10) has derived an expression for the differentiating effect resulting

from phase distribution when titrating a mixture of two acids of the charge type HA in an immiscible aqueous-organic solvent system. Cantwell and Mohammed performed photometric titrations in which weak acid drug substances were titrated with sodium hydroxide in the presence of a water immiscible organic solvent as the second phase (11) and in which the cationic ammonium conjugate acids of amine drugs were titrated with picrate anion in a chloroform-water medium.

Titrations have also been performed in aqueous solutions in the presence of solid adsorbents. Tendeloo et al. (12) have titrated acids of the charge type HA and H_2A in the presence of activated charcoal. Major shifts were observed in the titration curves compared to those obtained in the presence of charcoal, but attempts to develop an adequate quantitative model were unsuccessful (13,14). Stolkova (15) used the potentiometric titration curves of acids and bases obtained in the presence of norite, bonechar, kieselguhr and silica gel to estimate the quantity and degree of exhaustion of these adsorbents. Cantwell and Pietrzyk (4,5,6) studied the titration of weak bases with hydrochloric acid in an aqueous slurry of cation exchange resin and found that the resulting titration could be quantitatively described in terms of the aqueous phase acid-base equilibria and the phase-distribution equilibria of the conjugate acid-base species of the sample.

In Part I of this thesis, heterogeneous potentiometric titrations of weak acids are described in which the resin Amberlite XAD-2 is one phase and an aqueous solution is the other. Theoretical titration equations are derived and verified experimentally for several different charge type acids. Amberlite XAD-2 is a nonionic, hydrophobic macroporous adsorbent which is, chemically, a copolymer of styrene and divinylbenzene. It adsorbs chemical species from solution onto its surface. The detailed properties of Amberlite XAD-2 are discussed in Part II of this thesis.

2. PROPOSED MODEL

In this section, a physico-chemical model will be established which describes the acid-base titration of monofunctional acids of the charge types BH^+ and HA , mixed charge types BH^+ with HA , and charge type AH_2^+ , in an XAD-2 resin-aqueous solution two-phase medium. The details of the derivations are given in Appendices I, II, III, and V.

In the case of a weak acid BH^+ (e.g. benzylammonium) and its conjugate base B (e.g. benzylamine), there are two types of distribution equilibria which exist between the hydrophobic resin and aqueous phase: nonelectrolyte sorption and electrolyte sorption. The former one can be represented as:



The parenthesis and subscript R refer to species in the resin phase. Species without a subscript are in the aqueous phase. An equilibrium constant may be written for the adsorption as:

$$K_B = \frac{[B]_R}{[B]} \quad (2)$$

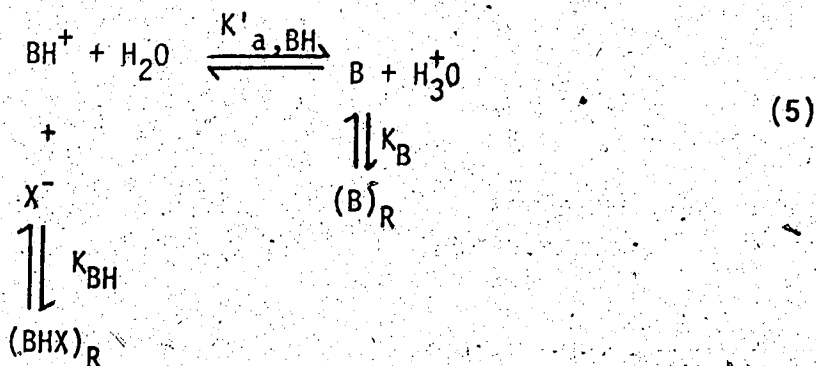
Similarly, the equilibrium constant for the electrolyte sorption:



can be written as:

$$K_{BH} = \frac{[BHX]_R}{[BH][X]} \quad (4)$$

In the titration of a BH^+ species, an overall equilibrium equation can be given:



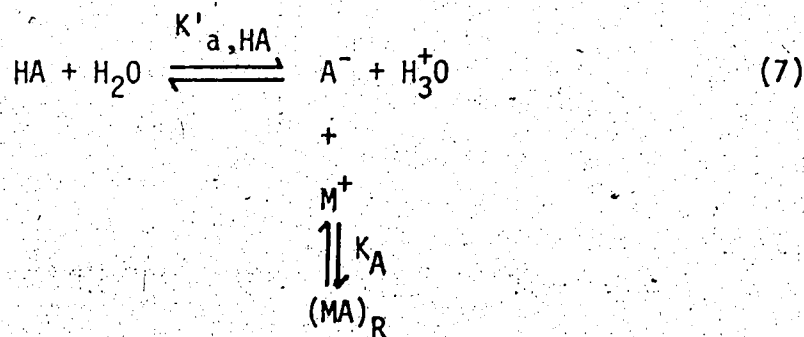
and



The X^- in the above equation is the conjugate base of a strong acid (e.g. Cl^- , Br^- , NO_3^-). It has been assumed that the ion-pair species BHX as well as the neutral species B can be sorbed by the resin. The mechanism of sorption of the electrolyte BH^+X^- onto the resin is the subject of Part II of this thesis. For simplicity of presentation at this point, the equilibrium is written as a simple 1:1 ion pair formation in which the concentration of ion pairs, BHX , in the aqueous phase are neglected. The titration equation presented below is not limited to an ion pair sorption.

mechanism since its derivation implies only that BH^+ partitions between resin and aqueous phase, without implying the mechanism of sorption on the resin. Sorption of H_3O^+ and OH^- onto XAD-2 resin can be neglected as shown later on.

In the case of the weak acid HA (e.g. nitrophenol) and its conjugate base (e.g. nitrophenolate), the equilibria are summarized by equations 6 and 7:



where M^+ is a small inorganic cation (e.g. Na^+ , K^+). In either case (i.e. BH^+ or HA), the amount of resin in the system is made large compared to the amount of sample acid, so that linear distribution isotherms are expected for species B and HA. In addition, the aqueous solution is made to contain a large excess of inert electrolyte (e.g. NaCl, NaBr) compared to the amount of sample, so that the concentration of X^- or M^+ becomes constant, independent of the amount of sample in the system. For a simple 1:1 ion pair retention mechanism, the sorption of BH^+ and A^- is described by the heterogeneous equilibrium constants:

$$K_{BH,eq} = \frac{a_{(BHX)_R}}{a_{BH} a_X} \quad \text{and} \quad K_{A,eq} = \frac{a_{(MA)_R}}{a_M \cdot a_A} \quad (8)$$

where a_i is the activity of species i . With large excess of M^+ or X^- , these equilibria can be represented by distribution coefficients:

$$K_{BH} = \frac{[BHX]_R}{[BH]} = K_{BH,eq} \frac{\gamma_{BH} \gamma_X [x]}{\gamma_{(BHX)}_R} \quad (9)$$

$$K_A = \frac{[MA]_R}{[A]} = K_{A,eq} \frac{\gamma_M \gamma_A [M]}{\gamma_{(MA)}_R} \quad (10)$$

where γ_i are activity coefficients, which are constant during a titration under the specified experimental conditions. If this ion-pair sorption mechanism prevails, K_{BH} and K_A will be constant (i.e. linear distribution isotherm). On the other hand, if more complex sorption mechanisms prevail, K_{BH} and K_A may not be constant, but experimentally measured nonlinear distribution isotherms will still accurately describe the system.

Table 1 lists the equilibrium constants and distribution coefficient expressions for the acids BH^+ and HA in the presence of an excess of resin and inert electrolyte. These are combined with the appropriate mass balance and electroneutrality equations to produce the potentiometric titration equations (Appendices I and II).

For the titration of n_{BH} moles of acid BH^+ with strong base $NaOH$, the titration equation is:

$$n_{OH} = \frac{n_{BH} K'_{a,BH} (V + K_B W)}{a_H (V + K_{BH} W) + K'_{a,BH} (V + K_B W)} + \frac{K_W V}{a_H \gamma_{OH}} - \frac{a_H V}{\gamma_H} \quad (11)$$

Table 1

Equilibrium constant and distribution coefficient expressions for acids of the charge type BH^+ and HA ^a

BH^+	HA
$K'_{a,BH} = \frac{[B] \cdot a_H}{[BH^+]}$	$K'_{a,HA} = \frac{[A^-] \cdot a_H}{[HA]}$
$K_W = a_H \cdot a_{OH}$	$K_W = a_H \cdot a_{OH}$
$K_{BH} = \frac{[BHX]_R}{[BH^+]}$	$K_{HA} = \frac{[HA]_R}{[HA]}$
$K_B = \frac{[B]_R}{[B]}$	$K_A = \frac{[MA]_R}{[A^-]}$

^a a_H is hydronium ion activity. All other symbols defined in text and Equations 5 and 7.

where V is the volume of aqueous phase, W is the weight of the resin, and n_{OH} is mole of titrant added. The titration equation for acid HA is identical except that n_{HA} , K_{HA} and K_A replace n_{BH} , K_{BH} and K_B . The titration equation for HA acid is:

$$n_{OH} = \frac{n_{HA} K'_{a,HA} (V + K_A W)}{a_H (V + K_{HA} W) + K'_{a,HA} (V + K_A W)} + \frac{K_W V}{a_{H,OH}} - \frac{a_H V}{\gamma_H} \quad (12)$$

The titration equations can be evaluated once the ionization constants and the distribution coefficients have been experimentally measured.

The influence of each of the heterogeneous distribution coefficients on the shape of the titration curve will now be considered. Figure 1 shows an example of the effect of K_B on the titration curve of a hypothetical acid BH^+ with $K'_{a,BH}$ of 10^{-10} . The effect can be understood in terms of LeChatelier's principle. The species B is a product of the titration reaction, so that its sorption by the resin shifts the acid-base equilibrium in the product direction. The portion of the titration curve before the equivalence point is shifted to lower pH values with increasing K_B , causing the acid BH^+ to appear as though it was a stronger acid. Data for these curves are presented in Tables 2 to 7.

The influence of K_{BH} is opposite to that of K_B . Here the removal of reactant species BH^+ from the aqueous phase is greater for higher K_{BH} , and the portion of the titration curve before the equivalence point shifts to higher pH values. Figure 2 shows the

effect of K_{BH} on the titration curve of an acid with $K'_{a,BH} = 10^{-10}$.

The data for these curves are tabulated in Tables 8 to 13. Although

a K_{BH} value of 10^4 has been assumed in curve 6 of Figure 2, it

is unlikely that K_{BH} for a real compound would ever be as large

as K_B where X^- is an anion such as Cl^- , Br^- , NO_3^- or ClO_4^- .

The effects of K_{HA} and K_A on the titration behavior of an acid HA are analogous to those of K_{BH} and K_B respectively, since

in this case HA is the reactant species and A^- the product species.

The detailed derivation of the above equation is given in Appendix

III.

Comparing titration curves for acid BH^+ in the presence (R) and absence of resin (NR), the difference in pH in the proton-binding region (5) of the curves is given by equation 13 (Appendix IV).

$$pH = pH(NR) - pH(R)$$

$$\approx \log \frac{V + K_B W}{V + K_{BH} W} \quad (13)$$

The analogous expression for acid HA:

$$pH = pH(NR) - pH(R)$$

$$\approx \log \frac{V + K_A W}{V + K_{HA} W} \quad (14)$$

Figure 1. Theoretical titration curves for acid BH^+ in a resin-solution medium. Effect of K_B . (Curves calculated from Equation 11).

For acid BH^+ . $K_{a,BH} = 1.0 \times 10^{-10}$; $V = 0.050$ l;
 $n_{BH} = 5.00 \times 10^{-4}$ mole; $K_{BH} = 0$; $W = 0$ (Curve 1), =
 0.0050 kg (Curves 2 - 6)

Curve No.	1	2	3	4	5	6
K_B	-	1	10	10^2	10^3	10^4

9

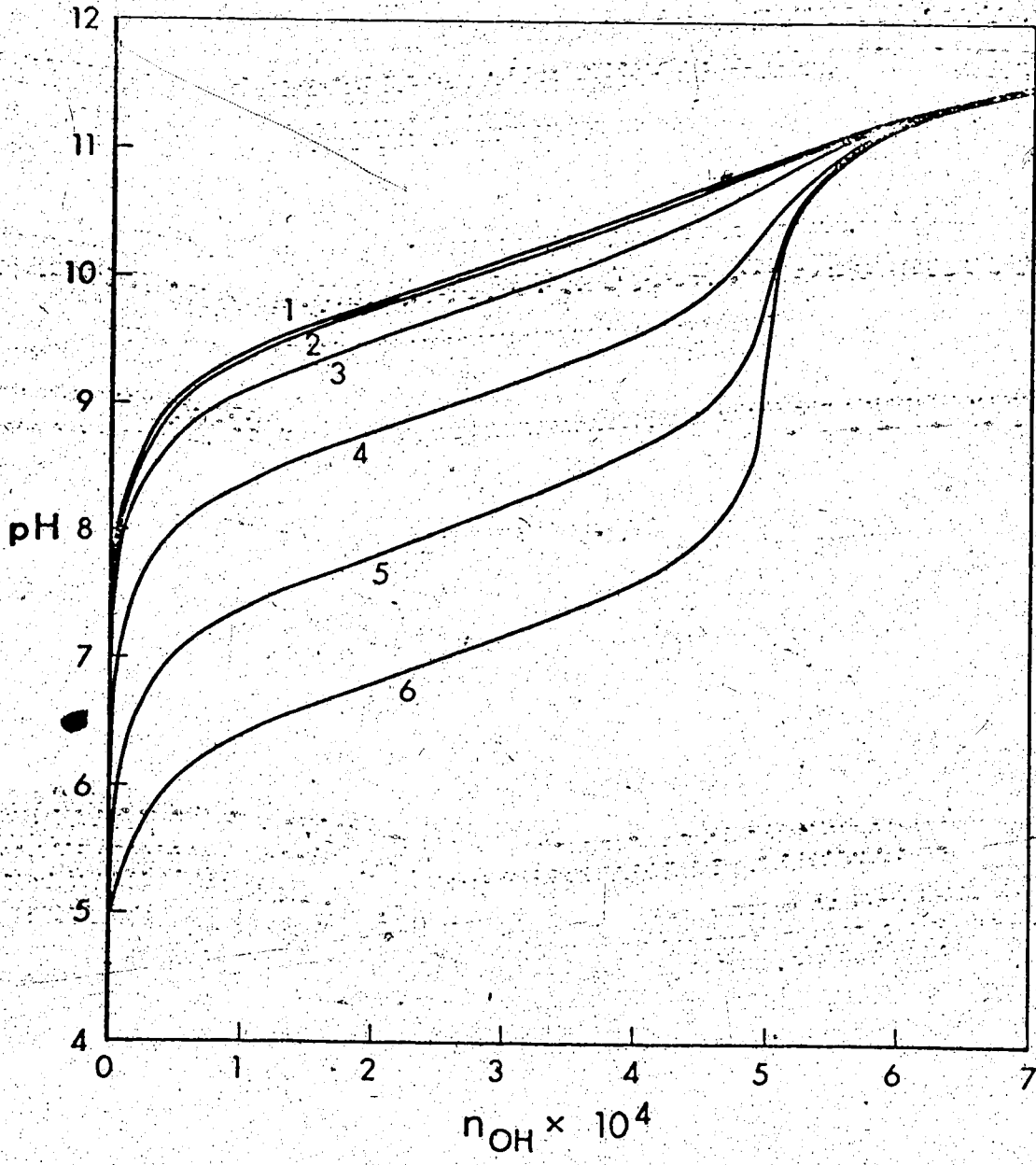


Figure 2. Theoretical titration curves for acid BH^+ in a resin-solution medium. Effect of K_{BH} . (Curves calculated from Equation 11).

For acid BH^+ . $K'_{a,BH} = 1.0 \times 10^{-10}$; $V = 0.050$ l;
 $n_{BH} = 5.00 \times 10^{-4}$ mole; $K_B = 10^4$; $W = 0$ (Curve 1), =
 0.0050 kg (Curves 2 - 6).

Curve No.	1	2	3	4	5	6
K_{BH}	10^4	10^3	10^2	10	1	-

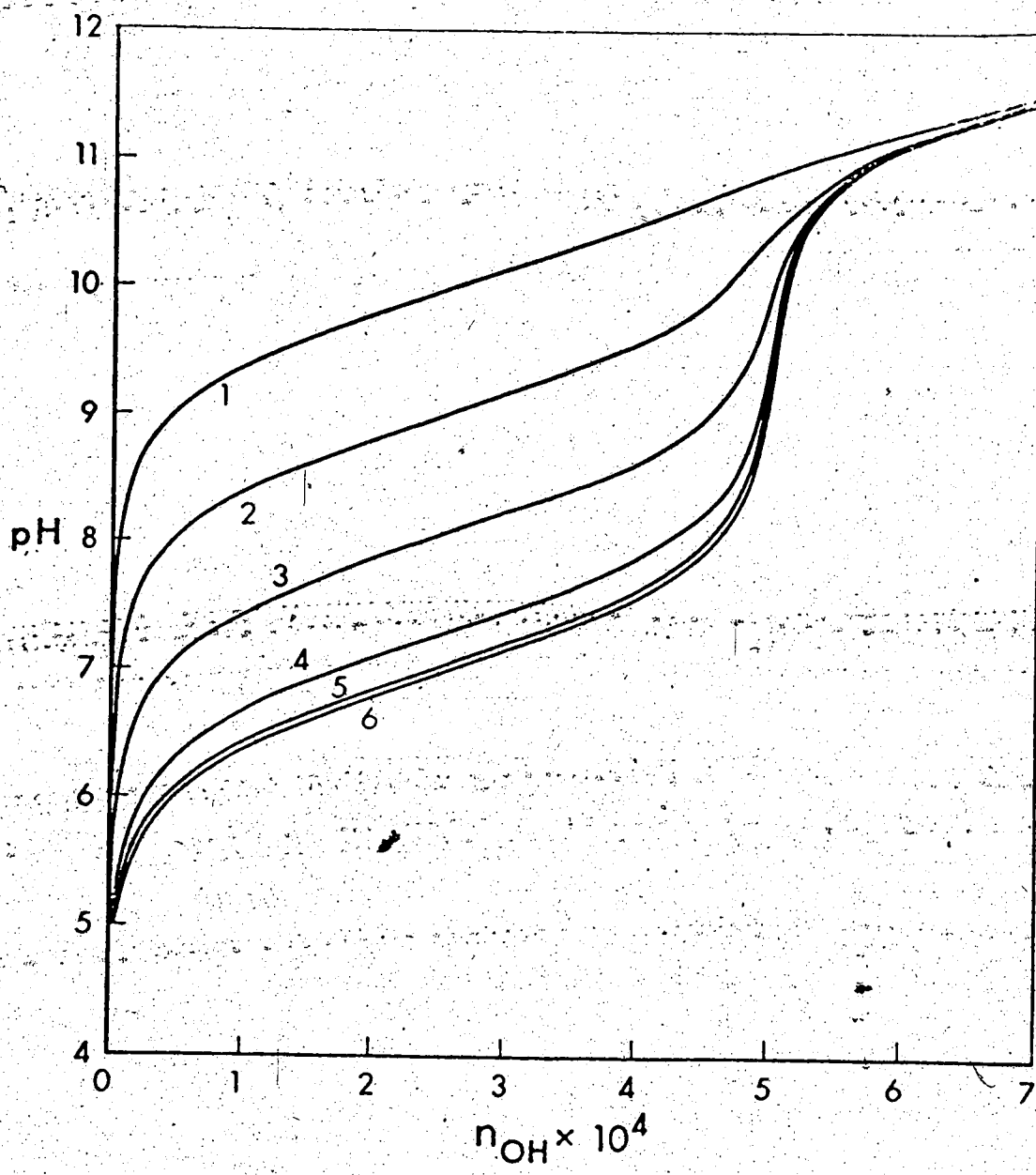


Table 2
Hypothetical titration data
for Curve 1; Figure 1.

$$K_{BH} = 0, K_B = 0^a$$

pH	Moles of NaOH added
6.5	1.41×10^{-7}
7.0	5.00×10^{-7}
7.5	1.60×10^{-6}
8.0	5.02×10^{-6}
8.5	1.55×10^{-5}
9.0	4.61×10^{-5}
9.5	1.22×10^{-3}
10.0	2.57×10^{-4}
10.5	4.01×10^{-4}
11.0	5.20×10^{-4}
11.5	6.93×10^{-3}
12.0	1.15×10^{-3}

^a All other information can be found
in Figure 1.

Table 3
Hypothetical titration data
for Curve 2; Figure 1.

$$K_{BH} = 0, K_B = 1^a$$

pH	Moles of NaOH added
6.5	1.57×10^{-7}
7.0	5.50×10^{-7}
7.5	1.75×10^{-6}
8.0	5.50×10^{-6}
8.5	1.70×10^{-5}
9.0	5.02×10^{-5}
9.5	1.31×10^{-4}
10.0	2.68×10^{-4}
10.5	4.09×10^{-4}
11.0	5.24×10^{-4}
11.5	6.94×10^{-4}
12.0	1.15×10^{-3}

^a All other information can be found
in Figure 1.

Table 4
Hypothetical titration data
for Curve 3; Figure 1.

$$K_{BH} = 0, K_B = 10^a$$

pH	Moles of NaOH added
6.0	4.04×10^{-8}
6.5	2.99×10^{-7}
7.0	9.99×10^{-7}
7.5	3.16×10^{-6}
8.0	9.87×10^{-6}
8.5	3.00×10^{-5}
9.0	8.40×10^{-5}
9.5	1.96×10^{-4}
10.0	3.40×10^{-4}
10.5	4.53×10^{-4}
11.0	5.42×10^{-4}
11.5	7.00×10^{-4}
12.0	1.16×10^{-3}

^a All other information can be found
in Figure 1.

Table 5

Hypothetical titration data
for Curve 4; Figure 1

$$K_{BH} = 0, \quad K_B = 10^2 \quad ^a$$

pH	Moles of NaOH added
6.0	4.90×10^{-7}
6.5	1.72×10^{-6}
7.0	5.44×10^{-6}
7.5	1.68×10^{-5}
8.0	4.96×10^{-5}
8.5	1.29×10^{-4}
9.0	2.63×10^{-4}
9.5	3.90×10^{-4}
10.0	4.65×10^{-4}
10.5	5.07×10^{-4}
11.0	5.61×10^{-4}
11.5	7.07×10^{-4}
12.0	1.16×10^{-3}

^a All other information can be found
in Figure 1.

Table 5
Hypothetical titration data
for Curve 5; Figure 1

$$K_{BH} = 0, K_B = 10^3 \text{ }^a$$

pH	Moles of NaOH added
5.5	1.40×10^{-6}
6.0	4.94×10^{-6}
6.5	1.55×10^{-5}
7.0	4.59×10^{-5}
7.5	1.21×10^{-4}
8.0	2.51×10^{-4}
8.5	3.81×10^{-4}
9.0	4.56×10^{-4}
9.5	4.87×10^{-4}
10.0	5.02×10^{-4}
10.5	5.19×10^{-4}
11.0	5.65×10^{-4}
11.5	7.08×10^{-4}
12.0	1.16×10^{-3}

^a All other information can be found
in Figure 1.

Table 7
 Hypothetical titration data
 for Curve 6; Figure 1

$$K_{BH} = 0, \quad K_B = 10^4 \text{ }^a$$

pH	Moles of NaOH added
5.0	4.35×10^{-6}
5.5	1.52×10^{-5}
6.0	4.54×10^{-5}
6.5	1.20×10^{-4}
7.0	2.50×10^{-4}
7.5	3.80×10^{-4}
8.0	4.55×10^{-4}
8.5	4.85×10^{-4}
9.0	4.96×10^{-4}
9.5	5.01×10^{-4}
10.0	5.06×10^{-4}
10.5	5.21×10^{-4}
11.0	5.66×10^{-4}
11.5	7.08×10^{-4}
12.0	1.16×10^{-3}

^a All other information can be found
 in Figure 1.

Table 8

Hypothetical titration data
for Curve 1; Figure 2.

$$K_{BH} = 10^4; K_B = 10^4 \text{ }^a$$

pH	Moles of NaOH added
6.5	1.41×10^{-7}
7.0	5.00×10^{-7}
7.5	1.60×10^{-6}
8.0	5.02×10^{-6}
8.5	1.55×10^{-5}
9.0	4.61×10^{-5}
9.5	1.22×10^{-4}
10.0	2.57×10^{-4}
10.5	4.01×10^{-4}
11.0	5.20×10^{-4}
11.5	6.93×10^{-4}
12.0	1.15×10^{-3}

^a All other information can be found
in Figure 2.

Table 9
Hypothetical titration data
for Curve 2, Figure 2

$$K_{BH} = 10^{-3} \quad K_B = 10^{-4} \quad ^a$$

pH	Moles of NaOH added
6.0	4.36×10^{-7}
6.5	1.55×10^{-6}
7.0	4.91×10^{-6}
7.5	1.52×10^{-5}
8.0	4.52×10^{-5}
8.5	1.20×10^{-4}
9.0	2.50×10^{-4}
9.5	3.81×10^{-4}
10.0	4.61×10^{-4}
10.5	5.05×10^{-4}
11.0	5.61×10^{-4}
11.5	7.07×10^{-4}
12.0	1.16×10^{-3}

^a All other information can be found
in Figure 2.

Table 10
Hypothetical titration data
for Curve 3; Figure 2

$$K_{BH} = 10^2, K_B = 10^4 \text{ }^a$$

pH	Moles of NaOH added
5.5	1.24×10^{-6}
6.0	4.45×10^{-6}
6.5	1.40×10^{-5}
7.0	4.17×10^{-5}
7.5	1.12×10^{-4}
8.0	2.38×10^{-4}
8.5	3.71×10^{-4}
9.0	4.51×10^{-4}
9.5	4.85×10^{-4}
10.0	5.01×10^{-4}
10.5	5.19×10^{-4}
11.0	5.65×10^{-4}
11.5	7.08×10^{-4}
12.0	1.16×10^{-3}

^a All other information can be found
in Figure 2.

Table 11

Hypothetical titration data
for Curve 4; Figure 2

$$K_{BH} = 10; K_B = 10^4 \text{ }^a$$

pH	Moles of NaOH added
5.0	1.89×10^{-6}
5.5	7.60×10^{-6}
6.0	2.38×10^{-5}
6.5	6.83×10^{-5}
7.0	1.67×10^{-4}
7.5	3.06×10^{-4}
8.0	4.17×10^{-4}
8.5	4.71×10^{-4}
9.0	4.91×10^{-4}
9.5	5.00×10^{-4}
10.0	5.06×10^{-4}
10.5	5.21×10^{-4}
11.0	5.66×10^{-4}
11.5	7.08×10^{-4}
12.0	1.16×10^{-3}

^a All other information can be found
in Figure 2.

Table 12

Hypothetical titration data
for Curve 5; Figure 2

$$K_{BH} = 1, K_B = 10^4 \text{ }^a$$

pH	Moles of NaOH added
5.0	3.91×10^{-6}
5.5	1.38×10^{-5}
6.0	4.17×10^{-5}
6.5	1.12×10^{-4}
7.0	2.38×10^{-4}
7.5	3.71×10^{-4}
8.0	4.51×10^{-4}
8.5	4.83×10^{-4}
9.0	4.95×10^{-4}
9.5	5.00×10^{-4}
10.0	5.06×10^{-4}
10.5	5.21×10^{-4}
11.0	5.66×10^{-4}
11.5	7.08×10^{-4}
12.0	1.16×10^{-3}

^a All other information can be found
in Figure 2.

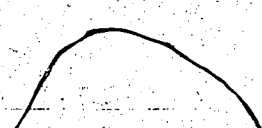


Table 13
Hypothetical titration data
for Curve 6; Figure 2

$$K_{BH} = 0, K_B = 10^4 \text{ }^a$$

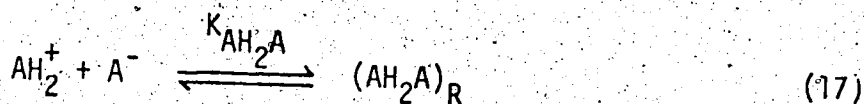
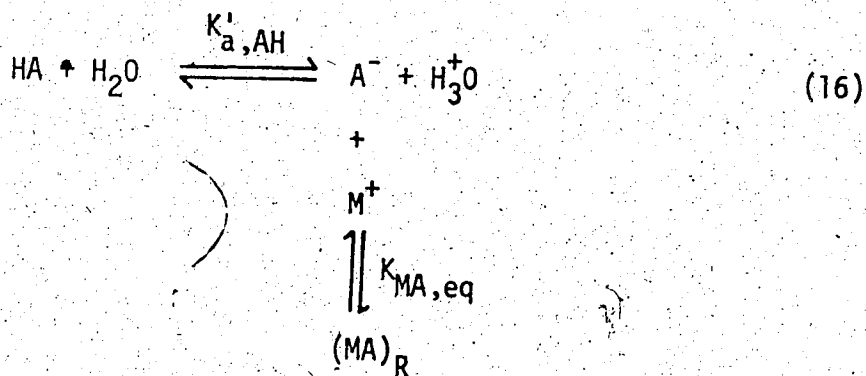
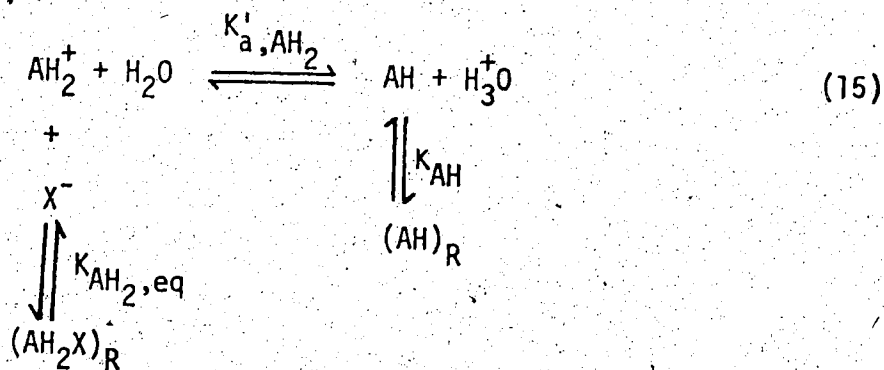
pH	Moles of NaOH added
5.0	4.35×10^{-6}
5.5	1.52×10^{-5}
6.0	4.54×10^{-5}
6.5	1.20×10^{-4}
7.0	2.50×10^{-4}
7.5	3.80×10^{-4}
8.0	4.55×10^{-4}
8.5	4.85×10^{-4}
9.0	4.96×10^{-4}
9.5	5.00×10^{-4}
10.0	5.06×10^{-4}
10.5	5.21×10^{-4}
11.0	5.66×10^{-4}
11.5	7.08×10^{-4}
12.0	1.16×10^{-3}

^a All other information can be found
in Figure 2.

Equations 13 and 14 are valid when both $\text{pH}(\text{NR})$ and $\text{pH}(\text{R})$ lie between 4 and 10 for the condition n_{BH} or $n_{\text{HA}} \geq 5 \times 10^{-4}$ moles and $V \leq 0.05$ L. For larger sample size or smaller volume, the equations are valid over a wider range of pH and n .

Titrations involving BH^+ or HA type acids have been described above. More complicated cases such as the titration of an AH_2^+ type acid or an acid mixture will now be presented.

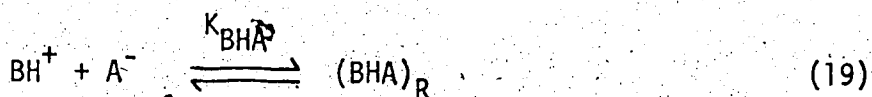
The equilibria likely to exist in an aqueous phase solution of AH_2^+ (as the X^- salt) in contact with a nonionic resin phase are presented in equations 15 - 18:





Here X^- is the conjugate base of a strong acid (e.g. Cl^- , Br^- , NO_3^- or ClO_4^-) and M^+ is a non-acidic cation (e.g. Na^+ , K^+).

Equilibria existing in a solution of a mixture of weak acids BH^+ and HA in contact with nonionic resin are given by equations 5, 7 and 19:



In both of the systems described above, the aqueous phase contains a large excess of inert electrolyte MX (e.g. NaCl , NaBr) compared to the amount of sample, so that the concentration of X^- or M^+ becomes constant, independent of the amount of sample in the solution. For a simple 1:1 ion pair mechanism, the sorption of BH^+ and A^- has been described previously. The sorption of AH_2^+ can be described by a heterogeneous equilibrium constant:

$$K_{\text{AH}_2, \text{eq}} = \frac{a_{(\text{AH}_2\text{X})_R}}{a_{\text{AH}_2} \cdot a_X} \quad (20)$$

where a_i is the activity of the different species, i . With large excess of X^- , this equilibrium can be described by a distribution coefficient, that is:

$$K_{AH_2} = \frac{[AH_2X]_R}{[AH_2^+]} = K_{AH_2,eq} \frac{\gamma_{AH_2} \gamma_X}{\gamma_{AH_2X,R}} [X] \quad (21)$$

Table 14 lists the equilibrium constants and distribution coefficients for the acid AH_2^+ and acid mixtures of BH^+ and HA in the presence of an excess of resin and inert electrolyte.

By combining equations from Table 14 with the appropriate mass and charge balance equations (Appendix V) potentiometric titration equations may be derived. For a titration of n_{AH_2} moles of acid AH_2^+ with strong base $NaOH$, the titration equation has the form:

$$n_{OH} = \frac{K_W V}{a_H \gamma_{OH}} - \frac{a_H V}{\gamma_H} + \frac{K'_{a,AH}}{a_H} [AH] \cdot (V + K_A \cdot W) - \frac{a_H}{K'_{a,AH_2}} [AH] \cdot (V + K_{AH_2} \cdot W) \quad (22)$$

where V is the volume of the aqueous phase, W is the weight of resin, and n_{OH} is the number of moles of titrant added. AH is a variable that has to be found by solving the quadratic equation:

$$a [AH]^2 + b [AH] + c = 0 \quad (23)$$

Table 14

Equilibrium constants and distribution coefficients
for acid AH_2^+ and acid mixture BH^+ and HA ^a

AH_2^+	BH^+, HA
$K'_{a,AH_2} = \frac{[AH] \cdot a_H}{[AH_2^+]}$	$K'_{a,BH} = \frac{[B] \cdot a_H}{[BH^+]}$
$K'_{a,AH} = \frac{[A^-] \cdot a_H}{[AH]}$	$K'_{a,HA} = \frac{[A^-] \cdot a_H}{[HA]}$
$K_W = a_H \cdot a_{OH}$	$K_W = a_H \cdot a_{OH}$
$K_{AH_2} = \frac{[AH_2X]_R}{[AH_2^+]}$	$K_{BH} = \frac{[BHX]_R}{[BH^+]}$
$K_{AH} = \frac{[AH]_R}{[AH]}$	$K_{HA} = \frac{[HA]_R}{[HA]}$
$K_A = \frac{[MA]_R}{[A^-]}$	$K_A = \frac{[MA]_R}{[A^-]}$
$K_{AH_2A} = \frac{[AH_2A]_R}{[AH_2^+][A^-]}$	$K_{BHA} = \frac{[BHA]_R}{[BH^+][A^-]}$

^a a_H is hydronium ion activity. All other symbols defined in text and Equations 15, 16, 17 and 19.

where

$$a = \frac{2 \cdot W \cdot K_{AH_2A} \cdot K'_{a,AH}}{K'_{a,AH_2}} \quad (24)$$

$$b = (V + WK_{AH}) + \frac{K'_{a,AH}}{a_H} (V + K_A) + \frac{a_H}{K'_{a,AH_2}} (V + WK_{AH_2}) \quad (25)$$

$$c = -n_{AH_2} \quad (26)$$

Since a and b are positive while c is negative in the above quadratic equation, both positive and negative roots exist. Only the positive root will be taken as the solution of equation 23 since the value of AH can not be negative. The titration equation 22 can be evaluated once the ionization constants and the distribution coefficients have been measured. Acid mixtures of $[HA]$ and $[BH^+]$ can be treated in a similar way and the final titration equation can be written as:

$$n_{OH} = \frac{K_w \cdot V}{a_H \cdot \tau_{OH}} - \frac{a_H \cdot V}{\tau_H} + \frac{K'_{a,HA}}{a_H} (V + WK_A) \cdot [HA] + [B] (V + WK_B) + W \cdot K_{BHA} \frac{K'_{a,HA}}{K'_{a,BH}} [B] \cdot [HA] \quad (27)$$

where $[HA]$ and $[B]$ are two dependent variables in equation 27, and $[HA]$ can be expressed as the function of $[B]$:

$$[HA] = n_{HA}/f([B]) \quad (28)$$

where

$$f([B]) = WK_{HA} + V\left(1 + \frac{K'_{a,HA}}{a_H}\right) + WK'_{a,HA} \left([B] \frac{K_{BHA}}{K'_{a,BH}} + \frac{K_A}{a_H}\right) \quad (29)$$

and $[B]$ is the solution of the following quadratic equation:

$$p[B]^2 + q[B] + s = 0 \quad (30)$$

where

$$p = WK_{BHA} \frac{K'_{a,HA}}{K'_{a,BH}} \left[(V + WK_B) + \frac{a_H}{K'_{a,BH}} (V + WK_{BH}) \right] \quad (31)$$

$$q = WK_{BHA} \frac{K'_{a,HA}}{K'_{a,BH}} (n_{HA} - n_{BH}) + \left[(V + WK_{HA}) + \frac{K'_{a,HA}}{a_H} (V + WK_A) \right] \cdot \left[(V + WK_B) + \frac{a_H}{K'_{a,BH}} (V + WK_{BH}) \right] \quad (32)$$

$$s = -n_{BH} \quad (33)$$

Here n_{HA} and n_B are the number of moles of HA and BH^+ acids being titrated. As in the solution to the quadratic equation 23, only the positive root will be taken as the solution of equation 30.

The effect of K_{AH} on the titration curve can be understood as follows: In the presence of the nonionic resin, AH, which is the product of the first acid association step would be adsorbed on the resin. This would shift the equilibrium and show a sharper first end point break. However, this would weaken the second end point, since HA is the reactant for the second dissociation step.

Figure 3. Theoretical titration curves for acid AH_2^+ in the presence of resin. Effect of K_{AH_2A} (Curves calculated from equation 22).

For acid AH_2^+ , $K'_{a,AH_2} = 1.0 \times 10^{-6}$; $K'_{a,AH} = 5.0 \times 10^{-8}$;
 $V = 0.0501$; $n_{AH_2} = 5.0 \times 10^{-4}$ mole; $K_{AH_2} = 10$;
 $K_{AH} = 10^3$; $K_A = 10$; $W = 0$ (Curve 1); $= 0.0050$ Kg
 (Curves 2-5).

Curve No.	1	2	3	4	5
K_{AH_2A}	-	0	10^8	10^{10}	10^{12}

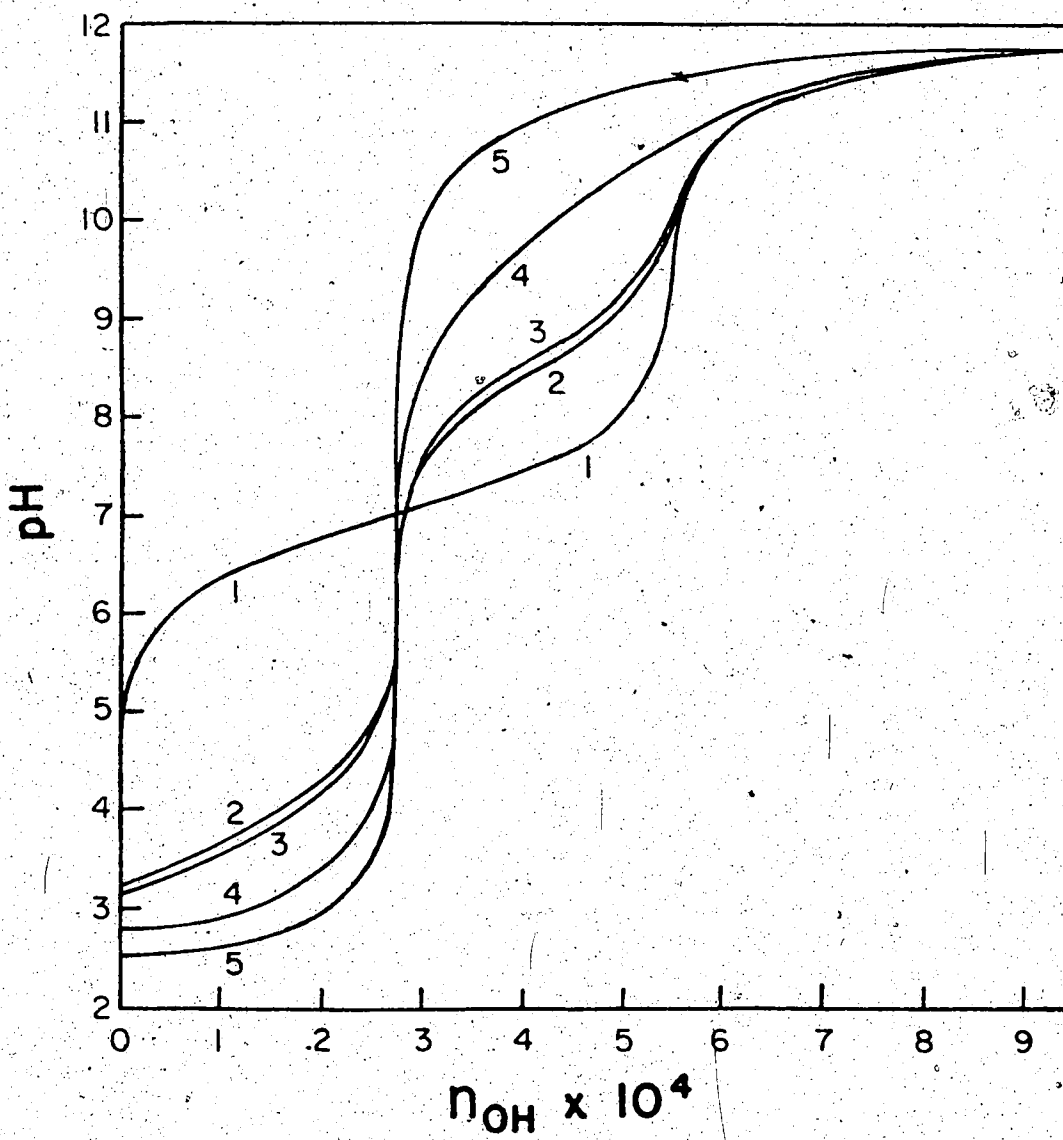


Figure 3 shows an example of the titrating curve of a hypothetical acid H_2A^+ with K'_{a, AH_2} of 1.0×10^{-6} and $K'_{a, HA}$ of 5.0×10^{-6} . Curve 1 is the titration curve in the absence of the nonionic resin. Curve 2 to 5 are the titration curves with various values of K_{AH_2A} . Curve 2 is obtained when K_{AH_2A} is zero. There is not much difference between the titration curves until K_{AH_2A} is very large (Curve 3). For values larger than 10^8 , the titration curve changes drastically, e.g. Curve 4 with K_{AH_2A} of 10^{10} and Curve 5 with K_{AH_2A} of 10^{12} . The effect of K_{AH_2A} is illustrated in Figures 4 and 5. In Figure 4, $[AH]$, which is the product of the first end point, is plotted against pH on a logarithmic scale. Curve 1 of Figure 4 is obtained in the absence of resin. Curve 2 which is obtained in the presence of resin is essentially the same for K_{AH_2A} up to 10^6 . Curves 3 and 4 are obtained when K_{AH_2A} is 10^{10} and 10^{12} respectively. Because of the larger value of K_{AH_2A} in the last two cases, H_2A^+ and A^- as AH_2A on the resin and show a relatively small but constant value of $[AH]$. Figure 5 describes the effect of K_{AH_2A} on the concentration of $[AH_2A]_R$ which increases rapidly from K_{AH_2A} of 1 (Curve 1) to 10^{12} (Curve 5) as expected.

Figure 6 shows the titration curves for an equivalent mixture (2.75×10^{-4} mole each) of two hypothetical acids with $K'_{a, BH}$ and $K'_{a, HA}$ both 1.0×10^{-7} . Curve 1 is the titration result without resin present. Only the second equivalence point exhibits a "break"

Figure 4. Plots of $-\log [AH]$ versus pH in the presence of resin.
Effect of K_{AH_2A} . All other data is the same as in
Figure 3.

Curve No.	1	2	3	4
K_{AH_2A}	-	$\leq 10^6$	10^{10}	10^{12}

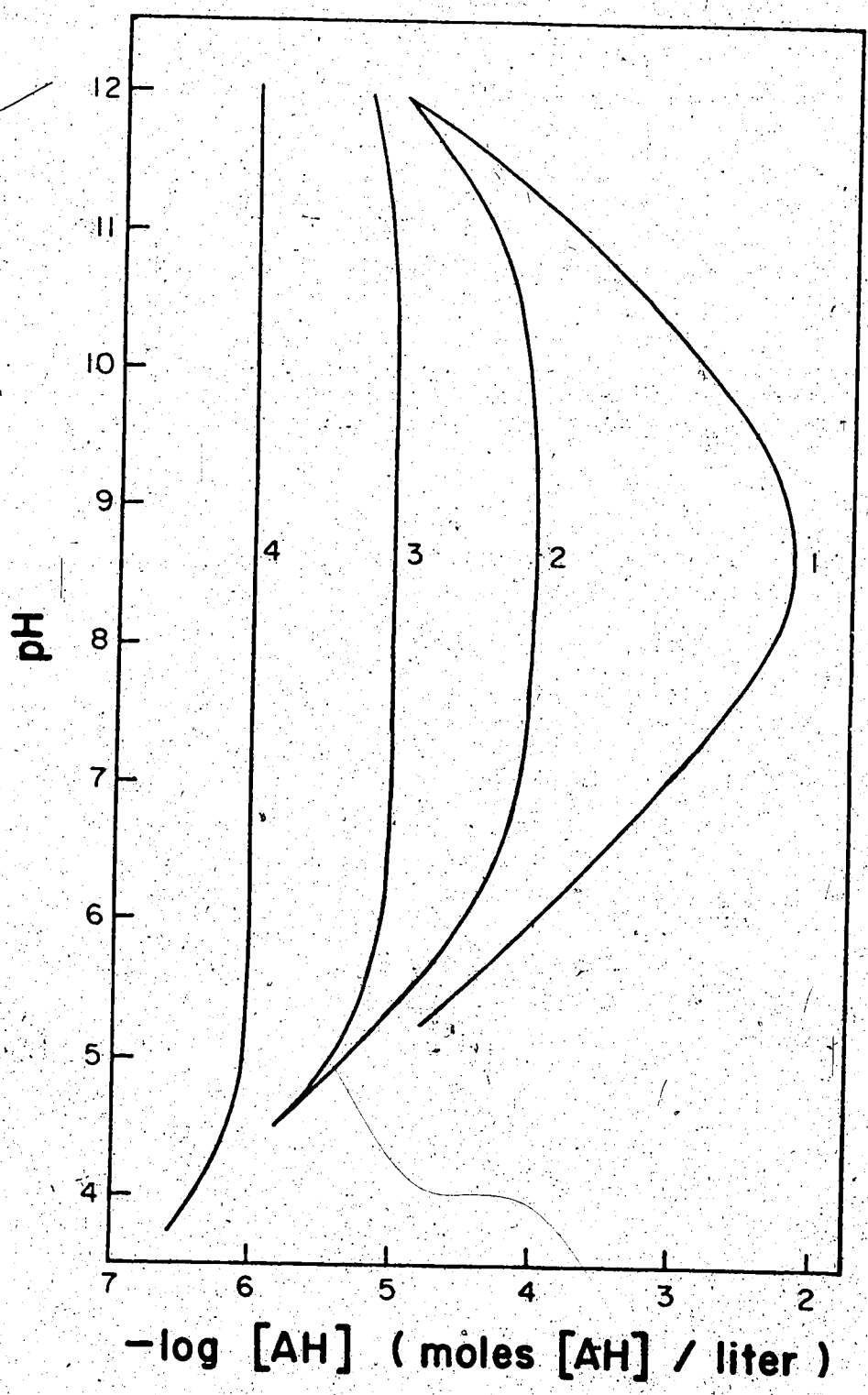


Figure 5. Plots of $-\log[AH_2A]_R$ versus pH in the presence of resin. Effect of K_{AH_2A} . All other data is the same as in Figure 3.

Curve No.	1	2	3	4	5
K_{AH_2A}	1	10^4	10^6	10^8	10^{12}

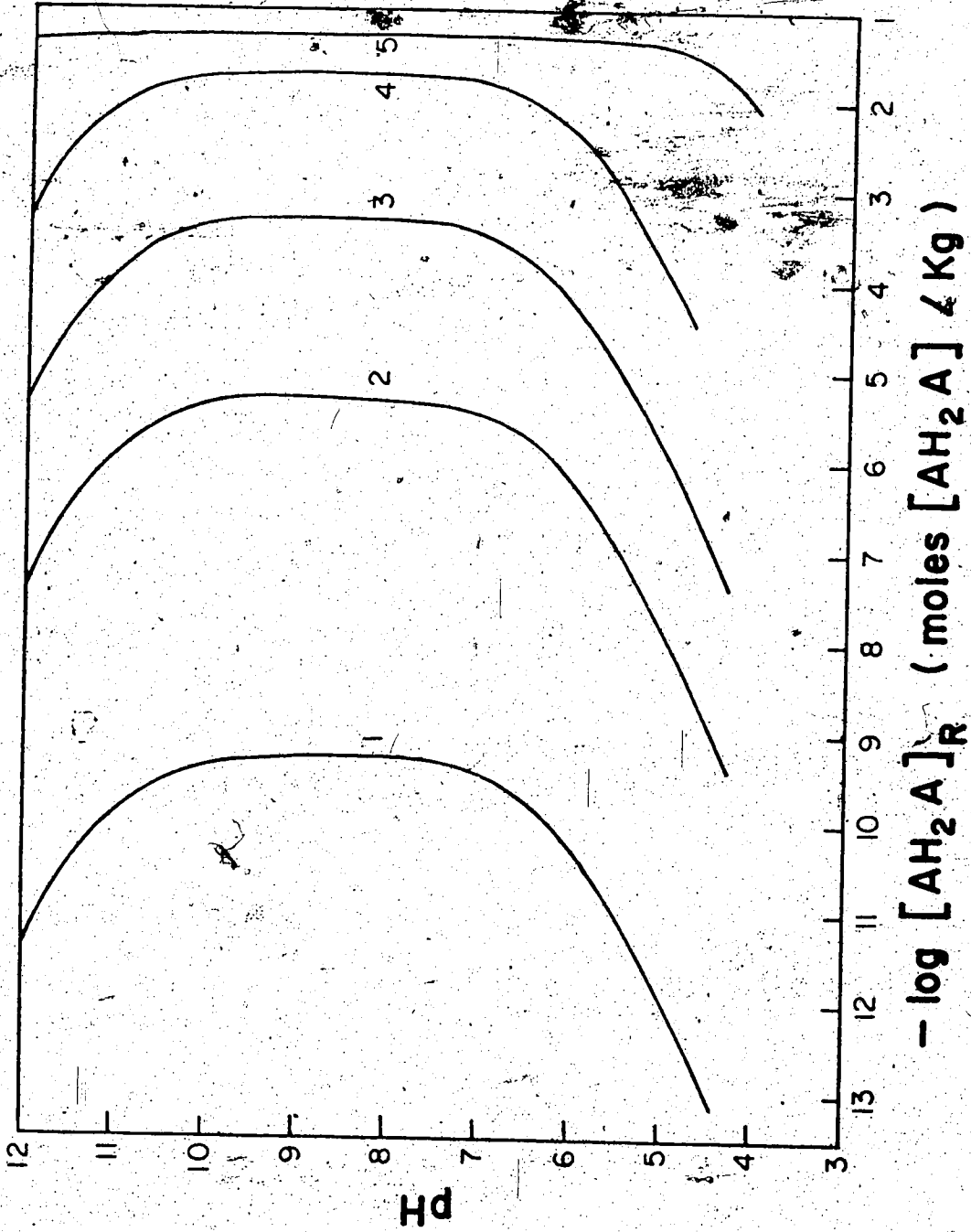
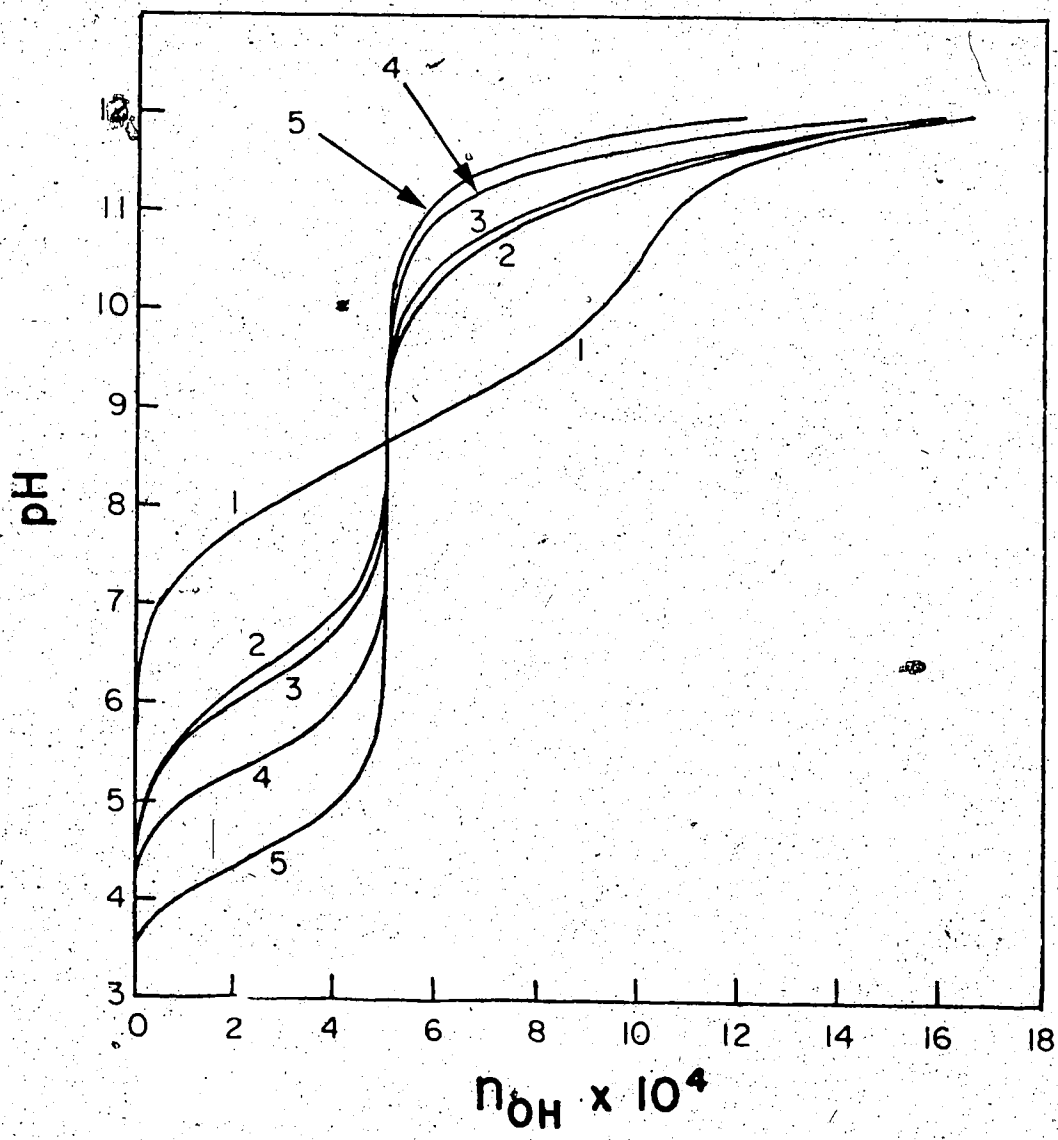


Figure 6. Theoretical titration curves for acid mixture of BH^+ and HA in the presence of resin. Effect of K_{BHA} (Curves calculated from equation 27).

For acid mixture, $K'_{a,HA} = 1.0 \times 10^{-7}$; $K'_{a,BH} = 1.0 \times 10^{-7}$; $V = 0.050$ l; $n_{BH} = n_{HA} = 2.75 \times 10^{-4}$; $K_A = 4.8$; $K_{HA} = 430$; $K_{BH} = 10$; $K_B = 2.9 \times 10^4$; $W = 0$ (Curve 1); $= 0.0050$ Kg (Curves 2-5)

Curve No.	1	2	3	4	5
K_{BHA}	-	0	10^8	10^{10}	10^{12}



In the presence of resin, a first equivalence point appears and becomes larger with increasing K_{BHA} at the expense of the second equivalence point break. This effect can be explained in the same way as the result in Figure 3. K_{BHA} plays the same role as K_{AH_2A} in the AH_2^+ titration. When K_{BHA} is less than 10^6 , it has virtually no effect on the titration curve. The effect of K_{BHA} on two of the species are shown in Figures 7 and 8. Figure 7 illustrates the effect of K_{BHA} on $[B]$, the titration product of BH^+ . Curve 1 indicates a large value B in the absence of resin after the first equivalence point. Curve 2 is the result of the presence of resin with K_{BHA} up to 10^6 . The sorption of B onto the resin phase decreases B . Curves 3, 4 and 5 represent K_{BHA} values of 10^8 , 10^{10} and 10^{12} .

With a larger and larger K_{BHA} , $[B]$ is diminishing from the aqueous phase. Figure 8 shows the opposite effect on $[BHA]_R$ from the increasing of K_{BHA} . Curve 1 is the result of a K_{BHA} value of 10^6 . With an increase in K_{BHA} (Curves 2, 3 and 4 with K_{BHA} of 10^8 , 10^{10} and 10^{12}), BHA is largely adsorbed on the resin phase. Hence a large value of $[BHA]_R$ is obtained.

The titrations of AH_2^+ type acids, and acid mixtures of BH^+ and HA are complicated by sorption of the AH_2A and BHA species on the nonionic resin. If K_{BHA} is equal to zero then the titration of the acid mixtures is the same as titrating two independent acids, BH^+ and HA . In solving the titration equations, unless K_{AH_2A} and K_{BHA} are unusually large, the titration curves will not be effected much by omitting them.

Figure 7. Plots of $-\log[B]$ versus pH in the presence of resin.
Effect of K_{BHA} . All other data is the same as in
Figure 6.

Curve No.	1	2	3	4	5
K_{BHA}	-	$< 10^6$	10^8	10^{10}	10^{12}

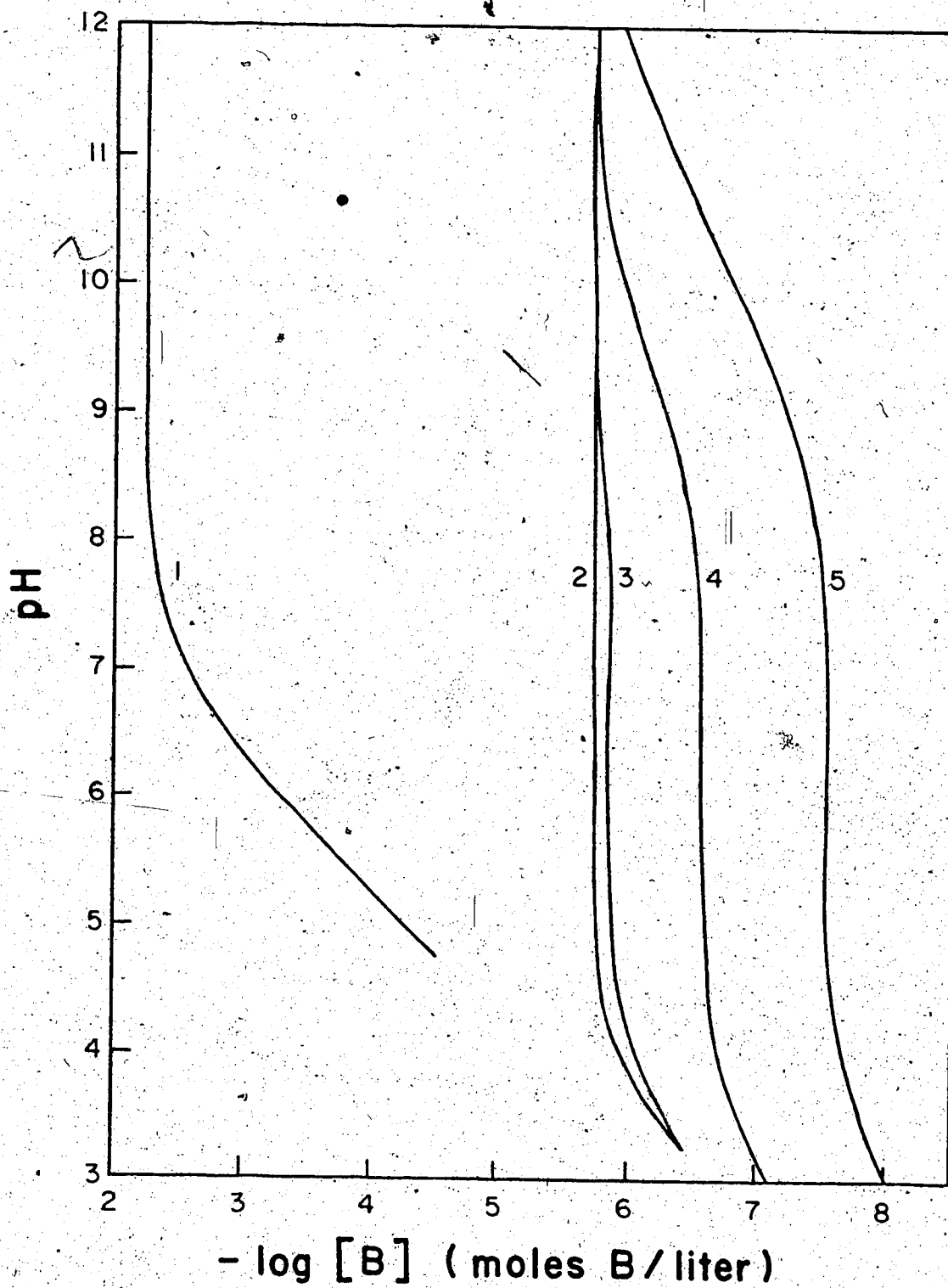
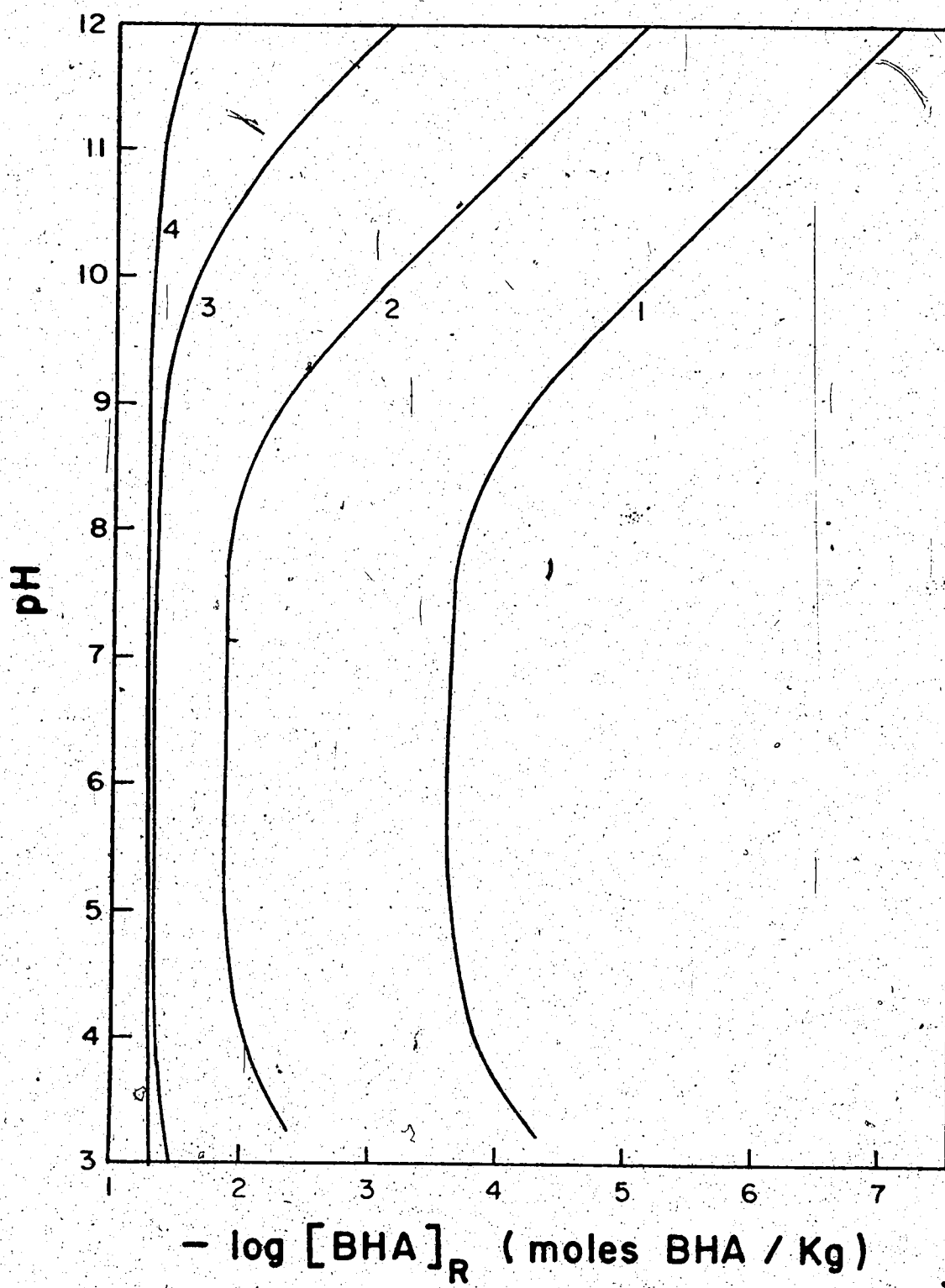


Figure 8. Plots of $-\log[BHA]_R$ versus pH in the presence of resin. Effect of K_{BHA} . All other data is the same as in Figure 6.

Curve No.	1	2	3	4
K_{BHA}	10^6	10^8	10^{10}	10^{12}



3. EXPERIMENTAL

3.1 Apparatus

Titration equipment for this work consisted of a titration vessel, electrodes, pH meter, polytetrafluoroethylene stopper and micrometer burette. The titration vessel was a lipless glass beaker with a volume of about 150 ml. The stopper was machined to fit the vessel. It has four holes, two of which are for the electrodes, the third passing nitrogen gas over the solution, and the fourth for the microburette tip. The titration vessel was put in a constant temperature water bath that was kept at 25 ± 1 C. The pH meter was from Fisher Scientific, Model 320. It was equipped with a glass electrode (Fisher Scientific Company) and a saturated calomel electrode (Fisher Scientific Company). The meter was standardized with pH=7 phosphate buffer and checked with pH=10 carbonate-borate-hydroxide buffer. The accuracy of the pH values reported is ± 0.05 to 0.10 pH units.

It was demonstrated that the pH obtained in a stirred resin suspension did not usually differ by more than 0.1 unit from that measured after allowing the resin to settle. In all the titrations, titrant was delivered from a 2 ml micrometer burette (Roger Gilmont Instruments, Great Neck, N.Y.). A 10 cm thin-drawn piece of flexible polyethylene tubing was fitted over the burette tip in order to allow it to be used in the horizontal position. This micrometer burette was calibrated by cumulatively weighing

0.100 ml increments of double distilled water. The error was found to be - 1.3% throughout the entire 2 ml range. Thus, in the titrations, the observed volume was increased by 1.3%.

Chromatographic measurements were performed with a model CMP-2V pump (Laboratory Data Control, Riviera Beach, Fla.) and a model 230 Absorbance Detector (Spectra-Physics, Santa Clara, Calif.). Glass chromatographic columns (2.8 mm I.D.) and additional valves and gauges were all obtained from Laboratory Data Control. Two different columns of 30 cm and 5 cm length were used. The glass columns were dried and packed with less than 325 mesh XAD-2 resin (less fines). The flow rate of this pump was checked by collecting the effluents in a 50 ml burette. It was found to have no more than 2% error when the pump was set at 0.5 ml per minute.

Other than being used in measuring the distribution coefficients directly, chromatography was also employed in determining the aqueous phase concentration in the batch equilibration method. When the concentration of the desired species is too low, it is more advantageous to concentrate it in a pre-column (5 cm) prior to the analytical column. Figure 9 shows the apparatus used in this study. The operation of this apparatus is similar to that of Cantwell's work (17), that is, the sample was loaded onto C1, the pre-column, through an injection valve V2. The electrolyte was eluted through P2 (solid line operation on the rotary valve V1). After a proper time, the sample was transferred from C1 to C2, analytical column (dotted line operation in V1), by using a different solvent (e.g., higher methanol percentage in the

Figure 9. Diagram of the liquid chromatograph.

P1, Main pump;

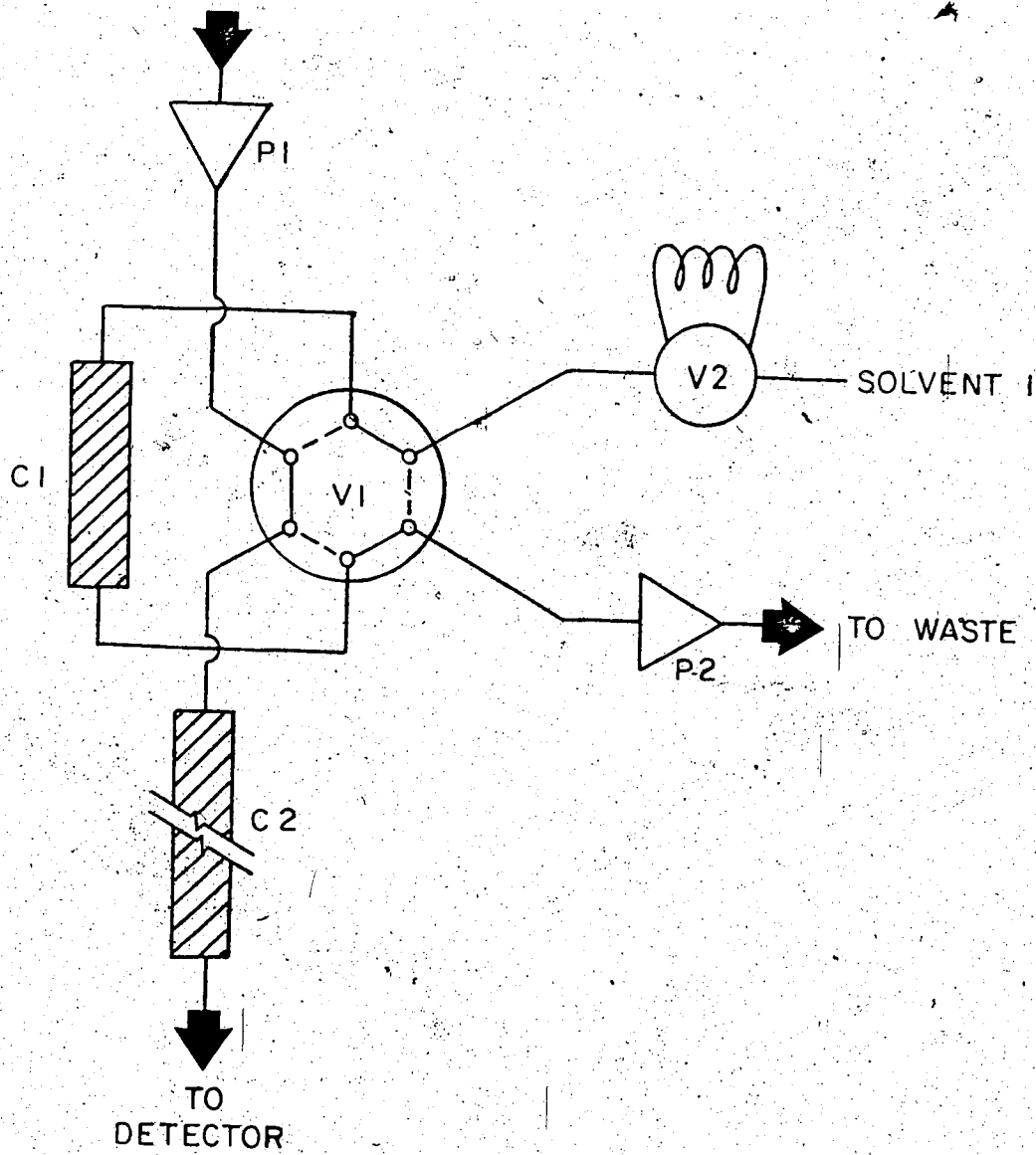
P2, Auxiliary pump;

C1, Pre-column (5 cm long);

C2, Analytical column (30 cm long);

V1, Rotary valve;

V2, Sample injection valve.



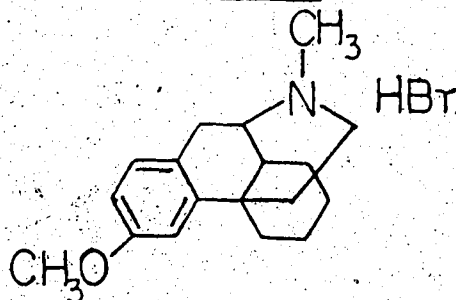
mobile phase) and eluted.

A Blue M agitating constant temperature bath (Blue M Company, Blue Island, Ill.) was used for isotherm studies. Spectrophotometric measurements were made on a Unicam SP 800 Spectrophotometer (Pye Unicam, Cambridge, England).

3.2 Chemicals

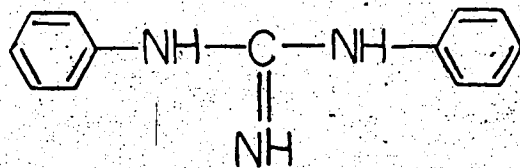
Benzylamine was obtained from British Drug House and was used without further purification. Titration with hydrochloric acid yielded an assay value of 98.07%.

Dextromethorphan Hydrobromide

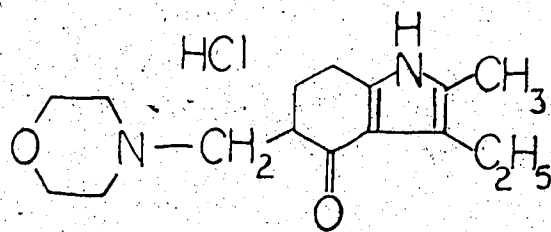


Dextromethorphan hydrobromide was kindly supplied by Endo Laboratories (Garden City, N.Y.). It was analyzed by Fajan's titration as 95.0%; the other 5% is water.

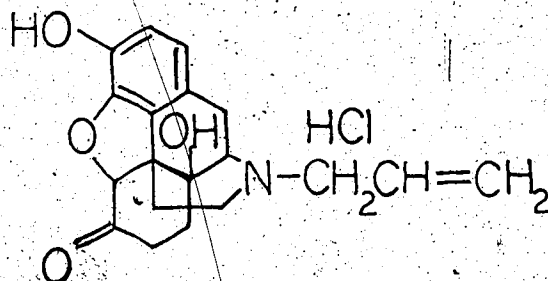
Diphenylguanidine



Diphenylguanidine was obtained from British Drug House. It was recrystallized twice from ethanol, then once from toluene. The melting point of this compound was found as 149.8-150.1°C.

Molindone Hydrochloride

Molindone hydrochloride was kindly supplied by Endo Laboratories and was used without further purification. It was analyzed by Fajan's titration as 99.74%.

Naloxone Hydrochloride

Naloxone hydrochloride was kindly supplied by Endo Laboratories. It was used as received. Fajan's titration of this compound yielded an assay value of 91.66%; the remainder is water.

m-Nitrophenol was obtained from Eastman Kodak Company (Rochester, N.Y.). It was recrystallized twice from 95% ethanol. The melting point of this compound was 96.7-97.2°C.

Tetra-n-Butylammonium Bromide (TBABr) was obtained from Eastman Kodak Company. It was used as received. The absence of acid-base impurities in TBABr was verified by titrating identical aliquots of hydrochloric acid with sodium hydroxide. In one case the titration

was performed in 50 ml of water and in the other case it was performed in 50 ml of 0.5 M TBABr. Identical potentiometric titration curves were obtained.

Tetraethylammonium Bromide (TEABr) and Tetramethylammonium Bromide (TMABr) were obtained from Eastman Kodak Company. They were used without further purification.

Other chemicals, including sodium carbonate, sodium chloride, hydrochloric acid, sodium hydroxide, sodium bromide, and silver nitrate were all analytical reagent grade chemicals. Potassium acid phthalate was primary standard grade.

3.3 Reagents

0.5 Molar Hydrochloric Acid was prepared from the concentrated reagent by diluting with double distilled water and standardized against sodium carbonate.

0.5 Molar Sodium Hydroxide was prepared by diluting 1 : 1 sodium hydroxide solution to the appropriate volume with freshly boiled and cooled double distilled water. The sodium hydroxide was stored in a polyethylene bottle and standardized with primary standard potassium hydrogen phthalate.

Double distilled water was prepared by distilling the laboratory distilled water from alkaline permanganate. The first 10-20% of the distillate was discarded and the middle fraction was used. This water was used to prepare all aqueous solutions in this work.

0.10 Molar Diphenylguanidine Hydrochloride. A stock solution was prepared by first suspending 2.11 grams of the purified compound in water, then adding 0.5 M HCl to within 2 ml of the equivalent amount. The solution was finally titrated to the potentiometric inflection with 0.5 M HCl in a 2-ml microburette, transferred quantitatively into a 100-ml volumetric flask, and diluted to volume with water. A 5.00 ml aliquot of this solution contained 0.5 milliequivalent of diphenylguanidinium ion and was used as the source of BH^+ in titrations with sodium hydroxide.

3.4 Resins

All the resin used in this study was originally taken from one bottle of Amberlite XAD-2 resin (Rohm & Haas Co., Lot no. 2-0218, 60-80 mesh). A portion of the resin was ground in a mortar and different mesh sizes were separated by using stainless steel sieves (W.S. Tyler Company of Canada). The 200 to 325 mesh cut and the less than 325 mesh portion were saved for the titration and isotherm experiments. The less than 325 mesh size with fines removed was dry packed into glass chromatographic columns.

Resin was purified as follows: In the case of the 200-325 mesh size, it was suspended in a large amount of methanol. After about 30 minutes, the fines were decanted. This process was repeated two or three times. This methanol-resin mixture was then transferred into a large flask, water was added, and the flask swirled so that the resin was settled with water. This water-resin mixture was decanted through a 10-20 μ sintered-glass filter to remove supernatant liquid. The resin was transferred into a flask filled with 3 M HCl and the swirling-decantation procedure repeated to wash the resin free of iron. After collecting the resin it was then added to 0.1 M sodium hydroxide, swirled and decanted. Then, finally, the resin was washed with water and dried. It was stored in a screw cap bottle under laboratory conditions.

Acid content of XAD-2 resin was determined by potentiometrically titrating a sample of this resin (5g) with 0.10 M sodium hydroxide in 0.10 M sodium chloride. This titration curve was compared with

the one obtained in the absence of resin. The difference between these two curves gives an estimate of the acid content. Base content of the resin was determined in a similar way by titrating a portion of the resin with 0.10 M hydrochloric acid in 0.10 M sodium chloride and comparing with a blank titration.

3.5 Potentiometric Titrations

Potentiometric titrations were usually carried out in 50.0 ml of aqueous phase and 5 g of resin. The total amount of sample acid added to the beaker was 0.5 meq, whether it was a monoprotic acid, a diprotic acid, or a mixture of monoprotic acids. The titrant concentration was 0.5 M. Thus the amount of added titrant was generally between 1.0 and 1.5 ml. Under these conditions, no account was taken of volume change during the titration, since the maximum volume change was never greater than three percent.

Before a titration was begun, a proper amount of inert salt was added to 45 ml of doubly distilled water. Then 5 g of wetted resin was added into the above solution. The system was flushed with nitrogen for about ten minutes. An aliquot of an aqueous solution of the sample acid was then pipetted into the beaker and titration was begun. If there was a need of calculating the theoretical titration curve, the beaker with the double distilled water was weighed before and after the wetted resin was added. When a titration was completed, the resin was collected in a pre-weighed Buchner funnel and was washed with a few portions of methanol and dried. The exact volume of the aqueous phase could be determined after the exact weight of the XAD-2 resin was known.

During the titration, an increment of titrant was added to the well-stirred resin suspension and stirring continued until the pH meter reading had drifted to a steady value. Then the pH value was

recorded. This value was compared with the pH recorded when the stirrer was shut off. No significant change was noted. The recording process, which usually required about five minutes per increment, was then repeated until the total number of equivalents of added titrant was in sufficient excess of the number of equivalents of acid in the system.

3.6 Distribution Isotherms

Distribution coefficients of H_3O^+ and OH^- on XAD-2 were determined as follows: a 100 ml stoppered flask was usually used. The proper quantity of sodium chloride (which made 0.10 M in the final solution) and a small amount of doubly distilled water was added to the flask and the flask was weighed. Then wetted resin was added and the flask was weighed again. From the difference of the two weights, the amount of water required to make the final volume 50 ml would be calculated. Then the known amount of HCl or NaOH solution was pipetted into the resin-aqueous solution mixture. The flasks were put in a shaker which was kept at $25 \pm 1^\circ C$. After equilibrium had been reached, the resin phase was collected in a Buchner flask, washed with methanol and dried. Aqueous phase was titrated with NaOH or HCl. The difference in the amount titrated and added was the amount sorbed on the resin phase. Distribution isotherms were obtained by repeating the distribution coefficient measurements at several different sample concentrations.

All the distribution coefficients of diphenylguanidine with the exception of that obtained in 0.10 M sodium chloride at pH 11 were determined by using the batch equilibration method. This procedure was similar to the one used for H_3O^+/OH^- determinations. After the aqueous phase was separated, the sample concentration was measured by either UV spectrophotometry or liquid chromatography as follows: In 0.10 M NaCl and at pH = 3, the sample concentration was measured by UV spectrophotometry using a calibration curve.

Since diphenylguanidinium ion has a large absorptivity, dilution of the sample solution was necessary. In 0.10 M TBABr and pH 3 or 11 (acid and base forms) concentrations were determined chromatographically on a column of XAD-2. Chromatographic peak areas were measured by a planimeter and the concentrations were found by comparing with a calibration curve. For the base form (pH = 11), which had a very low concentration, a precolumn was employed (see Section 3 - 1, Part I) in the following way: sample solution was injected onto the 5-cm XAD-2 column through an injection valve. The mobile phase was 20% methanol-aqueous solution which eluted the TBABr from the sample solution. After ten minutes, the diphenylguanidine base form was then eluted through the analytical column by changing the mobile phase to a 90% methanol-aqueous solution.

A chromatographic method, as opposed to the batch equilibration technique described above, was used to determine the distribution coefficient of DPG in 0.10 M NaCl at pH = 11. A known weight of XAD-2 was used as the stationary phase and the mobile phase was aqueous-methanol solution containing 0.10 M NaCl and adjusted to a pH reading of 11 by the addition of NH_4OH . Since the retention volume of diphenylguanidine was too large to be measured chromatographically when an aqueous mobile phase was used, a series of aqueous-methanol solutions were used as the mobile phases and a plot of $\log(\text{net retention volume})$ vs percent methanol yielded a straight line over the measurable range (50% to 70% methanol). Extrapolation of this line to 0% methanol yielded the net retention volume with aqueous mobile phase.

3.7 Solubility

The solubility of diphenylguanidine in aqueous 0.09 M NaCl - 0.01 M NaOH was determined by adding the solid to 50 ml of aqueous phase, shaking at $25 \pm 1^\circ \text{C}$ for 5 hours and 10 hours, and spectrophotometrically analyzing the filtrate for diphenylguanidine. Both equilibration times produced the same concentration. The solubility is 21.0 mg per 100 ml solution.

4. RESULTS AND DISCUSSION

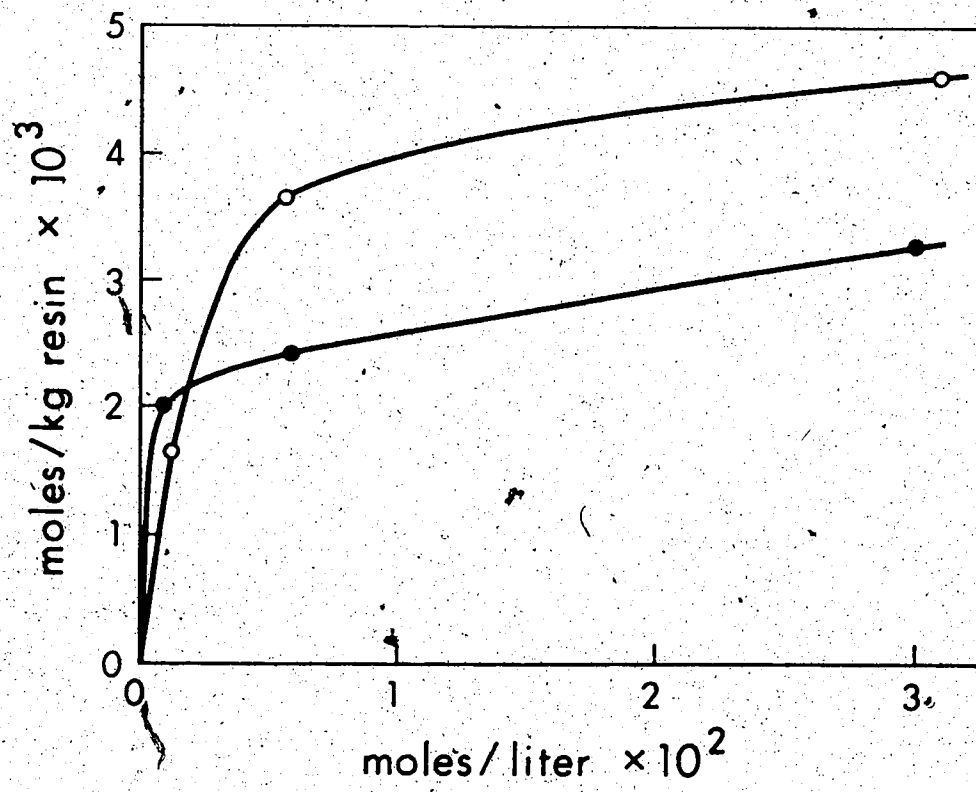
4.1 Sorption of H_3O^+ and OH^-

In spite of the fact that Amberlite XAD-2 is nominally a nonionic resin, an earlier study (17) suggests that it does possess some ion-exchange character. In Figure 10 are presented distribution isotherms for H_3O^+ and OH^- , from which it can be seen that the resin is capable of sorbing small amounts of both strong acid and strong base. This behavior is tentatively inferred to result from the presence in the resin of a relatively small number of acid-base functional groups. From the isotherms, it is evident that the resin will sorb less than 2×10^{-4} mmol of OH^- per gram at an aqueous phase pH of 10 or lower, and that it will sorb less than 1×10^{-3} mmol of H_3O^+ per gram at an aqueous phase of pH 4 or higher. Since the titrations of BH^+ and HA acids described later are performed with 0.5 mmol of sample acid in the presence of 5 g of XAD-2 resin, and the titration end points occur at pH values between 8 and 10, an end-point error of not more than 0.2% is expected from this source.

Figure 10. Distribution isotherms for H_3O^+ and OH^- between Amberlite XAD-2 resin and 0.10 M aqueous sodium chloride.

○ Hydrochloric Acid

● Sodium Hydroxide



4.2 Diphenylguanidine Hydrochloride

In order to test the validity of the proposed heterogeneous titration model, diphenylguanidine hydrochloride, which is a BH^+ type acid, was titrated in the presence and absence of XAD-2 resin. The resulting titration curves were compared to equation 11. Curve A in Figure 11 is the titration of diphenylguanidinium ion in the absence of resin. It is essentially identical whether the swamping electrolyte is sodium chloride, sodium bromide, or tetra-n-butylammonium bromide (TBABr). Its shape is understood as follows: the solid line for n_{OH} values below about 2.5×10^{-4} and the dashed line extending it are the curves predicted for an acid with $pK'_{a,BH} = 10.0$ which does not precipitate. However, during the actual titration the solution becomes supersaturated in diphenylguanidine base which suddenly precipitates at n_{OH} about 2.5×10^{-4} . The solid line at n_{OH} values higher than this is calculated on the assumption that $[B]$ is constant in the (saturated) solution (16). The poorer agreement between experimental points and the calculated line after precipitation is likely due to the slowness of the system to achieve saturation equilibrium.

The distribution coefficient of diphenylguanidine at $pH = 3$ (BH^+ form) in 0.10 M sodium chloride has been determined by batch equilibration. The result is shown in Table 15. The distribution isotherm (Figure 12, Curve A) is nonlinear, indicating that K_{BH} decreases markedly with an increase of BH^+ in the system. The consequence of this severe nonlinearity of the BH^+ distribution

Table 15

Distribution coefficient of diphenylguanidine HCl
(BH⁺) in 0.10 M sodium chloride and aqueous phase
pH = 3.

Concentration on XAD-2 resin (moles/kg)	Concentration in aqueous phase (moles/l)	K($\frac{\text{moles/kg}}{\text{moles/l}}$)
1.87×10^{-1}	1.10×10^{-2}	17
5.82×10^{-2}	4.91×10^{-4}	118
1.05×10^{-2}	1.60×10^{-5}	656

isotherm on the resultant titration curve is seen in Figure 11, Curve B. As the titration proceeds, the amount of the BH^+ species in the system decreases and its distribution coefficient K_{BH} therefore increases. The effect of this larger K_{BH} is to shift the titration curve to higher pH. Comparing Curve B with the hypothetical titration curves in Figure 1, it is evident that it shows considerably more upward curvature as the titration proceeds than would be found if K_{BH} were constant. As a result, the pH "break" at the end point is gradual.

In an attempt to reduce K_{BH} and, hopefully, make it independent of sample concentration the swamping electrolyte was changed from sodium chloride to tetra-n-butylammonium bromide (TBABr). Tetrabutylammonium is a large organic cation which, it was hoped, might adsorb on the XAD-2 and block the adsorption of diphenylguanidinium ion. (The mechanism of its action is discussed in Part II of this thesis). The isotherm obtained for BH^+ in the presence of 0.10 M TBABr is shown in Figure 12, Curve B (table 16). The value of K_{BH} is much smaller in the presence of the quaternary ammonium salt and, while not constant, varies much less with the amount of BH^+ in the system than is the case with sodium chloride swamping electrolyte. The value of K_B on the other hand is not significantly different in the presence of the two different swamping electrolytes. The distribution isotherm for species B in the presence of TBABr is shown to be linear with $K_B = 2.9 \times 10^4$ (Figure 13, Table 17). The experimental error in these data is about 10% because of the difficulty in measuring such low aqueous

Figure 11. Titration of diphenylguanidine hydrochloride with sodium hydroxide. Comparison of experimental with theoretical titration behavior. (Points are experimental. Solid lines calculated from Equation 11; see Appendix VII).

$K'_{a,BH} = 1.0 \times 10^{-10}$; $V = 0.050$ l; $n_{BH} = 4.97 \times 10^{-4}$ moles.

- A. Aqueous phase 0.10_0 M TBABr, $W = 0$;
- B. Aqueous phase 0.10_0 M NaCl, $W = 0.0050$ kg XAD-2;
- C. Aqueous phase 0.10_0 M TBABr, $K_B = 2.9 \times 10^4$,
 $K_{BH} =$ (varies, see text). $W = 0.0055$ kg XAD-2.

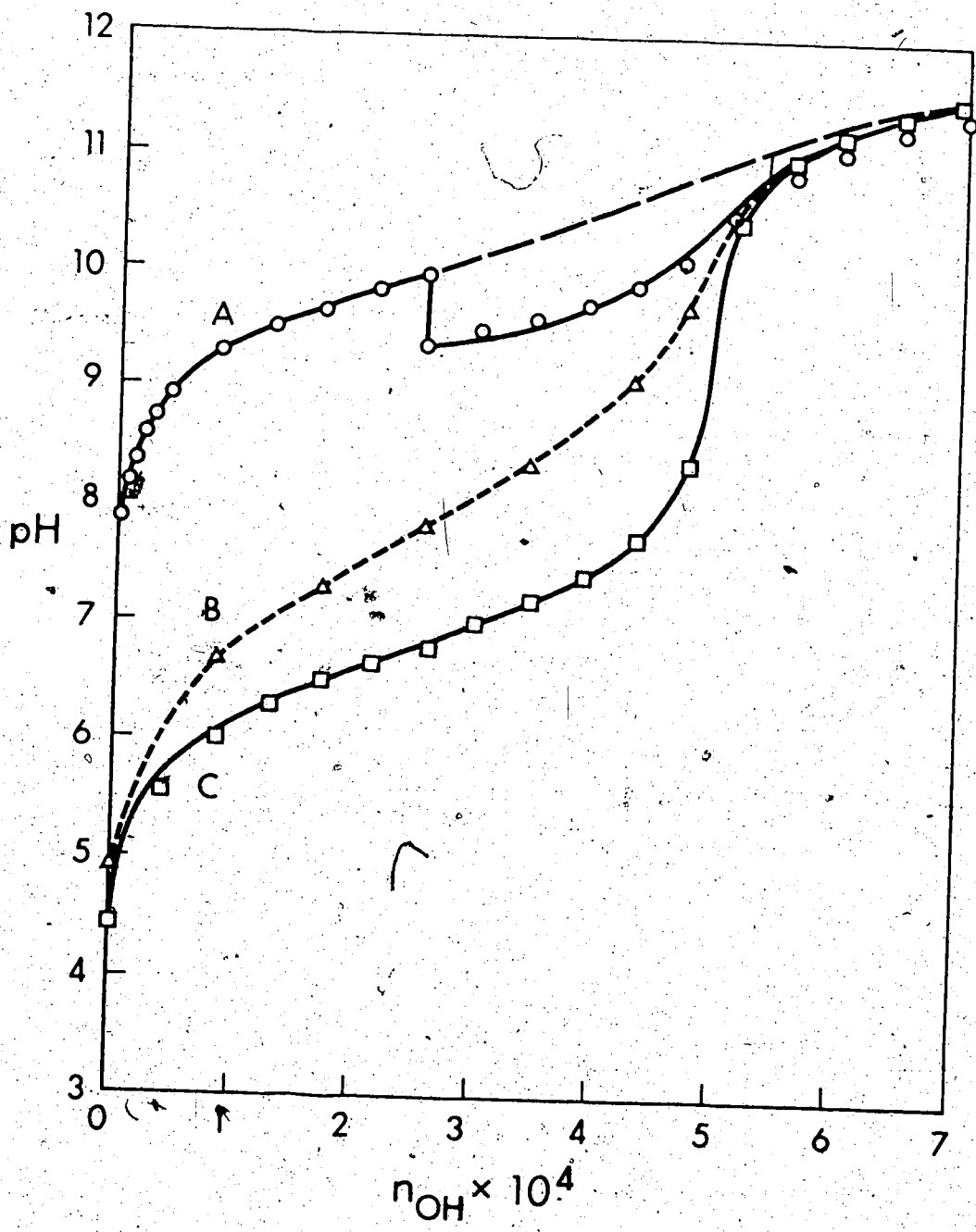


Table 16

Distribution coefficients of diphenylguanidine·HCl
in 0.10 M TBABr and aqueous phase pH = 3

Concentration on XAD-2 resin (moles/kg)	Concentration in aqueous solution (moles/l)	K ($\frac{\text{moles/kg}}{\text{moles/l}}$)
4.19×10^{-2}	6.10×10^{-3}	6.8
2.23×10^{-2}	2.55×10^{-3}	8.7
1.06×10^{-2}	9.90×10^{-3}	10.7
5.38×10^{-3}	4.92×10^{-4}	10.7

Figure 12. Distribution isotherm for diphenylguanidine·HCl between Amberlite XAD-2 and aqueous electrolytes

- A. Aqueous phase, 0.10 M Sodium Chloride, pH = 3
- B. Aqueous phase, 0.10 M TBABr, pH = 3

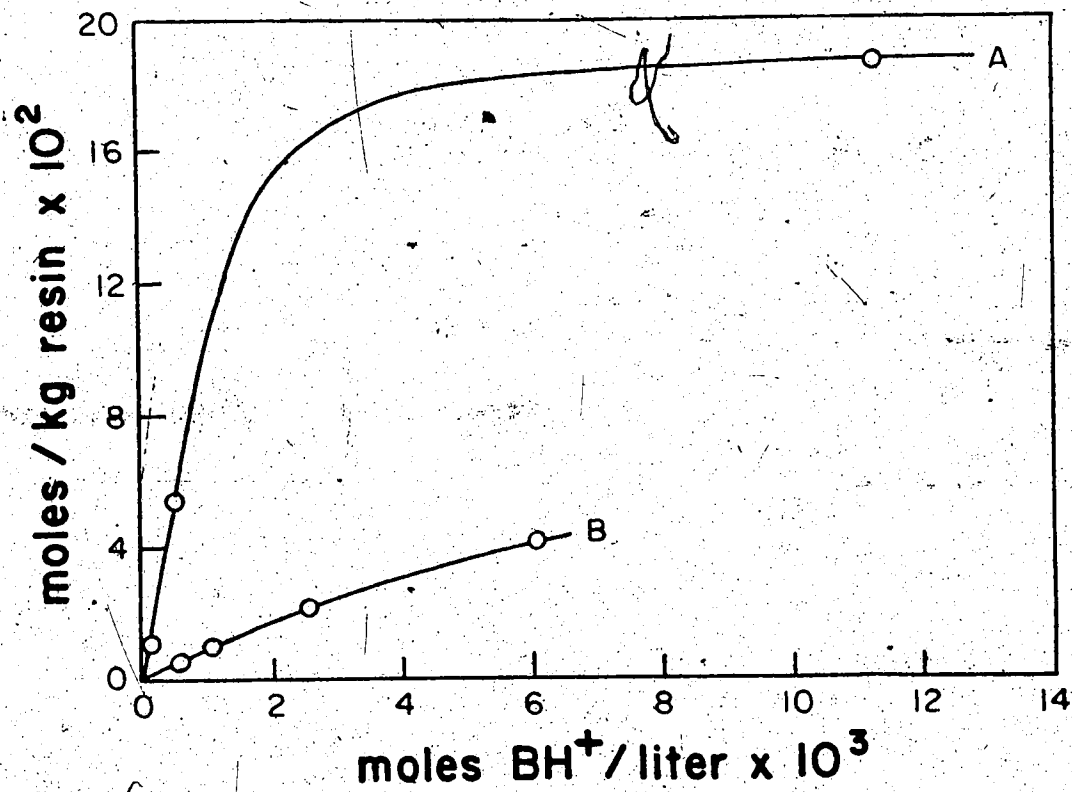


Figure 13. Distribution isotherm for diphenylguanidine between Amberlite XAD-2 resin and 0.10 M TBABr aqueous phase at pH = 11.0.

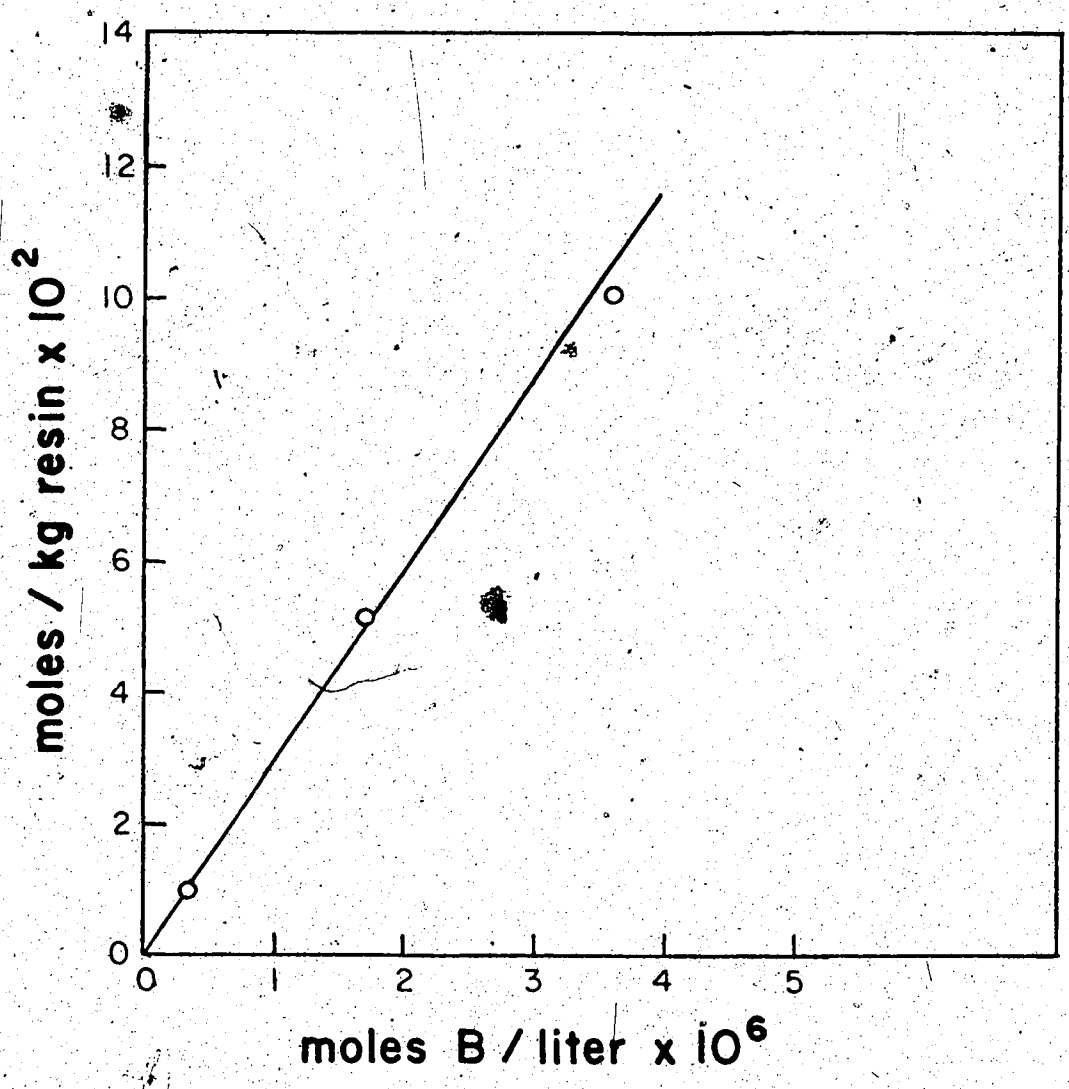


Table 17
Distribution coefficients of diphenylguanidine
base in 0.10 M TBABr and aqueous phase pH = 11

Concentration on XAD-2 resin (moles/kg)	Concentration in aqueous solution (moles/l)	K ($\frac{\text{moles/kg}}{\text{moles/l}}$)
0.0099	3.60×10^{-7}	2.75×10^4
0.0517	1.70×10^{-6}	3.13×10^4
0.101	3.60×10^{-6}	2.82×10^4

Average: 2.90×10^4

phase concentrations of diphenylguanidine. The value of K_B in the sodium chloride swamping electrolyte was obtained by the extrapolated chromatographic procedure as follows: The distribution coefficient K_B is related to the chromatographic retention volume V_R and void volume V_M by the expression:

$$V_R - V_M = K_B \cdot W \quad (34)$$

where W is the weight of resin in the column. K_B can be found if $(V_R - V_M)$ and W are known. By this method, K_B values were determined in 70%, 60% and 50% methanol-aqueous solution (with 0.10 M NaCl) and extrapolated to 0% methanol-aqueous solution. Table 18 shows the results for $(V_R - V_M)$ and K_B at different methanol concentrations. Figure 14 is a plot of $\log K_B$ vs % methanol; on extrapolation to 0% methanol a K_B of 4.0×10^4 is obtained. This value must be assumed to have an uncertainty of about one hundred percent as a result of the long extrapolation. Linearity of plots of $\log K$ vs % methanol has previously been found for such compounds as the alkyl esters of p-hydroxybenzoic acid, vanillin, and a number of drugs (17,18). The heterogeneous titration curve obtained in 0.10 M TBABr is presented in Figure 11, Curve C. The points are experimentally measured and the solid line is calculated from equation 11. Curve C is shifted to lower pH values than Curve B and does not exhibit undesirable curvature in the proton-binding region. The end-point pH break is now sharp and occurs at the theoretical end point. In the presence of XAD-2 resin, the weak acid diphenyl-

Table 18

Determination of K_B of diphenylguanidine base (chromatographic method) using different percentages of methanol in the mobile phase (pH = 11)

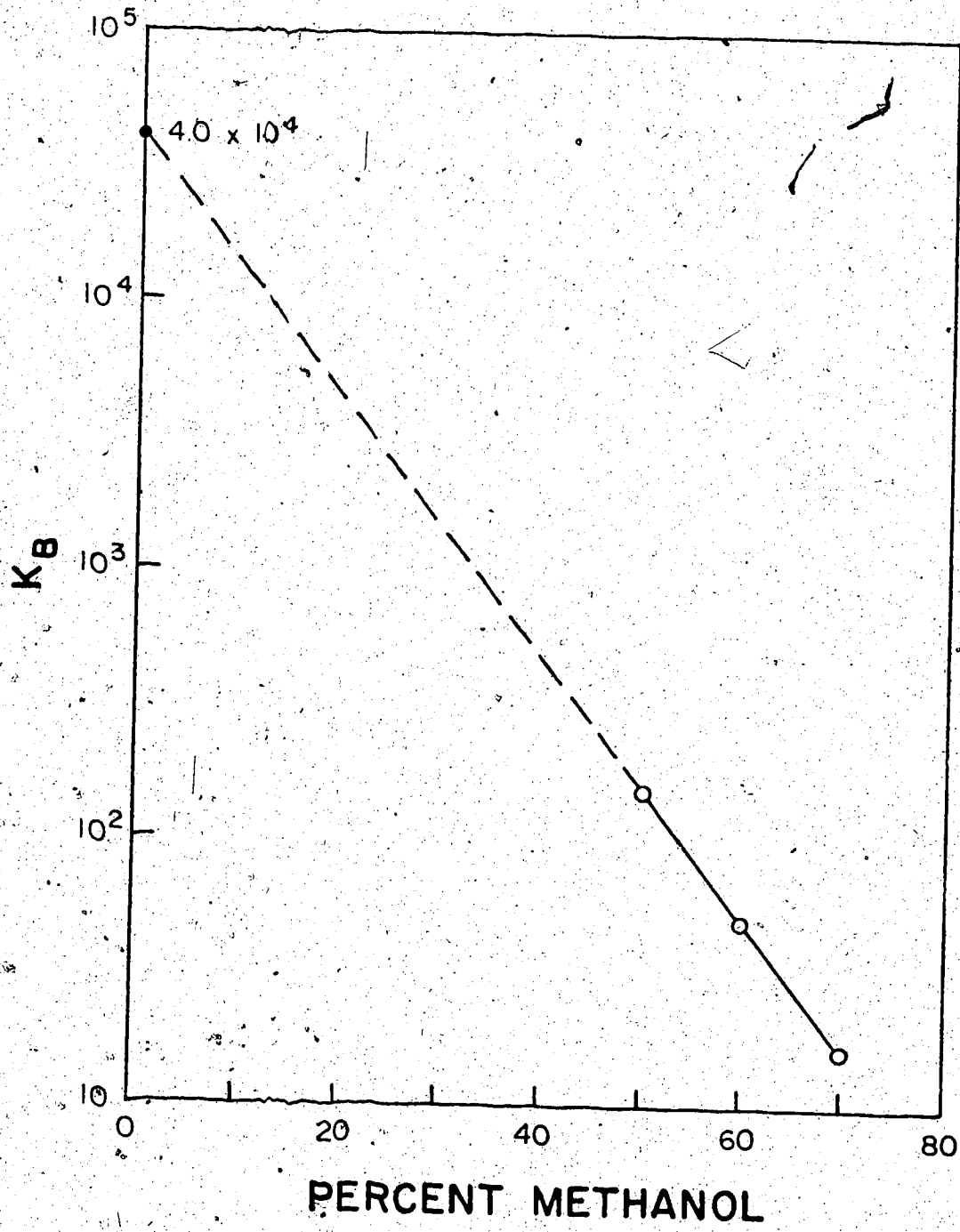
$(V_R - V_M)^a$ ml	percent methanol	K_B^b
1.50	70	16
4.99	60	51
13.50	50	150

a V_M , the void volume, is 0.34 ml.

b Weight of the resin in the column is 0.09 gm.

guanidinium ($pK'_{a,BH} = 10.0$) titrates as though it had a pK_a of about 6.8. The calculation of curve C is shown in Appendix VII.

Figure 14. Distribution coefficient of diphenylguanidine
base form in 0.10 M NaCl and 10^{-3} M NaOH.



4.3 Diphenylguanidine Hydrochloride: Effect of Concentration of TBABr on the Titration

The titration of diphenylguanidine hydrochloride was performed at various TBABr concentrations. In all of the titrations, the total bromide concentration was kept constant by adding the proper amount of sodium bromide (except in the 0.50 M TBABr, to which no sodium bromide was added). The effect of variation in concentration of TBABr can be best illustrated by comparing the pH difference at the half neutralization point. In the absence of the resin, the titration curves were essentially the same at all TBABr concentrations, but the titration curves in the presence of resin were affected to different degrees (Table 19; Figure 15). The influence of TBABr is marked at concentrations between 0.0 M and 0.05 M. From 0.05 M to 0.10 M the effect gradually diminishes, and it shows a reverse effect if the concentration of TBABr was made as high as 0.5 M. This may partly be accounted for by the fact that the ionic strength of the aqueous solution has been increased five fold. The increase of the ionic strength would change the proportionality between surface-potential; concentration of TBABr and concentration of diphenylguanidinium ion (see Part II).

Figure 15. Dependence of $\Delta pH_{1/2}$ for diphenylguanidinium ion on concentration of tetra-n-butylammonium bromide.

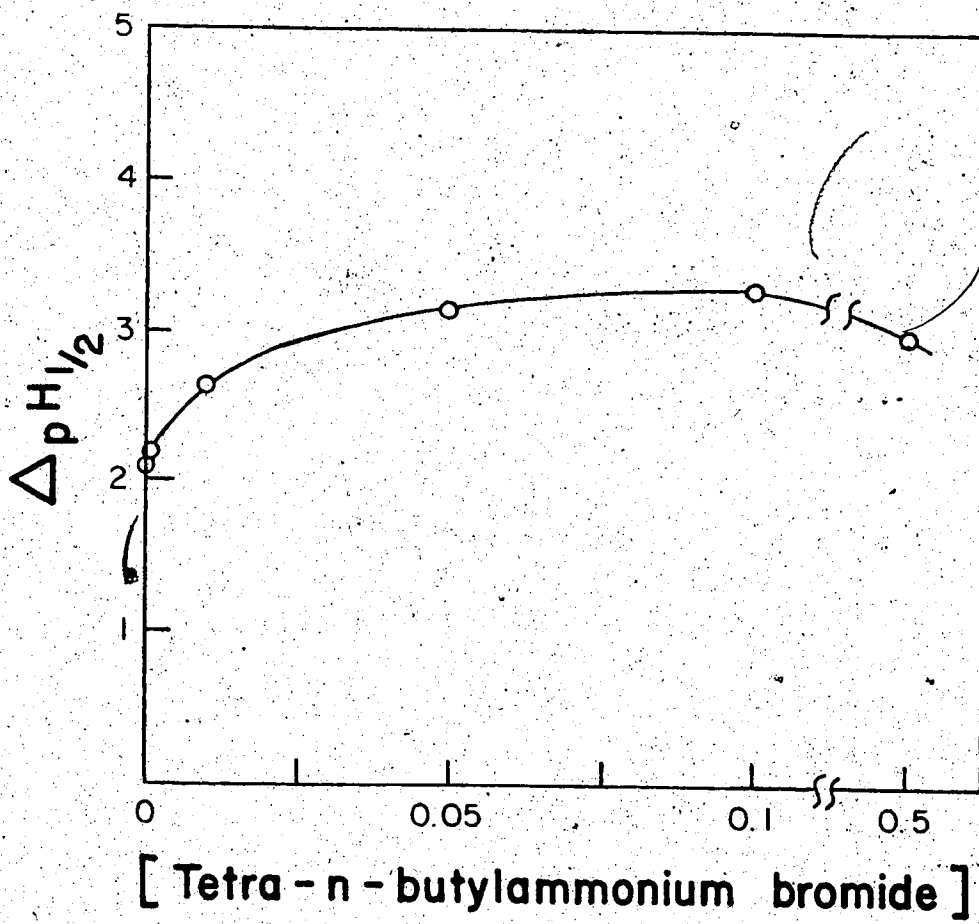


Table 19

Dependence of $\Delta\text{pH}_{1/2}$ for diphenylguanidinium ion on concentration of tetra-n-butylammonium bromide

M TBABr	M·Br ^{-a}	$\Delta\text{pH}_{1/2}^b$
0	0.10	2.1 ₀
0.0010	0.10	2.1 ₇
0.010	0.10	2.6 ₅
0.050	0.10	3.1 ₅
0.10	0.10	3.3 ₀
0.50	0.50	3.0 ₀

a Total bromide concentration maintained at 0.10 M, for all but the last entry, by addition of sodium bromide.

b $\Delta\text{pH}_{1/2} = \text{pH}_{1/2}(\text{NR}) - \text{pH}_{1/2}(\text{R})$, where $\text{pH}_{1/2}$ is the half-neutralization point pH value in the titration of diphenylguanidine hydrochloride with sodium hydroxide.

4.4 Diphenylguanidine Hydrochloride: Effect of Various Quaternary Ammonium Ions

Beside tetra-n-butylammonium bromide (TBABr), tetramethylammonium bromide (TMABr) and tetraethylammonium bromide (TEABr) were also used as the swamping electrolyte in the heterogeneous titration of diphenylguanidinium ion (Table 20). For 0.10 M TMABr, the effect on $pH_{1/2}$ was similar to that of sodium chloride. The same concentration of TEABr increases $\Delta pH_{1/2}$ by an additional 0.70 units, while TBABr has the greatest effect. The differences in effect of the three quaternary ions arise as follows: the larger the quaternary ion the more strongly it is adsorbed. Thus at 0.10 M aqueous concentration the surface concentration of quaternary ion used increases in the order $TMA^+ < TEA^+ < TBA^+$. The electrical potential of the surface would increase in the same order and, consequently, the repression of adsorption of diphenylguanidinium ion would increase in the same sequence (see Part II).

Table 20

Dependence of $\Delta\text{pH}_{1/2}$ for diphenylguanidinium ion on different quaternary ammonium bromides (0.10 M)

Salt used	Concentration of the salt used, M	$\Delta\text{pH}_{1/2}$ ^a
NaBr	0.10	2.1 ₀
TMABr	0.10	2.1 ₂
TEABr	0.10	2.8 ₂
TBABr	0.10	3.1 ₅

^a $\Delta\text{pH}_{1/2}$ defined in Table 19.

4.5 Benzylammonium Chloride

Benzylammonium chloride is a BH^+ type acid. The titration of this compound was performed in 0.10 M sodium bromide. Both the 200 - 325 mesh and < 325 mesh sizes of XAD-2 resin were used. There was no difference in the titration curves obtained, although equilibration was more rapid with the smaller particles. Benzylamine-free base is a moderately polar molecule, so that this compound is not strongly sorbed by the nonionic resin. Distribution coefficients K_B and K_{BH} were determined in 0.10 M sodium bromide (Table 21).

Experimental titration curves are shown in Figure 16. Curve A was obtained in the absence of XAD-2 resin and curve B was obtained with resin present. The value of ΔpH in the proton binding region is predicted from equation 13 to be 1.59. The observed value varies between 1.66 at 10% titrated and 1.35 at 80% titrated. The value of K_{BH} was small enough in this case that it was not necessary to add TBABr in order to produce a distinct end point pH break.

Benzylammonium chloride has a K_a of 3.18×10^{-10} (19). Titrated in aqueous phase alone it will not give a distinct end point break. In the presence of resin, the end point can be more easily located as 5.33×10^{-4} moles. The amount actually present was 5.29×10^{-4} moles. The error in the titration is thus about 1%.

Table 21

Distribution coefficients of benzylamine/
benzylammonium ion from batch equilibration

Species	NaBr Con- centration M	Weight of XAD-2 used (g)	Aqueous volumes (ml)	Distribution coefficient
BH ⁺ ^a	0.10	5.04	56.16	7.0 ^b
B ^c	0.10	5.17	50.00	650 ^d

a. benzylammonium ion

b. After equilibrium, aqueous phase concentration was 2.38×10^{-3} M,
resin phase concentration was 1.62×10^{-2} M.

c. benzylamine.

d. After equilibrium, aqueous phase concentration was 5.88×10^{-5} M,
resin phase concentration was 3.82×10^{-2} M.



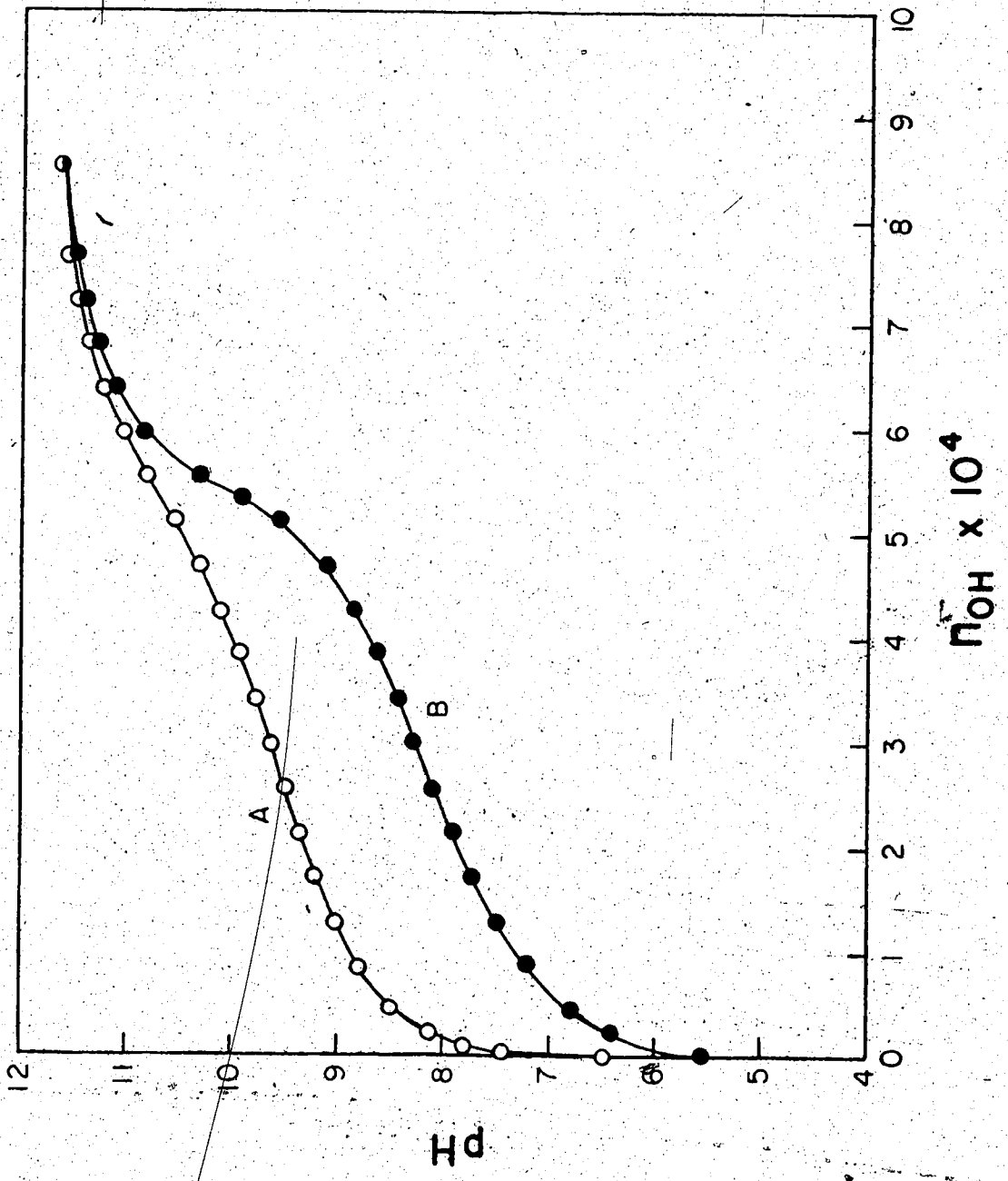


Figure 16. Experimental titration curves of benzylamine hydrochloride with sodium hydroxide in 50 ml of 0.10 M sodium bromide in the presence (○) and absence (●) of 5.0-g of Amberlite XAD-2 resin.

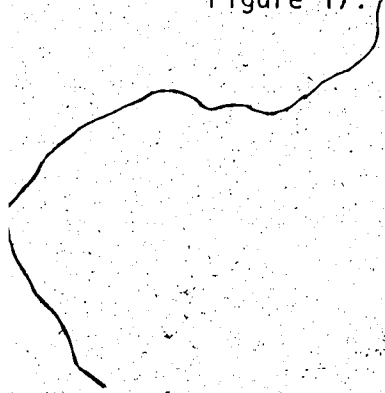


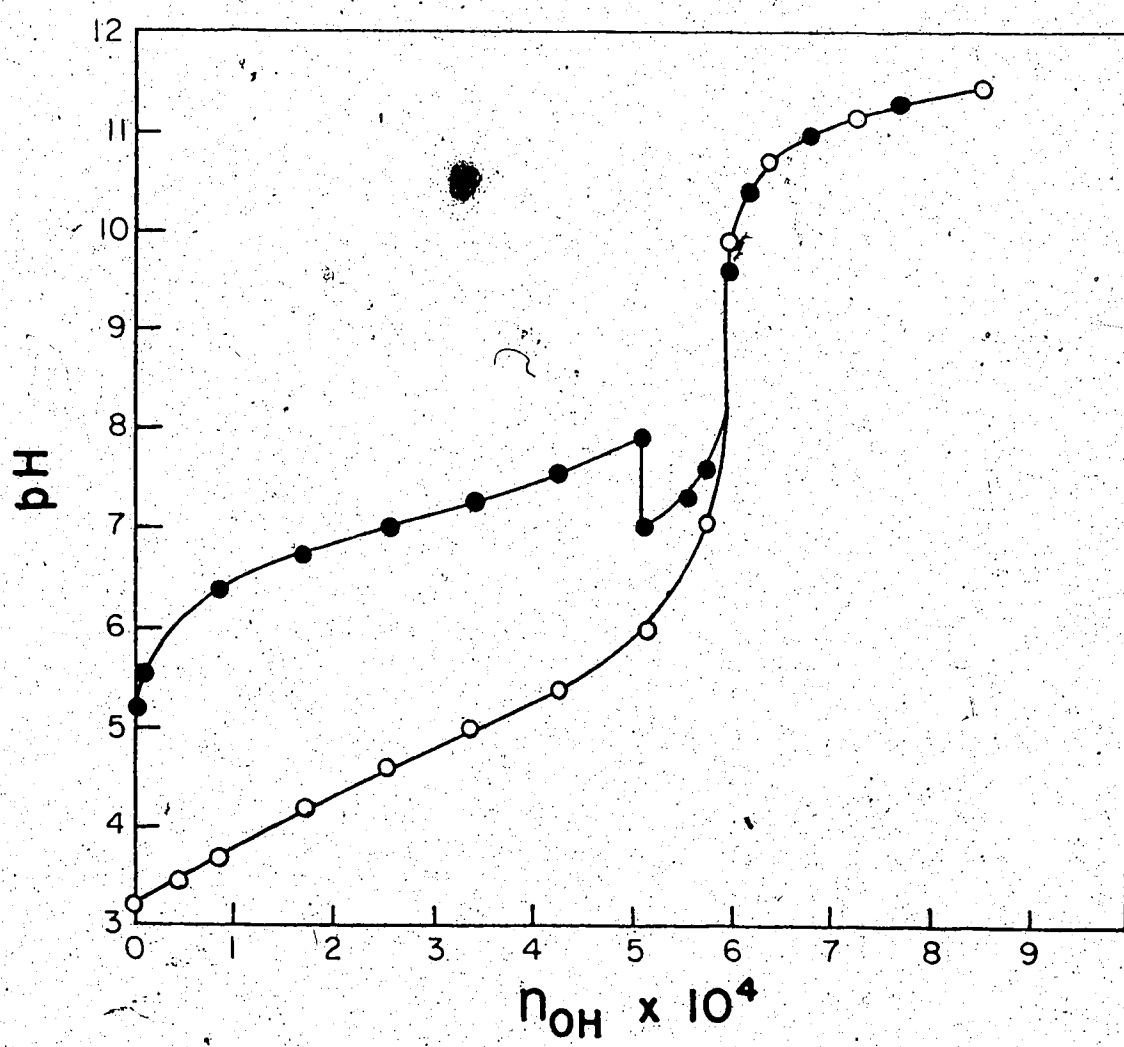
4.6 Molindone Hydrochloride

Molindone hydrochloride is another example of a BH^+ type acid. It has a pK_a of 7.13 (20). Figure 17 shows the titration of this acid in the absence and presence of XAD-2 resin. The swamping electrolyte used in this titration was TBABr. During the titration, free base was produced. After about 5×10^{-4} moles of NaOH was added, the (supersaturated) free base suddenly precipitated out. In the presence of the resin, the proton binding region was shifted down about 2.5 pH units. This suggests a strong interaction existing between the base form and the nonionic resin. The theoretical end point was 5.960×10^{-4} moles and the observed value was 5.960×10^{-4} moles.

Figure 17.

Experimental titration curves of molindone hydrochloride with sodium hydroxide in 50 ml of 0.10 M TBABr in the presence (o) and absence (●) of 5.0 g of Amberlite XAD-2 resin.

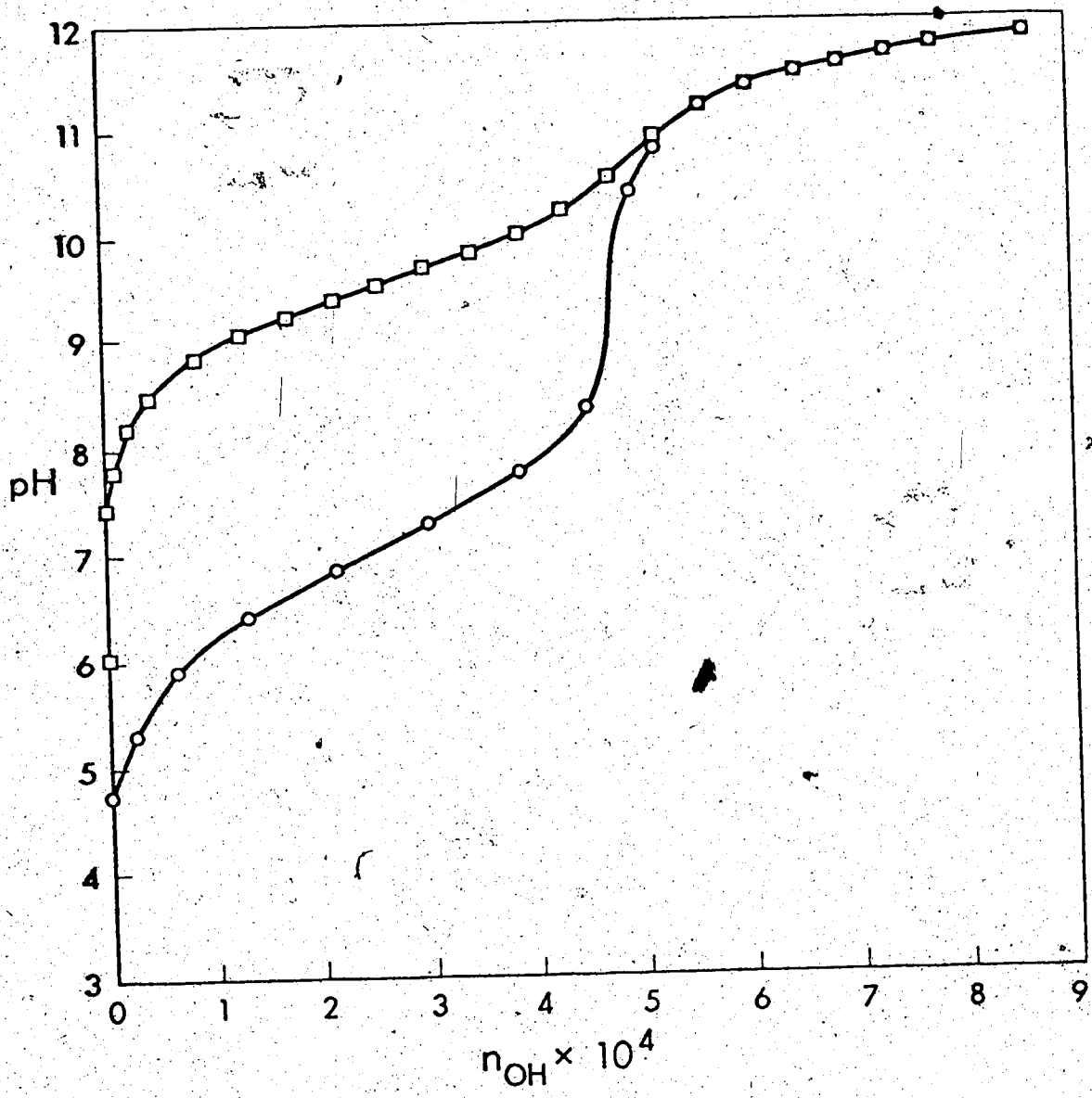




4.7 Dextromethorphan Hydrobromide

The titration curves of dextromethorphanium ion are shown in Figure 18. While the curve obtained in the absence of resin shows only a slight end point break, the curve obtained in the presence of resin exhibits a distinct end point break. This titration was performed in a 30% methanol - aqueous solution because the product of the titration in water was an oily precipitate which seriously reduced the rate of equilibration. The addition of methanol kept the free base dissolved. This compound, which has a pK_a of 8.30 (21), behaved as if it had a pK_a of 6.90. The theoretical end point was 4.78×10^{-4} moles while 4.75×10^{-4} was taken from the titration curve.

Figure 18. Experimental titration curves of dextromethorphan hydrobromide with sodium hydroxide in 50 ml of 0.10 M TBABr - 30 percent methanol in the presence (o) and absence (□) of 2.5 g of Amberlite XAD-2 resin.



4.8 m-Nitrophenol.

All the previous titrations involved a BH^+ type acid. In these titrations, BH^+ behaved as though it were a stronger acid, since the product B was strongly adsorbed on XAD-2 resin. m-Nitrophenol, which is an HA type acid, exhibits the opposite effect. m-Nitrophenol has a pK_a of 8.4 (22). Titrating it in the presence of XAD-2 is equivalent to titrating an acid with a pK_a of 9.70 (Figure 19). Distribution coefficients of K_{HA} and K_A at one concentration are listed in Table 22. The ΔpH in the proton binding region predicted by equation 14 is -1.47. The observed value is -1.49 at the half neutralization point. This agreement again supports the validity of the heterogeneous titration model. The addition of quaternary ammonium salts (Q^+X^-) should be avoided when titrating acids of the HA charge type since the "ion pair" Q^+X^- , formed with the conjugate base A^- , is strongly sorbed by the resin.




Figure 19. Experimental titration curves of m-nitrophenol with sodium hydroxide in 50 ml of 0.10 M sodium bromide in the presence (o) and absence (□) of 5.0 g of Amberlite XAD-2 resin. (Used 2.26×10^{-4} mole.)

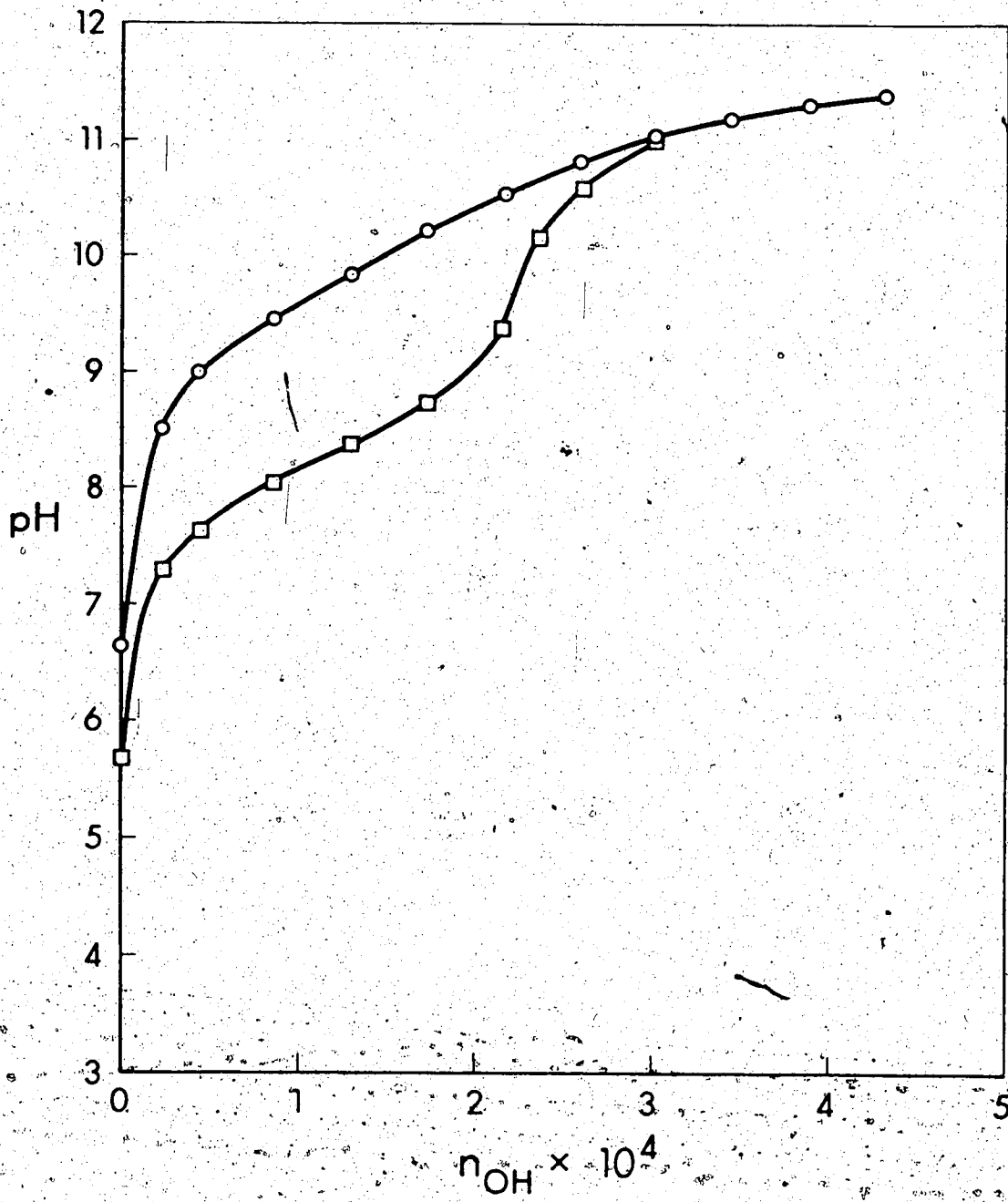


Table 22

Batch analysis data for obtaining the distribution coefficients of m-nitrophenol / m-nitrophenolate

Species	NaBr Concentration, M	Weight of XAD-2 used (g)	Aqueous volumes (ml)	Distribution coefficient
HA ^a	0.10	4.95	53.94	4.8
A ^{-b}	0.10	5.02	56.65	430.

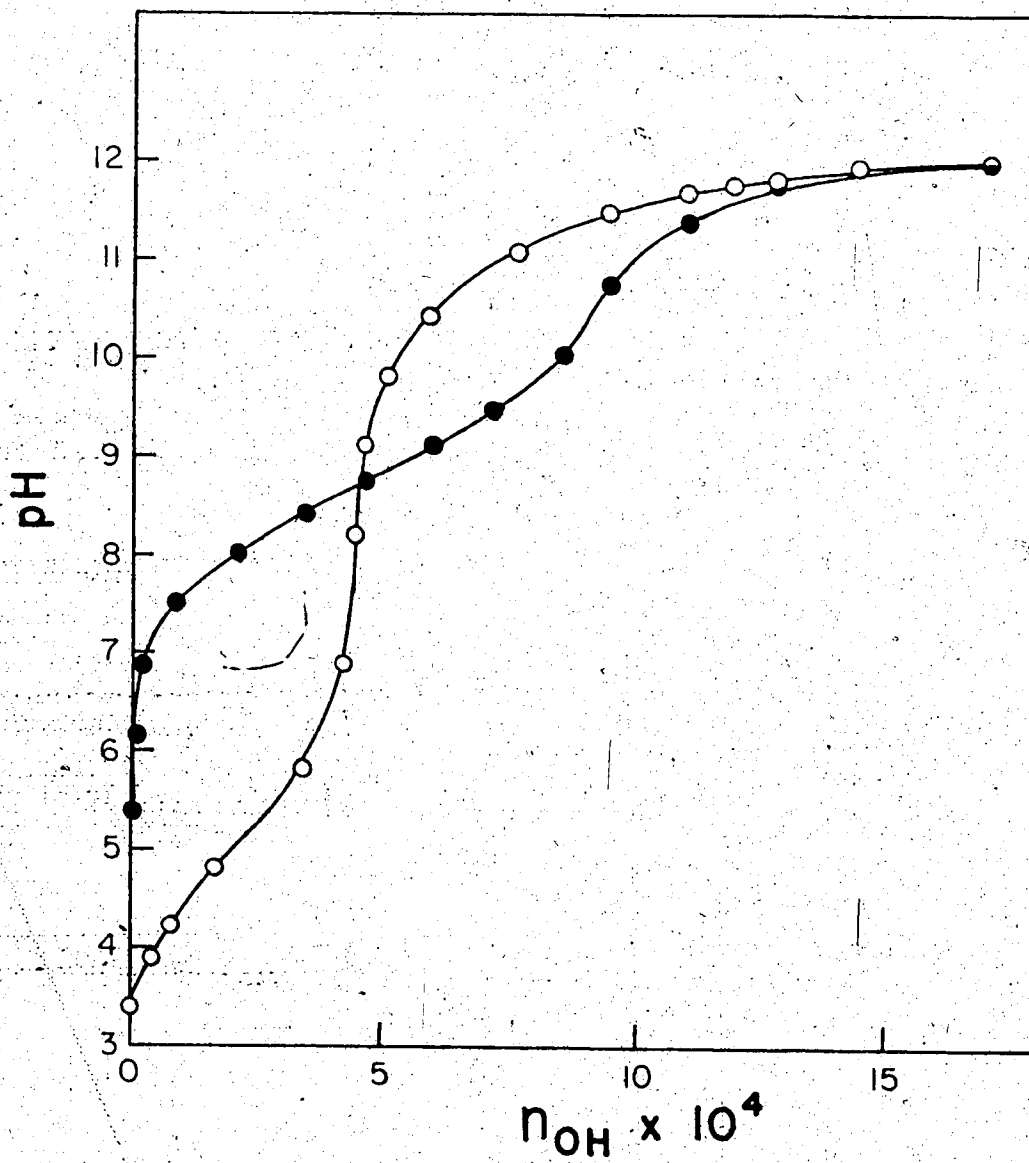
a. m-nitrophenol

b. m-nitrophenolate

4.9 Naloxone Hydrochloride

Naloxone hydrochloride is an AH_2^+ type acid with $pK_{a1} = 7.9$ and $pK_{a2} = 9.1$ (20). If titrated in aqueous solution with NaOH only the second end point is observed (Figure 20). If XAD-2 resin is added, the first end point is enhanced but the second point is weakened since the distribution coefficient K_{HA} is expected to be much greater than K_{AH_2} and K_A (see Figure 3). The theoretical first end point for the titration in Figure 20 is 4.538×10^{-4} moles; the value found was 4.50×10^{-4} moles for the first end point in the presence of resin.

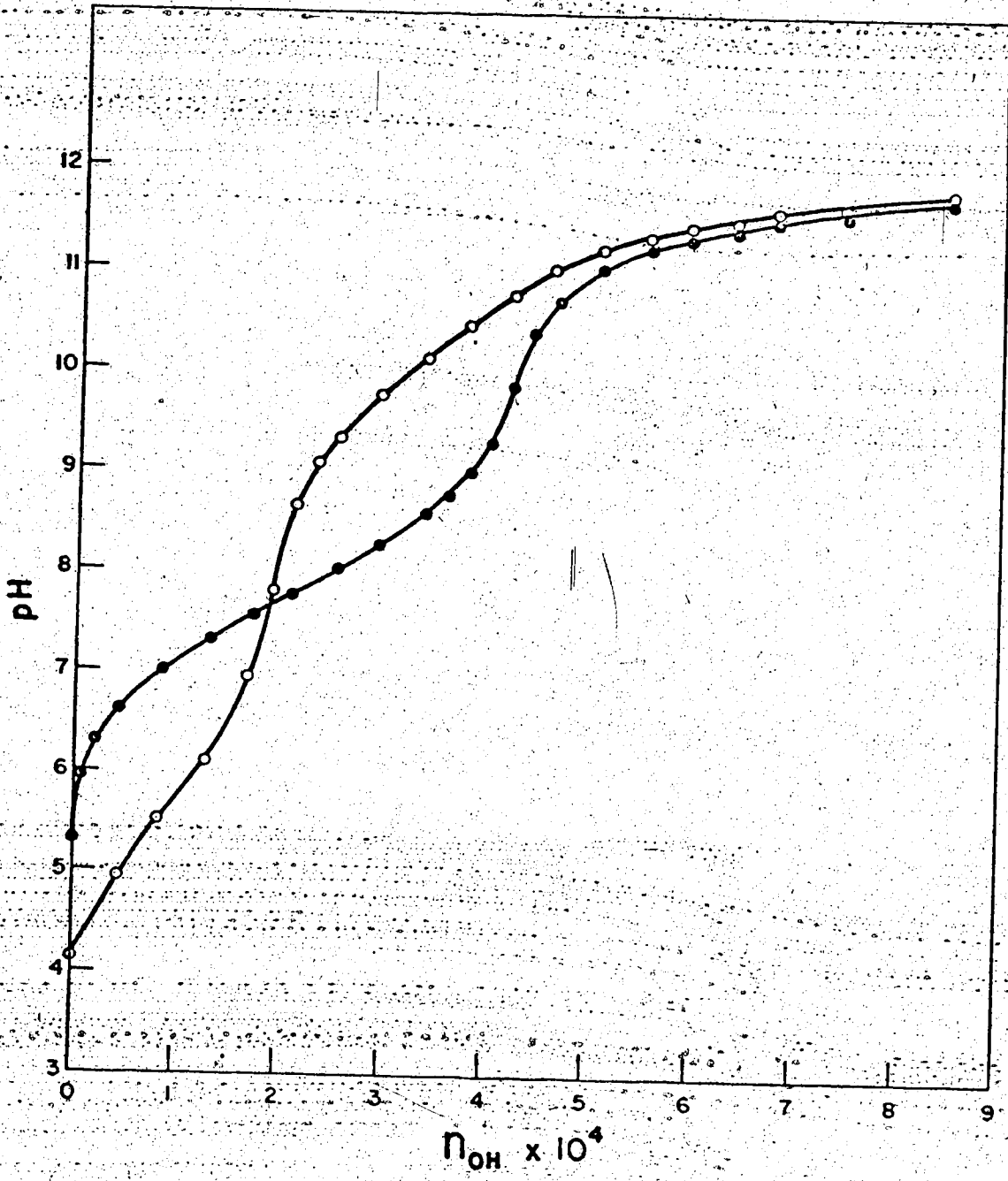
Figure 20. Experimental titration curves of naloxone hydrochloride with sodium hydroxide in 50 ml of 0.10 M sodium bromide in the presence (o) and absence (●) of 5.0 g of Amberlite XAD-2 resin.



4.10 Mixture of Molidone Hydrochloride and m-Nitrophenol

The titration of molidone hydrochloride and m-nitrophenol as individual acids was shown in the previous sections. In the absence of XAD-2 resin a mixture of the two exhibits only the second end point (Figure 21). This second end point corresponds to the total number of moles present in the solution. In the presence of XAD-2 resin BH^+ is titrated as a stronger acid and HA as a weaker acid so that the first end point break is enhanced while the second end point break is weakened. Figure 21 gives the result of this titration. The pK_a values of molidone hydrochloride and m-nitrophenol are 7.3 (20) and 8.4 (22) respectively. In the presence of the resin, they appear to have pK_a values of 5.8 and 9.9. Theoretical first and second end points are at 1.96×10^{-4} and 4.20×10^{-4} moles. Experimental findings from the two end points yield 1.94×10^{-4} (resin present) and 4.20×10^{-4} moles (resin absent).

Figure 21. Experimental titration curves of a mixture of molidone hydrochloride and m-nitrophenol with sodium hydroxide in 50 ml of 0.10 M sodium bromide in the presence (o) and absence (●) of 5.0 g of Amberlite XAD-2 resin.



5. CONCLUSION

Heterogeneous titrations in the presence of Amberlite XAD-2 resin permit the accurate determination of acids of the BH^+ charge type which are too weak to be titrated in a homogeneous aqueous solution. Such titrations show promise as an alternative to nonaqueous titrations. The opposite sign of the pH shift (ΔpH) of HA and BH^+ charge-type acids makes possible differentiating titrations of acids with similar strength but different charge-type. It also allows the possibility of detecting the first end point in the titration of an AH_2^+ type of acid. The principal limitation to the method is the relatively long equilibration times required after the addition of each increment of titrant. This time can be reduced, however, by the use of smaller particle size and more efficient stirring.

This work has revealed the sorption of ions on Amberlite XAD-2 resin. The detailed mechanisms of this sorption and its significance for liquid chromatography are presented in the second part of the thesis.

6. FURTHER WORK

a. Theoretical titration curves of AH_2^+ type acids in the presence of XAD-2 (or any other kind of nonionic second phase) have been derived. Qualitatively, the results agree with the experimental titration of naloxone hydrochloride. No quantitative evaluation was attempted. More work can be done on the quantitative aspects, which need a knowledge of distribution coefficients determined by batch equilibration methods.

b. The titration work can be extended to zwitterions such as amino acids. Naloxone hydrochloride is probably not a zwitterion, though the microscopic constants have not been reported.

c. The presence of a second phase in the titration is not limited to potentiometric titrations. It could also be used in photometric and amperometric titrations, to mention two.

d. Heterogeneous potentiometric titrations in the presence of XAD-2 resins can be performed routinely. It is a useful method for the titration of a BH^+ type weak acid and acid mixtures in water. The development of an autotitrator system can be an immediate study. It would be desirable, in this connection, to increase the rate of attainment of equilibrium.

PART II. STUDIES OF ADSORPTION MECHANISM
OF IONIC SPECIES ON AMBERLITE
XAD-2 RESIN

1. INTRODUCTION

Amberlite XAD-2 resin is one of a series of synthetic polymers developed by Rohm and Haas Co., Philadelphia, Pa. (Amberlite is a registered trade name of the Rohm and Haas Co.) Methods of synthesis involve the suspension polymerization of styrene-divinylbenzene copolymers in the presence of a substance that is good solvent for the monomer but a poor swelling agent for the polymer (23, 24, 25, 26, 27). Unlike conventional homogeneous gels, this kind of resin has a rigid macroporous structure, with large surface area and large pore size. Amberlite XAD-2 is a hydrophobic adsorbent. Its use for organic compounds has been studied by several workers (28,29). Basically, adsorption of a sample molecule or ion increases as the length of hydrocarbon residue increases, as the number of hydrocarbon substituents increases or as the number of aromatic rings increases.

XAD-2 resin has been used widely in biological studies. Most workers use this kind of resin to remove and/or concentrate a compound from an aqueous sample. The sorbed compound is later washed off. Compounds that have been studied in this way include: steroid conjugates (30,31,34,35,38), corrinoids (32,33), steroids (36,37,39,40) and benzoyl ecognine (41) from urine. The use of XAD-2 resin from the extraction of pharmaceutical compounds include: barbiturates in urine (42,43), morphine in aqueous solution (44),

or from urine (45,46,47) and narcotic analgesics (48,49,50,51,52,53). The possible clinical use of XAD-2 in detoxification was also investigated: an XAD-2 packed column was used in hemoperfusion to remove phenobarbital from blood (54,55). A disposable resin column of XAD-2 was reported for use in urine screening for abused drugs and excreted steroids (56). Reviews on the use of XAD-2 in biological studies have been given by different groups. Brusse et al. (57) gave a rather detailed review with 91 references. Fujimoto et al. (58) described the pharmacological procedures with 31 references. Stolman and Pranita (59) had a review of XAD-2 in pharmaceutical analysis and forensic chemistry with 14 references.

In the last decade, XAD-2 has been increasing its role in environmental analysis. Its usage is also based on its strong adsorptive ability towards the many organic compounds which are regarded as pollutants. It has been used in the following: water treatment (60), reducing the concentration of nitrobenzenes in aqueous effluent (61), removing chlorinated hydrocarbons and phenols from waste waters (62), adsorbing chlorinated pesticides from river water (63), removing alkali lignin from kraft waste water at low pH (64), concentrating DDT and its metabolites, dieldrin and polychlorobiphenyls in water (65,66,67,68), removal of phenolic waste from water (69), recovery of volatile organic compounds from municipal sewage (70), removing oil from water (71), trapping 2,4-D and its derivatives from air (72,73), recovering fenitrothion from environmental waste water (74), and removing colored agents from waste kraft water (75,76,77). In a recent work, Junk et al.

(78) discussed the use of a mini-column packed with XAD-2 or acylated resins to adsorb the organic compounds from water samples. Besides use in environmental studies, XAD-2 is used in the sugar industry to remove colored impurities (79,80,81). A few compounds have also been purified either by retaining the desired compound on the resin or by removing the impurities. Examples are 3,6-bis-(5-chloro-2-piperidinyl)-2,5-piperazinedione (82), pentaerythritol (83) and H_2O_2 (84). When 8-hydroxyquinoline (oxine) solutions of ^{60}Co , ^{59}Fe , ^{144}Ce , ^{95}Zr and ^{106}Ru are passed through the resin the metal-oxine neutral compounds are adsorbed (85). Iron(III) is adsorbed onto the resin by forming a complex with 1,10-phenanthroline (85).

Jyo et. al. (86) constructed an anion-selective electrode by chloromethylation and quaternization of the XAD-2 resin. It has also been used as a chelating liquid ion-exchanger in extraction chromatography (87); as a thin-layer chromatographic support (88); impregnated with β -diphenylglyoxime as adsorptive reagent for Pt, Pd and Ni (89); nitrated, reduced and then diazotized and coupled with Na_2AsO_3 to give phenylarsonic acid resins which were used to concentrate and separate trace metals in the ppb range from demineralized, tap and sea water (90).

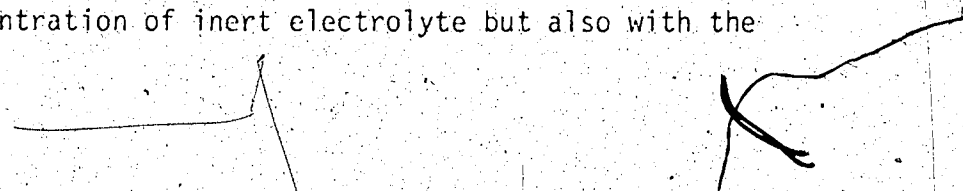
In recent years, XAD-2, due to its physical durability, low cost and useful pH range (78), has been used as a packing material for liquid chromatography (LC). Fritz and Willis (91) described the use of a gas pressure pump to force the liquid solvent through an XAD-2 column. Their work dealt with the separation

of phenols. Cantwell (17) used it to analyze p-hydroxybenzoates in complex pharmaceuticals. Cantwell and coworkers also used the XAD-2 column to analyze various pharmaceutical compounds (18,92). Use of XAD-2 in LC has been investigated by Pietrzyk and Chu (93,94,95) who have used it to separate various organic bases (93), anilines, substituted benzenes, phenols, benzoic acids, sulfonic acids and phenoxyacetic acids (94,95). More recently, Cantwell discussed its future role in reversed-phase hplc (96). Recent work of Pietrzyk et. al. involved studies on the effect of solute ionization on chromatographic retention on XAD-2 HPLC (97), and extended the theory to the separation and retention of amino acids, peptides and derivatives (98).

Although the use of XAD-2 resin is wide spread, studies directed towards an understanding of the mechanism of adsorption are rather limited. Seidl and Krska (99) studied the sorption of phenol and p-nitrophenol on XAD-2. They found that the adsorption is reversible and may be fitted to Freundlich isotherms. They also suggested that the phenol molecule is adsorbed in a horizontal orientation to the surface. Fritz (100) suggested that the nonpolar XAD-2 would retain nonpolar compounds best and that the sorption ability would increase with larger surface area of the sample molecule. Mantouri and Riley (101) studied the sorption of humic acid and fulvic acid on XAD-2 and found that the adsorption of humic acid fitted to the Langmuir isotherm; they also found that the adsorption increased with increased ionic strength. O'Conner (102) discussed the adsorption of organic acids at low pH where

their ionization was suppressed. In a review paper, Gustafson and Paleos (103) described the role of variables such as the chemical structure, surface area of the adsorbent, the concentration of the adsorbate, ionic strength and temperature. Generally speaking, the adsorption increases as the length of a hydrocarbon increases or as the number of the aromatic ring increases.

XAD-2 resin not only adsorbs nonionic species, it also adsorbs ionic species. Grieser's work (104), showed the effect of electrolyte concentration on the sorption of several compounds by XAD-2. The neutral form of the weak acids is highly sorbed and the anion is sorbed to a small extent. Gustafson et. al. (28) reported that the distribution coefficients of aliphatic and aromatic sulfonates increase with increasing concentration of sodium chloride and suggested that this effect might arise if the ions from the added salt distribute themselves in such a way as to minimize the electrostatic repulsions of neighboring adsorbed sulfonate anions. Sulfonate, benzoate and phthalate were chromatographically separated, and retention volumes were also found to increase with increasing concentration of sodium chloride in the mobile phase (105,106). More recent studies (94,95) have confirmed this electrolyte effect and have led to the suggestion that ion-pairing might account for the increased retention. But as will be seen below, the present investigation strongly supports an alternative mechanism. Retention volumes of cationic conjugate acids of pharmaceutical amines have been shown to vary not only with the concentration of inert electrolyte but also with the



nature of the electrolyte (18). For example, the cationic conjugate acid of phenylephrine is more strongly retained on XAD-2 in 0.1 M sodium perchlorate than 0.1 M sodium chloride. Lundgren and Schilt (107) have reported the same phenomenon in their study of the retention of the divalent cationic complex tris-3-(2-pyridyl)-5,6-diphenyl-1,2,4-triazine iron(II) on XAD-2. They suggest that this electrolyte effect may arise from partial charge neutralization of the adsorbed complex metal cations by the anions of the inert salt, promoting stronger retention by decreasing mutual electrostatic repulsion between adsorbed cations.

Up to now, no mechanistic model has been proposed to account for the adsorption of ions on Amberlite XAD-2 and no experimental studies directed to this end have been reported. Using a nonpolar stationary phase in LC to separate ionic compounds is not new. For example, "ion-pair" chromatography is a liquid-liquid partition technique in which the stationary phase is usually an aqueous solution containing a dissolved salt, one of the ions of which forms extractable ion pairs with oppositely charged ions in the sample; the mobile phase is a water-immiscible organic solvent. Sample solute is injected as an ion pair dissolved in the mobile phase. Eksborg and Schill (108) used an aqueous solution of a quaternary ammonium salt on an ethanolized cellulose as a stationary phase to separate carboxylic acids. The anions of the acids form ion pairs with the quaternary ammonium and migrate in that form with the mobile phase. Persson and Karger (109) used the same technique to separate amino compounds and amino acids as

perchlorate ion pairs and carboxylic acids as ion pairs with tetrabutylammonium ions. They found that this L-L partition chromatography has a lower efficiency than LSC (liquid-solid chromatography). Similar work was done by Santi et al. (110) who separated hyoscyamine, scopolamine and ergotamine as picrate ion pairs.

A different technique termed "Reversed-phase ion pair chromatography" has become popular in recent years. The column packing in this technique may be a reversed-phase bonded packing while the mobile phase contains a small amount of a salt which has the ability of forming ion-pairs with the sample species. (This complexing agent is called "hetaeron" or "detergent" by different people.) This detergent may form ion pairs which are sorbed on the bonded phase. Wittmer et al. (111) used this technique to analyze the anionic dye tartrazine and its intermediates, with quaternary or tertiary ammonium salt in the mobile phase for ion pairing. Knox and Laird (112) used this method to separate a wide range of sulphonic acids and derived dye stuffs. The detergent used is cetyltrimethyl ammonium bromide. They call this technique "soap chromatography". Knox and Jurand (113) did separations of catecholamines and their metabolites by LSC, ion-pair chromatography and soap chromatography. They found that soap chromatography has the best column efficiency. In this study, they suggested that the behavior of ions in soap chromatography is similar to ion exchange. In a communication from Kissinger (114), he also suggested that the ion

pair is formed on the surface rather than in the mobile phase and then is extracted. He suggests that the organic salt added to the mobile phase is modifying the stationary phase and the process of 1:1 ion pair partition is insignificant. Later work by Horvath et al. (117) suggests that ion pair formation does occur in the mobile phase and is followed by sorption of this neutral ion pair to the stationary phase.

Horvath et al. have proposed that the sorption of ions on reversed-phase bonded packings can be accounted for by solvophobic (Hydrophobic, if the mobile phase is water) interactions (115,116,117,118). Between the hydrocarbonaceous stationary phase and the hydrophobic moiety of the solute molecule. The hydrophobic effect has been derived by considering different free energies associated with the solute-stationary phase, eluent-solute and eluent-stationary phase interactions. After each of the free energy terms has been evaluated, the retention, or the capacity factor of an ionized solute can be represented as a function of ionic strength. Qualitatively, the increase of the salt concentration would have two effects: First, it decreases ionic activity coefficients in the mobile phase which tends to decrease the retention time of the sample ion; second, and more important, the increasing ionic strength increases the surface tension of the mobile phase which leads to an increase in retention time because of stronger hydrophobic interaction. Over a wider range of ionic strength, the capacity factor will show a

minimum near 0.3. This model apparently does not apply to Amberlite XAD-2 resin, since plots of adjusted retention volume on XAD-2 versus ionic strength do not show this minimum. (Compare Figure 4 in reference 18 with Figure 11 in reference 116) There is, perhaps, no strong reason to expect that the sorption mechanisms on Octadecylsilica (ODS)-bonded phases and XAD-2 would be the same. The former might be considered to possess a surface whose properties are between those of a liquid and solid, while XAD-2, at least in water, possesses a true adsorbent surface so that sorption from water onto XAD-2 is correctly viewed as solid-liquid adsorption.

In the present study two different experimental techniques have been used to elucidate the adsorption mechanism: (i) Adsorption isotherms for two organic cations were measured in the presence of different concentrations of inert electrolyte either by batch equilibrium or by a liquid chromatographic method. Values obtained from the isotherms were then compared with those predicted by the Stern-Gouy-Chapman (SGC) model of the electrical double layer; (ii) Microelectrophoresis measurements were made on individual resin particles suspended in solutions of an adsorbable cation and the observed zeta potentials were compared to those predicted by the SGC model. The results from both types of experiments suggest that adsorption of ions onto Amberlite XAD-2 can be explained in terms of the Stern-Gouy-Chapman model.

2. PROPOSED MODEL

2.1 Stern-Gouy-Chapman Model

The theory of the electric double layer deals with the distribution of counterions and coions in the locality of a charged surface, and with the magnitude of the electric potentials which occur in this region. When a surface is charged, counterions are electrostatically attracted by the oppositely charged surface. At the same time, however, these ions have a tendency to diffuse away from the surface toward the bulk of the solution, where their concentration is low. The simplest quantitative approach to this diffuse part of the double layer was proposed by Gouy (119) and Chapman (120). Their treatment is based on a flat surface with uniform distributed (smeared out) charge. Ions in the diffuse part of the double layer are assumed to be points distributed according to Boltzmann distribution. A single symmetrical electrolyte of valence z is assumed. Later, Stern (121) modified the Gouy-Chapman theory by proposing a model in which the double layer is divided into two parts separated by a plane (the Stern plane) located at about a hydrated ion radius from the surface. Stern also considered the possibility of specific ion adsorption. The Stern modified Gouy-Chapman model is called the Stern-Gouy-Chapman (SGC) model. A more sophisticated model than that of Stern was proposed by Grahame (122), who made a distinction between the plane through the centers of unhydrated counter ions at closest approach to the

surface (Inner Helmholtz Plane, IHP) and the limit of the diffuse layer or the position of closest approach of hydrated counterions and coions (Outer Helmholtz Plane, OHP).

The SGC model of the electrical double layer at a charged interface has been reviewed in many places (122,123,124,125,126), and a concise summary may be found in Shaw's book (127). The modification of the SGC theory proposed by Grahame is used in the present discussion except that the adsorbed "potential-determining ions" are considered to be part of the surface rather than part of the compact double layer. This formalism is more consistent with the usage of colloid chemistry (125,128) than of electrochemistry (122), although for the system under investigation both formalisms should lead to the same quantitative conclusions.

Since Amberlite XAD-2 has a non-ionogenic and electrically non-polarizable surface it acquires a surface charge by the adsorption of ions from solution. These ions are attached to the XAD-2 particles by van der Waal's forces (see section 4.1 below). The adsorbed ions are shown in Figure 22 as diphenylguanidinium cations (DPGH^+) which will be used as an example throughout the present discussion. The adsorbed ions are referred to as "potential-determining ions" and are responsible for the electrical potential difference, Ψ_0 , between the surface and the bulk solution (the potential of the bulk solution is defined as zero). The bulk solution is a region in the solution sufficiently far away from the charged surface that electroneutrality prevails throughout it, even on a microscopic scale. The relationship between activity of potential-determining

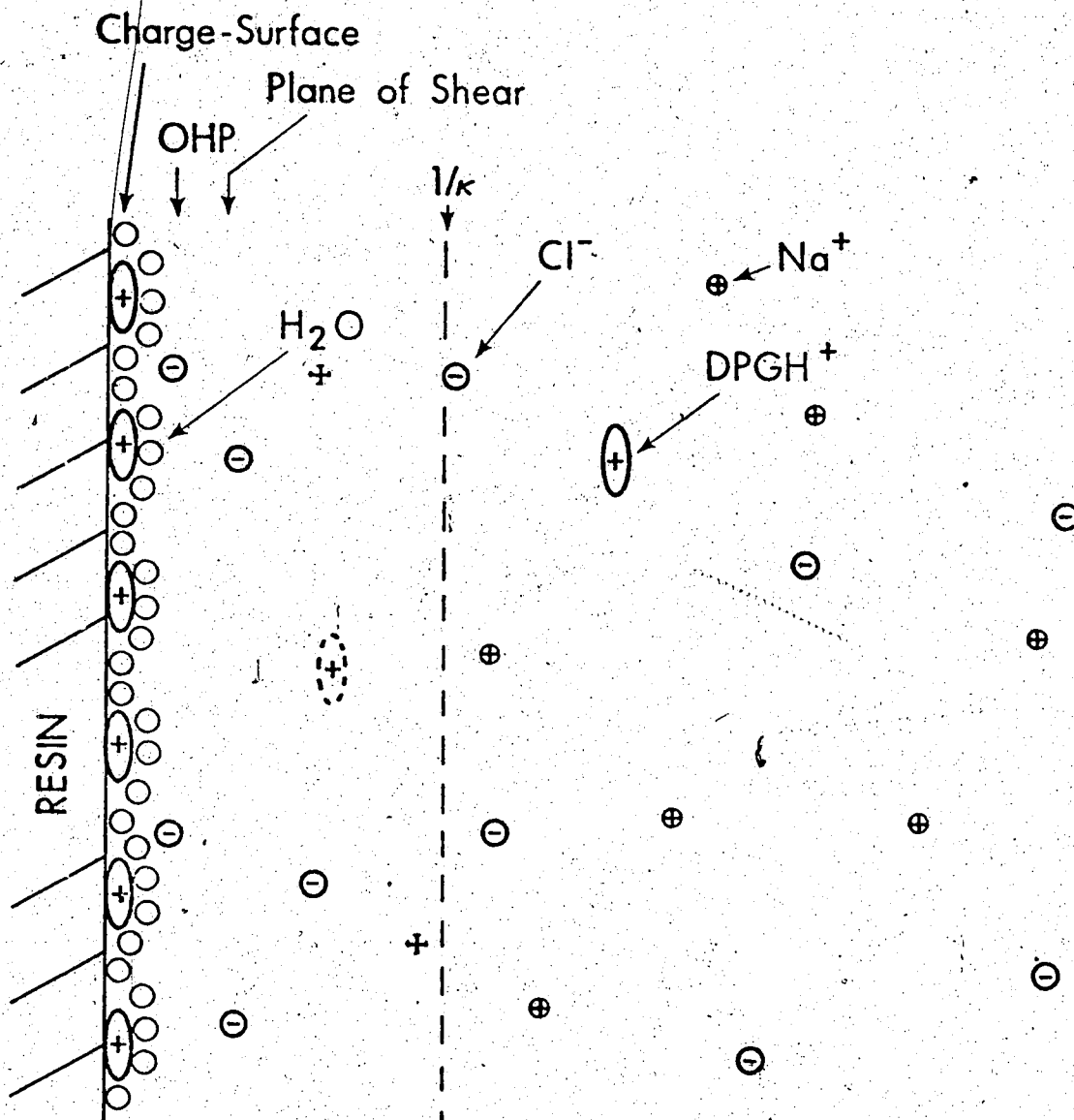
ions in the bulk solution, a_{DPGH} , and the surface potential in volts is often described by a Nernst equation (123,124,125).

$$\Psi_0 = k + \frac{RT}{ZF} \ln a_{DPGH} \quad (35)$$

where R is the ideal gas constant (8.314 coulomb-volt/mole°K); F is the Faraday constant (96,487 coulomb/equivalent); T is the absolute temperature; Z is the valence of the potential-determining ion (equivalent/mole) with appropriate sign; and k is a constant. Equation 35 is often found to apply when the surface coverage is well below a monolayer and it defines the "completely reversible electrode". In the present treatment it is not necessary that equation 35 be valid, but only that, regardless of their functional relationship, Ψ_0 is a constant at constant a_{DPGH} .

The region between the XAD-2 surface and the bulk solution is described by the SGC theory as follows: As a first approximation, the charges of the adsorbed potential-determining ions are viewed as smeared out on the resin surface, with the plane passing through them identified as the "charge-surface" (Figure 22). The surface charge density, σ_0 , is given in units of coulombs per cm^2 . In the absence of any other charged species the potential would decay linearly with distance, from a value of Ψ_0 at the charge surface to zero in the bulk solution. However, there are necessarily other ions present in solution, and counterions, such as chloride ions in the present example, which are of opposite sign to the potential-determining ions, are electrostatically attracted toward the charge

Figure 22. Schematic view of the interfacial region between Amberlite XAD-2 resin and aqueous electrolyte solution containing sodium chloride and diphenyl guanidinium chloride. Six DPGH^+ cations are adsorbed on the resin. Cations shown in dashed outline represent Na^+ and DPGH^+ that have been expelled from the double layer region.



surface so that their concentration near the surface is greater than in the bulk solution. At the same time, coions, such as sodium and DPGH^+ , which are of like sign, are repelled from the surface and their concentration near the surface is lower than in the bulk solution (dashed circles in Figure 22). The "surface excess", Γ_j , of any ion j_{\pm} is the number of moles of the species j_{\pm} contained on one cm^2 of surface and in its adjoining double layer in the solution, which are in excess of the moles of the same species contained in an equivalent volume of bulk solution containing the same total moles of charge of all species as there are in the one cm^2 of interface under consideration (128). The units of Γ_j are moles per cm^2 . An important distinction is that σ_0 , the surface charge density of DPGH^+ , includes only the moles of adsorbed potential-determining ion, while Γ_{DPGH} includes also the moles of DPGH^+ expelled from the adjoining double layer region (The expelled coion, by their absence from the double layer, are equivalent to an excess of oppositely charged counterion present in the double layer).

Because the hydrated counterions and coions have a finite size they cannot approach the charge surface any closer than about a hydrated radius. This plane of closest approach of counterions in the double layer is the Outer Helmholtz Plane (OHP) (122). The water molecules shown in Figure 22 between the charge surface and the OHP are intended merely to indicate the presence of water of hydration, and do not necessarily imply that it is only one molecule thick. It is possible for counterions to be "specifically

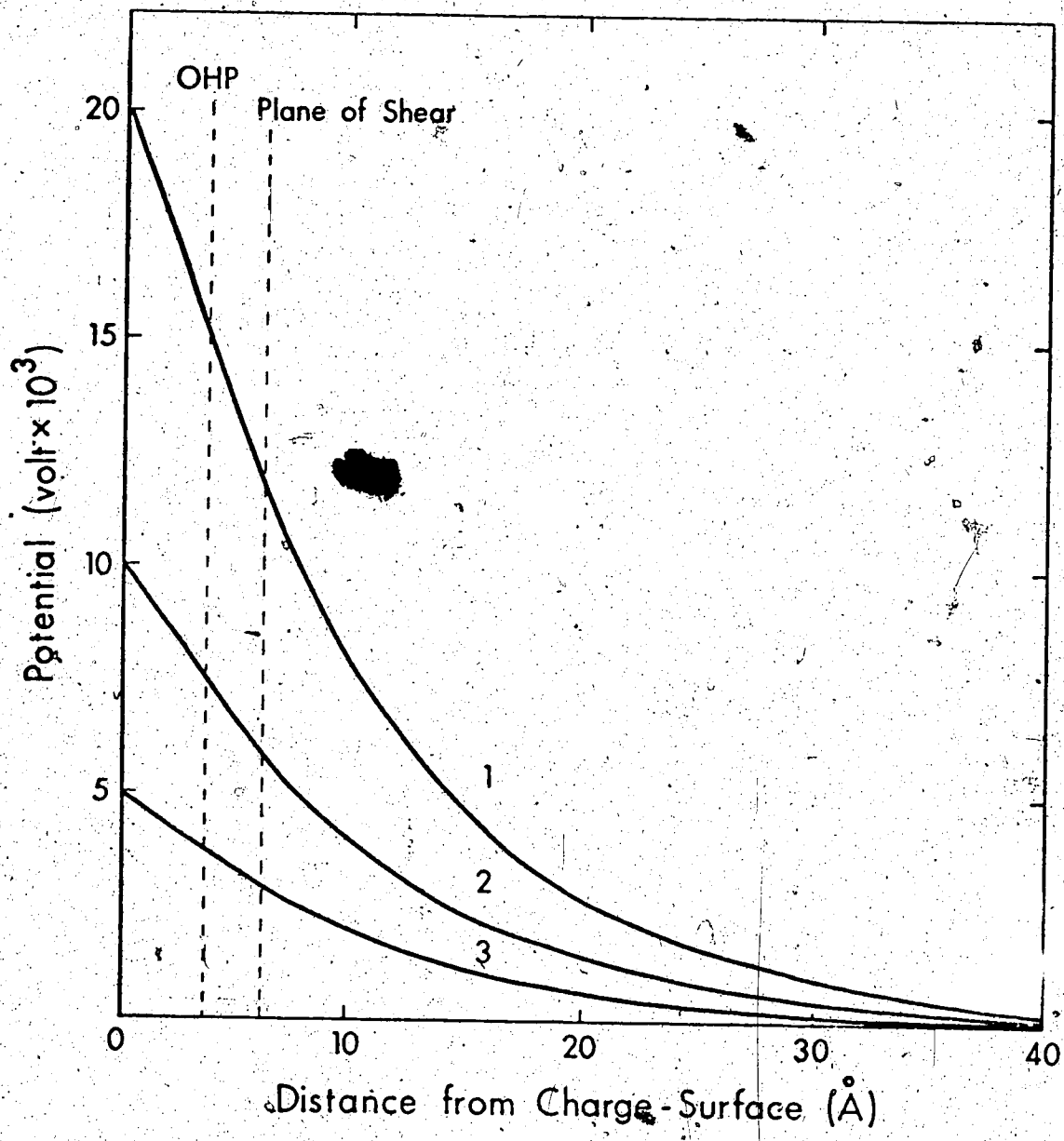
adsorbed" to the charge surface, with all or most of the hydrate water molecules being absent between the charge surface and the specifically adsorbed counterion. Such a layer would be called the "Inner Helmholtz Layer" or "Stern Plane" (122,123). However, in the present case the experimental data are inconsistent with specific adsorption, and therefore the OHP is considered to be the plane of closest approach of counterions.

Two regions are now distinguishable in the double layer. The first, lying between the charge surface and OHP, is called the "compact part" of the double layer and in it the potential decays linearly (Figure 23). The second region lies between the OHP and bulk solution and is called the "diffuse part" of the double layer. Here the potential decays not linearly, but nearly exponentially because the excess counterion charge nearer the OHP screens the ions farther away toward the bulk solution, causing the potential to decay more rapidly. The sum of the excess charges in the OHP and diffuse part of the double layer must be equal but opposite in sign to the surface charge in order that electro-neutrality be maintained.

If the activity of the potential-determining ion, DPGH^+ , in the bulk solution were reduced at constant ionic strength some DPGH^+ would desorb from the resin in order to re-establish electrochemical equilibrium. The net effect would be a decrease in Ψ_0 (Equation 35) and in surface charge density, σ_0 (Figure 23).

Now consider the effect of increasing the ionic strength in bulk solution by adding more inert electrolyte such as sodium

Figure 23. Dependence of the electrical potential in the double layer on distance from the charge surface for a fixed total concentration of univalent electrolyte in the bulk solution ($c = 0.10 \text{ M}$) and varying surface potential. $C_1 = 2.00 \times 10^{-4} \text{ farad/cm}^2$; $\Psi_0 = 20 \times 10^{-3} \text{ volt}$ (curve 1), $10 \times 10^{-3} \text{ volt}$ (curve 2), $5 \times 10^{-3} \text{ volt}$ (curve 3).



chloride while at the same time maintaining the activity of DPGH^+ constant in bulk solution. Since ψ_0 is constant and the electrolyte concentration has been increased, this leads to a corresponding and proportional increase of counterions attracted into the double layer and coions repelled from it. In order to maintain electro-neutrality in the double layer the number of DPGH^+ ions adsorbed must increase (larger σ_0). A second consequence of increased ionic strength is a compression of the diffuse part of the double layer (Figure 24). This occurs because the increased counterion concentration in the diffuse part of the double layer closer to the OHP provides an increased screening effect for ions farther out in the diffuse layer. The potential therefore decays faster.

The compact and diffuse parts of the double layer are usually treated as two parallel plate capacitors in series, and discussion of this idea requires that the above qualitative description of the double layer be expressed mathematically. The compact part of the double layer obviously has some analogy with a capacitor, with the charge surface constituting one "plate" and the OHP the other. The capacitance of the compact part of the double layer, C_1 , is given as:

$$C_1 = \frac{\sigma_0}{\psi_0 - \psi_{\text{OHP}}} \quad (36)$$

In the absence of specific adsorption C_1 is, nearly constant independent of electrolyte concentration (126,127).


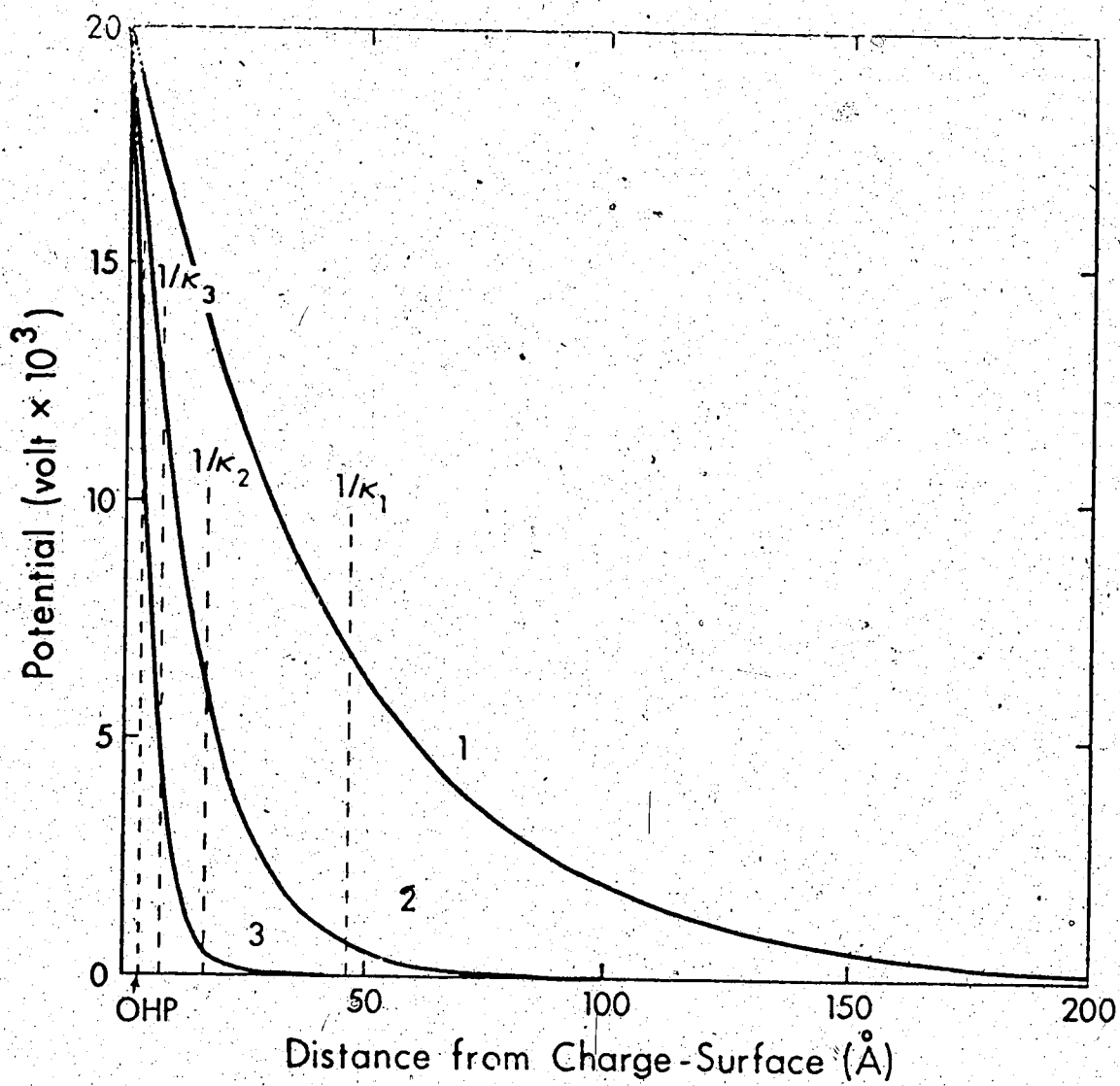


Figure 24. Dependence of the electrical potential in the double layer on distance from the charge surface for a fixed surface potential and varying total concentrations of uniunivalent electrolyte in the bulk solution. $C_1 = 2.00 \times 10^{-4}$ farad/cm²; $\Psi_0 = 20 \times 10^{-3}$ volt; $c = 0.005$ M (curve 1), $c = 0.05$ M (curve 2), $c = 0.5$ M (curve 3).



The second capacitor has the OHP as one "plate" and a hypothetical plane in the diffuse part of the double layer as the second plate. This latter point requires elaboration.

Mathematical treatment of the double layer (125,127) is based on the following assumptions: The surface is uniformly charged; solvent influences the double layer only through the dielectric constant; this dielectric constant has the same value throughout the entire diffuse part. Under these assumptions, the double layer is governed by: (1) Coulombic interaction which is described by Poisson's equation:

$$\nabla^2 \psi = - \frac{4 \pi \rho}{\epsilon} \quad (37)$$

where ∇^2 is the second derivative vector, ψ is the potential at distance x , ρ the charge density and ϵ the permittivity; and (2) Boltzmann distribution which can be described by the following equation:

$$n_i = n_0 \exp(-ZF\psi/RT) \quad (38)$$

where n_i and n_0 are the number of ions in the double layer and bulk solution respectively. The rest of the symbols have the same meaning as before. By combining equations 37 and 38, a second order differential equation results*:

$$\psi'' = \frac{8 \pi Z e n_0}{\epsilon} \sinh \frac{ZF\psi}{RT} \quad (39)$$

with boundary conditions of **:

$$\psi = \psi_{\text{OHP}} \quad \text{at } x=0$$

$$\psi = 0, \quad \psi' = 0 \quad \text{at } x = \infty$$

at low ψ_{OHP} (i.e. ≤ 0.025 V), the solution of the above differential equation is simplified to:

$$\psi = \psi_{\text{OHP}} \exp(-\kappa x) \quad (40)$$

$$\kappa = \left(\frac{8 \pi^2 \epsilon_0 Z^2 F^2}{\epsilon RT} \right)^{1/2} \quad (41)$$

* This second order differential equation is in the x direction only.

** x is from the OHP plane, not from the charge surface.

Equation (40) illustrates that at low ψ_{OHP} the potential decays in an exponential form in the double layer region. Figure 23 illustrates this phenomenon at three different ψ_{OHP} .

In the absence of a specifically adsorbed Inner Helmholtz Plane of counterions, electroneutrality requires that:

$$\sigma_0 = -\sigma_{\text{DL}} \quad (42)$$

where σ_{DL} is the charge density in coulombs/cm², in and beyond the OHP (122), produced by the positive surface excess of counterions

and negative surface excess of coions. σ_{DL} is related to Ψ_{OHP} by equating the σ_{DL} with the net space charge in the diffuse part of the double layer (i.e. $\sigma_{DL} = \int_0^{\infty} \rho dx$, the integration is from the OHP, not from the charge surface) and applying the Poisson-Boltzmann distribution (122). The resulting expression is:

$$-\sigma_{DL} = \left(\frac{\epsilon RT}{2000 \pi} \right)^{1/2} c^{1/2} \left(\exp\left[\frac{ZF\Psi_{OHP}}{2RT} \right] - \exp\left[-\frac{ZF\Psi_{OHP}}{2RT} \right] \right) \quad (43)$$

where Ψ_{OHP} is the electrical potential at the OHP in volts, c is the concentration of electrolyte in bulk solution in moles/l and $Z=1$ for uniunivalent electrolyte. The permittivity of the solution in the double layer, ϵ , is equal to the unitless dielectric constant times the constant 1.12×10^{-12} coulomb/volt-cm (122,127).

When $Z\Psi_{OHP}$ is smaller than about 0.025 volt, at 25°C then:

$$\exp\left[\frac{ZF\Psi_{OHP}}{2RT} \right] \approx 1 + \frac{ZF\Psi_{OHP}}{2RT}$$

and

$$\exp\left[-\frac{ZF\Psi_{OHP}}{2RT} \right] \approx 1 - \frac{ZF\Psi_{OHP}}{2RT} \quad (44)$$

and equation 43 becomes:

$$-\sigma_{DL} \approx \frac{\epsilon \Psi_{OHP}}{4\pi} \left(\frac{8\pi Z^2 F^2 c}{1000 RT} \right)^{1/2} = \frac{\epsilon \kappa}{4\pi} \Psi_{OHP} \quad (45)$$

By rearranging equation 45 and substituting σ_0 for $-\sigma_{DL}$ from equation 42 the following is obtained:

$$C_2 = \frac{\sigma_0}{\Psi_{\text{OHP}}} \approx \frac{\epsilon K}{4 \pi} \quad (46)$$

from which it is seen that the diffuse part of the double layer has the same capacitance, C_2 , as a parallel plate condenser with distance $1/K$ between the plates. For this reason $1/K$, the distance over which the potential decreases from Ψ_{OHP} to Ψ_{OHP}/e , is called the "thickness" of the diffuse part of the double layer.

At a fixed ionic strength in bulk solution (i.e. fixed concentration of electrolyte, c), σ_0 varies linearly with Ψ_{OHP} . On the other hand, if the ionic strength of the solution is varied then the capacitance C_2 varies directly as $c^{1/2}$ because the "thickness", $1/K$, of the diffuse part of the double layer decreases linearly with $c^{1/2}$ (Figure 24). At 25°C, with $Z=1$, and assuming the dielectric constant to be that of pure water, (i.e. 78.3) the capacitance has the value:

$$C_2 = 2.28 \times 10^{-4} \cdot c^{1/2} \frac{\text{farads}}{\text{cm}^2} \quad (47)$$

and its value is proportional to the square root of c , and therefore, to the square root of the ionic strength in the bulk solution.

It is important in the present study to know the relationship that prevails when $\Psi_{\text{OHP}} > 0.025$ volt. Substituting σ_0 for $-\sigma_{\text{DL}}$ from equation 42 into equation 43 and replacing the exponential terms with their hyperbolic sine equivalent allows equation 43 to be rewritten as:

$$\sigma_0 = \left(\frac{RT\epsilon}{2000\pi} \right)^{1/2} \cdot 2 \cdot c^{1/2} \cdot \sinh\left(\frac{ZF\Psi_{OHP}}{2RT} \right) \quad (48)$$

It can also readily be shown that:

$$2 \left(\frac{\epsilon RTc}{2000} \right)^{1/2} = \frac{\epsilon K}{4\pi} \left(\frac{2RT}{ZF} \right) \quad (49)$$

Substituting from equation 49 into 48 and simplifying gives:

$$\sinh\left(\frac{ZF\Psi_{OHP}}{2RT} \right) = \left(\frac{\epsilon K}{4\pi} \right)^{-1} \cdot \left(\frac{2RT}{ZF} \right)^{-1} \cdot \sigma_0 \quad (50)$$

Substituting numerical values yields:

$$\sinh\left(\frac{ZF\Psi_{OHP}}{2RT} \right) = 8.53 \times 10^4 \cdot c^{-1/2} \cdot \sigma_0 \quad (51)$$

Equation 51 allows an evaluation of Ψ_{OHP} from the known electrolyte concentration, c , and the experimentally measured value of σ_0 , since the value of $ZF\Psi_{OHP}/2RT$ can be found in tables (129) for any value of $\sinh(ZF\Psi_{OHP}/2RT)$. Starting, as in equation 46, with the definition of C_2 and substituting the value of σ_0 from equation 50 gives:

$$C_2 = \frac{\sigma_0}{\Psi_{OHP}} = \left(\frac{\epsilon K}{4\pi} \right) \left(\frac{ZF\Psi_{OHP}}{2RT} \right)^{-1} \sinh\left(\frac{ZF\Psi_{OHP}}{2RT} \right) \quad (52)$$

which is a more rigorous form of equation 46 that applies at all values of Ψ_{OHP} .

From equations 36 and 52 and the definition of K implied in equation 45 it is possible to write:

$$\frac{1}{\sigma_0} = \frac{1}{2.28 \cdot 10^{-4} \cdot c^{1/2} \cdot \psi_0 \left[\left(\frac{ZF\psi_{OHP}}{2RT} \right)^{-1} \sinh \left(\frac{ZF\psi_{OHP}}{2RT} \right) \right]} + \frac{1}{c_1 \cdot \psi_0} \quad (53)$$

When $\psi_{OHP} < 0.025$ volt the bracketed term in the denominator of equation 53 is equal to one and equation 52 simplifies to equation 46. Equation 53 provides a simple way to experimentally test whether the SGC theory describes the adsorption of ions on Amberlite XAD-2, since it predicts a straight line plot of σ_0^{-1} versus $(c^{1/2} \left[\left(\frac{ZF\psi_{OHP}}{2RT} \right)^{-1} \sinh \left(\frac{ZF\psi_{OHP}}{2RT} \right) \right])^{-1}$ under conditions where ψ_0 is constant (achieved by making the measurements in solutions of fixed activity of potential determining ion). Furthermore, if this plot is repeated for several different surface potentials, then the ratio of the intercept to the slope should be the same for each plot and should have the value $2.28 \times 10^{-4} / c_1$.

2.2 Microelectrophoresis

Electromigration of charged particles large enough to be seen with a microscope can be measured by microelectrophoresis, a technique in which the rate of movement of individual particles is observed (127). Charged particles migrate in an applied electric field because of the electrical potential difference between the particle and the bulk solution. Adsorbed potential determining ions as well as a certain amount of water of hydration will form part of the migrating unit. The boundary between the migrating unit and the solution phase, which in reality is a region of rapidly changing viscosity, is called the "plane of shear" (Figures 22 and 23) and its location, though unknown with any accuracy, is usually assumed to be at or slightly beyond the OHP (12,127). The potential difference between the plane of shear and the bulk solution is called the zeta potential (ζ) and it is ζ which is accessible by electrophoretic measurements.

In the microelectrophoresis experiment the measured quantity is the electrophoretic mobility U_E micrometer-cm/volt-sec. There are several equations relating the electrophoretic mobility to the zeta potential. The Huckel equation (130) applies for small particles (i.e. the ratio of the radius to the thickness of the double layer ($1/K$) is in the order of 0.1). In this case, the particle can be treated as a point charge in an unperturbed electric field. If Stoke's law applies here, then the following equation is obtained:

$$U_E = \frac{\zeta \epsilon}{6 \pi \eta} \quad (54)$$

where η is the viscosity of the liquid in poise. But the Huckel equation is not likely to be applicable to XAD-2 particles, since the XAD-2 particles under investigation have a very large radius. The Helmholtz-Smoluchowski equation (123,127) on the other hand is useful for large particles. Their treatment is based on the motion of liquid in the diffuse part of the double layer relative to a non-conducting flat surface when an electric field is applied parallel to the surface. By equating the electrical and viscous force on a liquid layer of unit area and applying the Poisson equation, the Helmholtz-Smoluchowsky equation results:

$$\begin{aligned} \zeta &= \frac{4 \pi \eta}{\epsilon} U_E \\ &= 1.28 \times 10^{-2} U_E \text{ volts} \end{aligned} \quad (55)$$

A particle is large if the ratio of its radius to the thickness of the double layer ($1/k$) is greater than about 300.

If the approximation is made (122):

$$\zeta \approx \psi_{OHP} \quad (56)$$

then equation 36 can be rewritten as:

$$c_1 \approx \frac{\sigma_0}{\psi_0 - \zeta} \quad (57)$$

and rearranging gives:

$$\sigma_0 \approx c_1 \psi_0 - c_1 \zeta \quad (58)$$

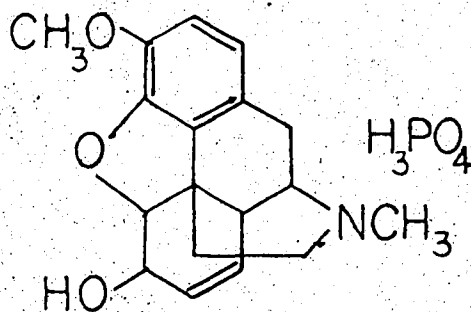
The value of ψ_{OHP} (or, from equation 56, the value of ζ) depends on the total electrolyte concentration, c , and on σ_0 via equations 42 and 43. Thus, a plot of the experimentally measured values of σ_0 versus those of ζ should give a straight line under conditions where the activity of potential-determining ion is held constant to provide constant ψ_0 , and the concentration of total electrolyte, c , is varied in order to vary ψ_{OHP} .

3. EXPERIMENTAL

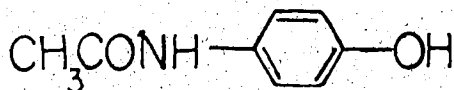
3.1 Chemicals

Diphenylguanidine, benzylamine and tetra-n-butylammonium bromide have been described in the first part of the thesis.

Codeine Phosphate was supplied by Endo Laboratories. It was used as received. It has the following structure:



Acetaminophen was supplied by Matheson Coleman & Bell. This compound was used without further purification. Its structure is shown as below:



Other chemicals, including sodium perchlorate, sodium chloride, sodium bromide, sodium phosphate dibasic, potassium phosphate monobasic, potassium chloride, hydrochloric acid, hydrobromic acid, perchloric acid, d-camphorsulfonic acid sodium salt, and propane-sulfonic acid sodium salt were all analytical reagent grade chemicals.

3.2 Reagents

0.1 M Potassium Chloride. Potassium chloride was dried at 50 - 60°C overnight or until a constant weight was obtained. This was used to prepare 1 liter of 0.100 M KCl solution.

Phosphate buffer consisted of 0.01334 M potassium dihydrogen phosphate (potassium phosphate monobasic) and 0.05333 M disodium hydrogen phosphate (sodium phosphate dibasic). This buffer solution yields a pH of 7.4.

Resin suspension. (1 mg/ml) was prepared by first weighing roughly 0.1 g of the dry resin. After rinsing with methanol, water was added to replace the methanol. Finally, a proper amount of water was added to make a total volume of 100 ml. This solution contained 1 mg of the XAD-2 resin per ml aqueous solution and was used in the microelectrophoresis measurements.

3.3 Chromatographic Apparatus

A Chromatronix model CMP-2VK pump, a 10 μ l injection valve (model CSV), a pressure gauge, Teflon tubing, and Cheminert fittings were all obtained from Laboratory Data Control. The U.V. absorbance detector was a model SP 8200 (Spectra Physics, Santa Clara, Calif.) and the recorder a Recordall model 5000 (Fisher Scientific Co.). The glass Microbore chromatographic columns (Laboratory Data Control) were 0.28 cm I.D. by 30/5 cm long and were dry-packed with < 325 mesh XAD-2. The columns were water jacketed and thermostatted at 25 \pm 1°C.

3.4 Resins

Amberlite XAD-2 resin (Rohm and Haas Co., Philadelphia, Pa.) was ground in a triple porcelain roller mill (Erweka-Apparatebau-GmbH), dried, and classified in U.S. standard sieves. The < 325 mesh portion which was used both in packing the chromatographic columns and in adsorption isotherm measurements were purified and "de-fined" as previously described (17). Particles of nominally 5 micrometer diameter for use in microelectrophoresis were prepared by elutriation of the < 325 mesh resin using methanol (This resin was prepared by Dr. Robert Baum). The elutriation apparatus was similar to that previously described (131) except that solvent was pumped at constant flow rate with a Chromatronix model CMP-3V pump (Laboratory Data Control, Riviera Beach, Fla.) and the column was kept at constant temperature by means of a water-jacket. Diameters of the irregular shaped particles were measured microscopically.

3.5 Adsorption Isotherms

Isotherms for the adsorption of DPGH^+ and acetaminophen on XAD-2 were measured at $25 \pm 1^\circ\text{C}$ by a batch equilibration technique. All solutions were adjusted to $\text{pH} = 3$ with hydrochloric acid. In the case of diphenylguanidine this insured that the concentration of diphenylguanidine free base was negligible. Twenty-five ml volumes of aqueous phase containing varying amounts of DPGH^+ or acetaminophen and sodium chloride were pipetted into stoppered flasks along with 2.5 g of XAD-2 resin. Five different NaCl concentrations were used: 0.01, 0.05, 0.10, 0.25, and 0.50 M, with five or six different concentrations of DPGH^+ or acetaminophen used for each NaCl concentration. The stoppered flasks were agitated in a mechanical shaker (Blue M Company, Blue Island, Ill.) for about 24 hours which was shown to be sufficient to establish adsorption equilibrium. The aqueous phase was filtered free of resin and analyzed for its DPGH^+ or acetaminophen concentration by U.V. spectroscopy on a Cary 118 spectrophotometer (Varian Instruments, Palo Alto, Calif). Concentrations of DPGH^+ or acetaminophen on the resin phase were determined by difference.

Because XAD-2 resin will not imbibe water into its pores when dry resin is placed directly in water, it was wetted with methanol before being used in the isotherm measurements. The methanol was filtered off and the methanol-wet resin washed thoroughly with water to displace the methanol. Excess water was sucked off and the resin, which now contained water in its pores,

3.6 Chromatographic Studies

Chromatography was used to obtain adsorption isotherms for BZH^+ , to study the effect of the concentration of both tetra-n-butylammonium bromide and total bromide on the retention volume of $DPGH^+$ and codeine phosphate and to study the effect of various salts on the retention of BZH^+ .

The chromatographic bed was rinsed by pumping methanol through it. Then methanol was replaced by the desired mobile phase. The 10 μ l injection valve was employed to assure that a constant amount of sample was loaded on the column. The flow rate was kept at 0.5 ml/min. This flow rate was checked by collecting the effluent in a buret for a known time period. Net retention volume was the difference of retention volume and void volume. Void volume of the column was determined by injecting an unretained compound such as methanol into the column. The void volume was 1.34 ml for the 30 cm long column. When the mobile phase was changed between experiments, samples were injected at various times until a constant retention volume was obtained, in order to insure that the resin bed and mobile phase were equilibrated. The wave length used for this study was 254 nm. Sensitivity settings on the U.V. detector were from 0.02 to 0.08, except that for acetaminophen, 0.32 was used.

was weighed into the flasks. The exact weight of resin in the flask was determined after equilibration by filtering off, washing, oven-drying, and weighing. The pore volume of water was included, for calculation purposes, in the aqueous phase volume.

Adsorption isotherms of benzylammonium ion (BZH^+) were measured by chromatography on XAD-2. The mobile phase was made to contain varying concentrations of hydrobromic acid. Concentration of BZH^+ was varied by varying the concentration of BZH^+ in the 10 μ l of sample solution injected. The chromatograph and the calculations used to obtain isotherms from chromatographic retention volumes are described below (Section 4.2.2).

3.7 Microelectrophoresis

Electrophoretic mobility was measured on a Mark II Micro-electrophoresis Apparatus (Rank Bros., Cambridge, England) using a flat quartz cell, 0.8 mm thick and 9.7 mm high, immersed in a 25±1°C water bath. The viewing axis of the microscope was horizontal so that observations were free of interference caused by gravitational sedimentation of the resin particles. The platinum electrodes supplied with the instrument were replaced with coils of silver wire previously anodized to give them a coating of AgCl. This was done in order to minimize "gassing" at the electrodes in the low-resistance sample solutions. The "effective length" or interelectrode distance was calculated from the equation (127):

$$L = r \cdot k \cdot A \quad (59)$$

where k is the specific conductance of 0.10 M KCl with which the cell was filled for calibration purposes, A is the cross-sectional area of the cell at the point of microscopic observation, and r is the resistance measured with an impedance bridge (Model 1650-A, General Radio Company, Concord, Mass.). The value of k is $1.289 \times 10^{-2} \text{ ohm}^{-1} \text{ cm}^{-1}$ (132). The value of A was determined as $7.76 \times 10^{-2} \text{ cm}^2$ and r was measured as 5790 ohm. With the value of L obtained from the calibration measurement it is possible to calculate the potential gradient in volts/cm during an electrophoresis

experiment by dividing the voltage applied between the electrodes by L.

Microscopic observations were made on particles of XAD-2 resin at the "stationary level" in the solution, which was located 20 percent of the distance from one cell wall to the other, in order to minimize convective movement due to electroosmosis (127). The time required for a given resin particle to migrate 50 micrometers was measured. The polarity of the applied potential was then reversed and the time required to migrate in the opposite direction was also measured. The measurements were repeated ten times at each applied potential and polarity. As a check on instrument calibration the electrophoretic mobility of unwashed human red blood cells was measured at 25°C in 6.67×10^{-2} M phosphate buffer at pH = 7.4. The anticoagulated blood sample was refrigerated for several days before use. The observed mobility was -1.11 micrometer-cm/volt-sec which is lower than the accepted mean value of -1.30 for fresh blood but close to the lowest value of -1.12 reported by Abramson (133) for aged blood.

Suspensions of XAD-2 resin for electrophoretic measurement were prepared at a concentration of 0.1 mg/ml. Three series of these resin suspensions were prepared. In each series the activity of DPGH^+ in the aqueous phase was constant, while the ionic strength was adjusted to four different values by adding NaCl. The activity of DPGH^+ varied between the series. All solutions were adjusted to pH = 3 by the addition of HCl. Mobilities of XAD-2 resin were found to be 0 when no DPGH^+ was present.

4. RESULTS AND DISCUSSION

4.1 Adsorbent Properties

Amberlite XAD-2 is hydrophobic, since its surface is not wetted by water (134). The forces of interaction between a sample species and the surface of XAD-2 are mainly dispersion forces which, in the case of aromatic samples, take the form of π - π interactions. Since XAD-2 resin is a styrene-divinylbenzene copolymer the electron donor properties of the benzene ring make it possible for it to also undergo weak hydrogen bonding interactions with sample species that carry proton-donor groups (135). Styrene-divinylbenzene copolymers such as Chromosorb 102 and Porapak P which are used as gas chromatographic stationary phases have been found to contain small numbers of polar impurity surface sites (136,137), and Zettlemyer (138) indicates that it is nearly impossible to synthesize any hydrophobic surface that is free of polar site-impurities. XAD-2 which is chemically identical to some of the gas chromatographic phases is probably not immune from these impurities. In Part I of this thesis, a small amount of H_3O^+ and OH^- were shown to be taken up by XAD-2 resin. It may well be that this occurs by reaction of the H_3O^+ or OH^- with acid-base surface impurities.

Various batches of Amberlite XAD-2 are reported to have specific surface areas ranging between 300 and 354 m^2/g as determined by the B.E.T. method, porosities of 0.42 ml/ml, and average pore diameters of 90 Å (28,139,140).

4.2 Distribution Isotherms of DPGH⁺ and BZH⁺ and the SGC Theory

4.2.1 Diphenylguanidinium ion (DPGH⁺)

The results of adsorption studies of DPGH⁺ by the batch equilibration technique are presented in Tables 23 to 27. If the concentration of DPGH⁺ on the resin (moles/kg) is divided by $3.30 \times 10^9 \text{ cm}^2/\text{kg}$, which is the average of the reported value of specific surface area of the XAD-2 resin, then it gives Γ_{DPGH} , the surface excess (moles/cm²). The distribution isotherms obtained in the presence of various bulk solution concentrations of sodium chloride are presented in Figure 25.

At higher concentrations of DPGH⁺ in solution the data can be described by the Langmuir equation (101):

$$\frac{1}{\Gamma_{\text{DPGH}}} = \frac{1}{K \cdot [\text{DPGH}] \cdot \Gamma_{\text{DPGH,MAX}}} + \frac{1}{\Gamma_{\text{DPGH,MAX}}} \quad (60)$$

where $[\text{DPGH}]$ is moles/l of DPGH⁺ in the solution, K is a heterogeneous equilibrium constant, and $\Gamma_{\text{DPGH,MAX}}$ is the surface excess corresponding to monolayer coverage of resin surface with DPGH⁺.

Figure 26 shows the data for DPGH⁺ plotted according to equation 60. The y-ordinate intercepts for all of the curves are the same, indicating that $\Gamma_{\text{DPGH,MAX}}$ is the same, regardless of the ionic strength of the solution. This intercept value of $(0.59 \pm 0.02) \times 10^{10} \text{ cm}^2/\text{mole}$ corresponds to $1.70 \times 10^{-10} \text{ moles/cm}^2$ for a monolayer of DPGH⁺, and to an area of $9.8 \times 10^{-15} \text{ cm}^2$ occupied by each DPGH⁺.

Figure 25. Adsorption isotherms for diphenylguanidinium ion in the presence of various bulk solution concentrations of sodium chloride. The numbers at the end of the curves are the molarities of sodium chloride.

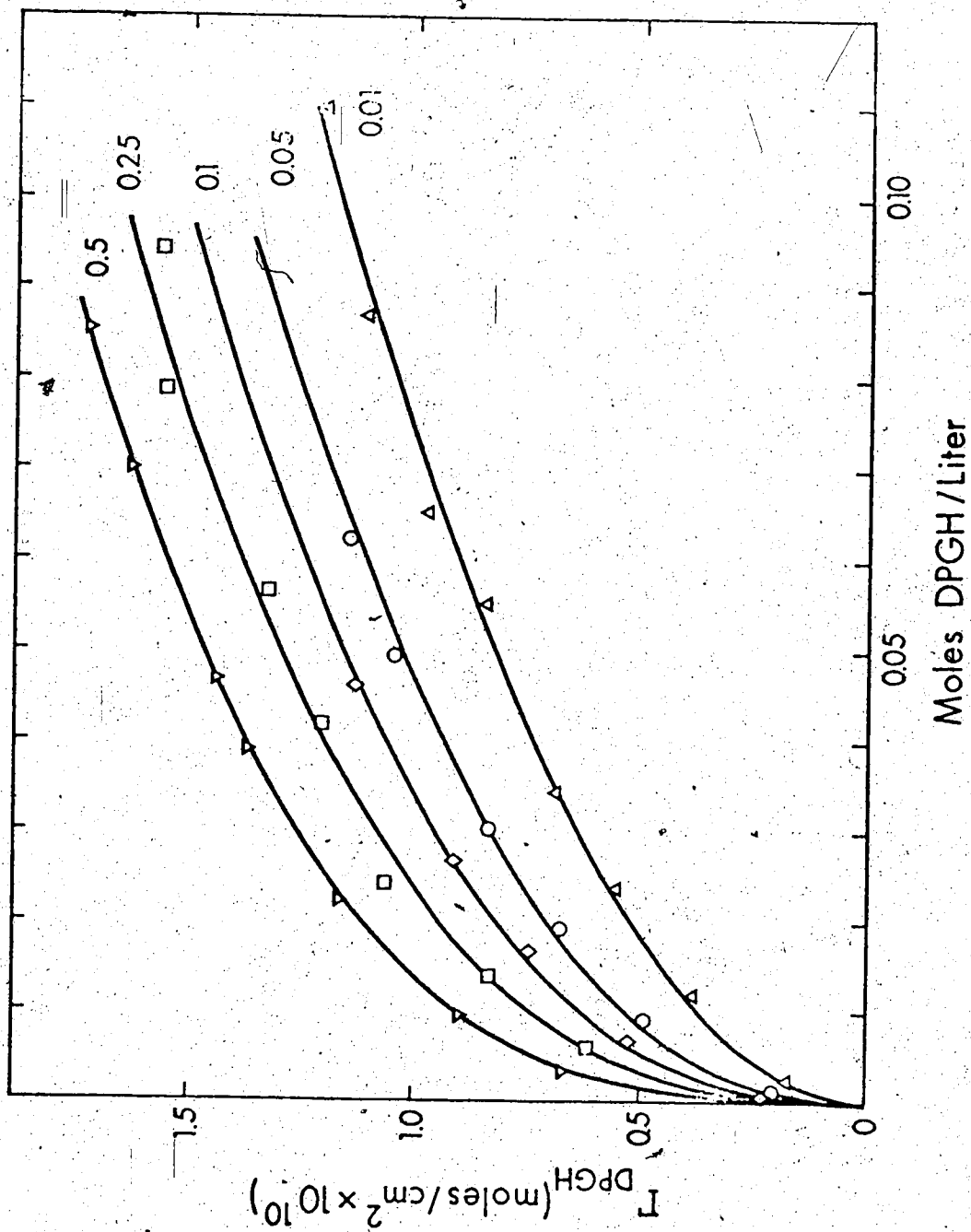


Table 23

Data for the distribution isotherm of
 DPGH^+ on XAD-2 resin in 0.011 M NaCl

No.	Wt. of XAD-2 used (g)	Aqueous phase volume (ml)	$[\text{DPGH}^+]$ moles/l	$[\text{DPGH}^+]_R$ moles/kg	$[\text{DPGH}^+] \times 10^{10}$ moles/cm ²
1	2.543	25.055	2.33×10^{-3}	0.0588	0.178
2	2.581	24.971	1.19×10^{-2}	0.126	0.382
3	2.443	25.037	2.47×10^{-2}	0.183	0.553
4	2.516	25.791	3.43×10^{-2}	0.227	0.688
5	2.534	24.970	5.50×10^{-2}	0.279	0.845
6	2.460	26.135	6.52×10^{-2}	0.322	0.976
7	2.602	24.880	8.68×10^{-2}	0.369	1.118
8	2.516	24.917	0.110	0.399	1.208

Table 24

Data for the distribution isotherm of
 DPGH^+ on XAD-2 resin in 0.050 M NaCl

No.	Wt. of XAD-2 used (g)	Aqueous phase volume (ml)	$[\text{DPGH}^+]$ moles/l	$[\text{DPGH}^+]_R$ moles/kg	$[\text{DPGH}^+ \times 10^{10}]$ moles/cm ²
1	2.647	25.030	1.03×10^{-3}	0.182	0.209
2	2.421	25.325	9.14×10^{-3}	0.393	0.491
3	2.483	25.311	1.92×10^{-2}	0.554	0.676
4	2.509	25.132	3.02×10^{-2}	0.696	0.841
5	2.381	25.480	4.92×10^{-2}	0.826	1.052
6	2.440	25.243	6.22×10^{-2}	0.926	1.150

Table 25

Data for the distribution isotherm of
 DPGH^+ on XAD-2 resin in 0.10 M NaCl

No.	Wt. of XAD-2 used (g)	Aqueous phase volume (ml)	$[\text{DPGH}^+]$ moles/l	$[\text{DPGH}^+]_R$ moles/kg	$\sqrt{[\text{DPGH}^+] \times 10^{10}}$ moles/cm ²
1	2.421	24.977	7.78×10^{-4}	0.0769	0.233
2	2.516	24.949	6.76×10^{-3}	0.174	0.528
3	2.383	24.637	1.66×10^{-2}	0.246	0.746
4	2.592	24.627	2.68×10^{-2}	0.301	0.912
5	2.434	24.828	4.60×10^{-2}	0.376	1.139

Table 26

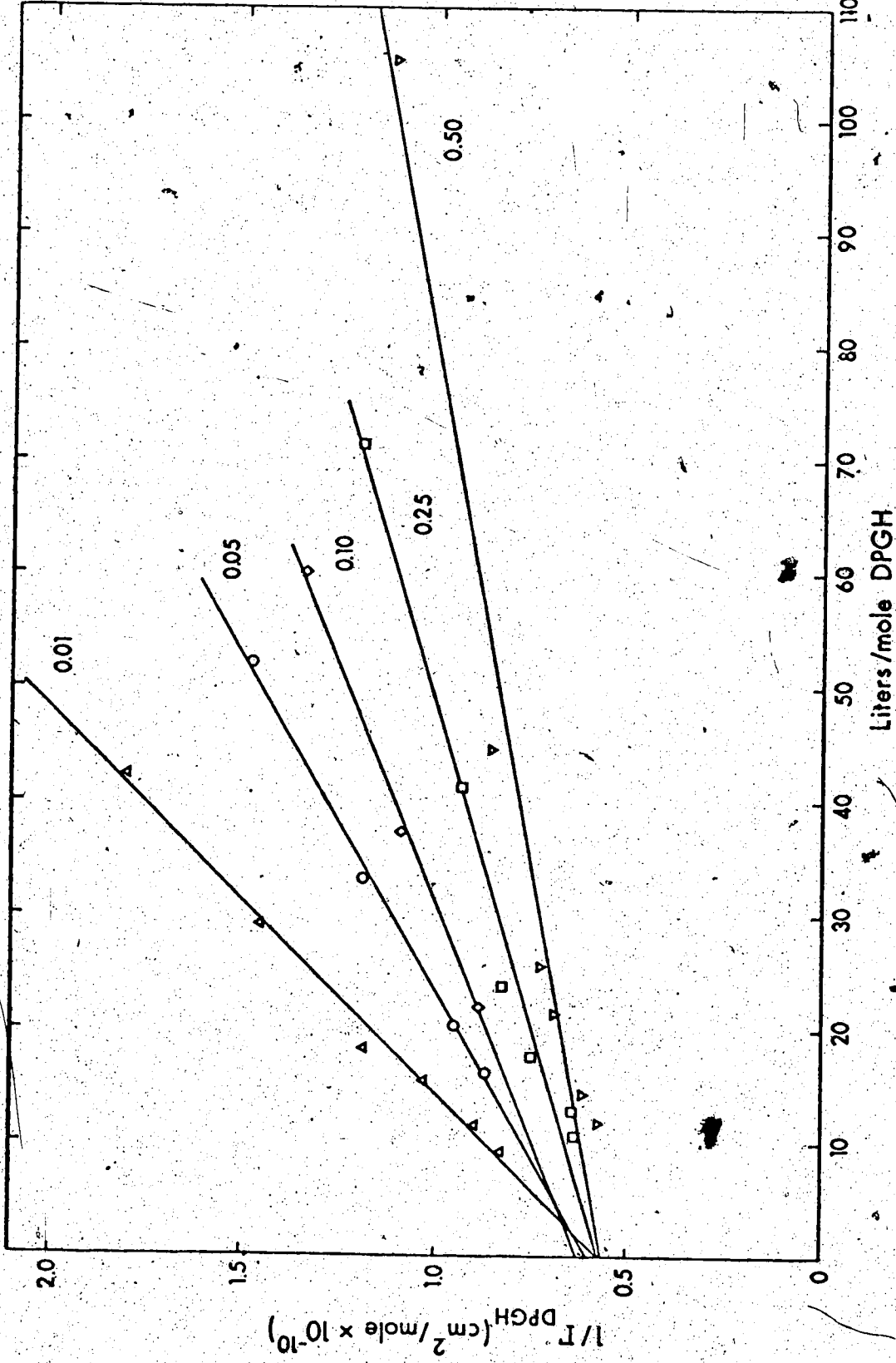
Data for the distribution isotherm of
 DPGH⁺ on XAD-2 resin in 0.25 M NaCl

No.	Wt. of XAD-2 used (g),	Aqueous phase volume (ml)	[DPGH ⁺] moles/l	[DPGH ⁺] _R moles/kg	$\sqrt{DPGH} \times 10^{10}$ moles/cm ²
1	2.403	25.172	4.93×10^{-4}	0.0804	0.244
2	2.329	25.017	5.91×10^{-3}	0.202	0.611
3	2.472	24.860	1.40×10^{-2}	0.276	0.835
4	2.366	25.132	2.42×10^{-2}	0.352	1.065
5	2.554	24.806	4.19×10^{-2}	0.399	1.207
6	2.415	24.798	5.67×10^{-2}	0.440	1.333
7	2.209	25.183	7.88×10^{-2}	0.514	1.558
8	2.645	25.122	9.42×10^{-2}	0.518	1.570

Table 27
 Data for the distribution isotherm of
 DPGH⁺ on XAD-2 resin in 0.50 M NaCl

No.	Wt. of XAD-2 used (g)	Aqueous phase volume (ml)	[DPGH ⁺] moles/l	[DPGH ⁺] _R moles/kg	$\sqrt{\text{DPGH} \times 10^{10}}$ moles/cm ²
1	2.692	24.577	2.20×10^{-4}	0.0744	0.225
2	2.353	24.897	3.96×10^{-3}	0.220	0.670
3	2.695	24.668	9.50×10^{-3}	0.295	0.894
4	2.280	25.061	2.24×10^{-2}	0.385	1.167
5	2.405	24.820	3.90×10^{-2}	0.453	1.373
6	2.727	24.986	4.68×10^{-2}	0.476	1.442
7	2.504	24.837	7.00×10^{-2}	0.538	1.636
8	2.525	24.503	8.54×10^{-2}	0.570	1.727

Figure 26. Langmuir adsorption isotherms for diphenylguanidinium ion in the presence of various bulk solution concentrations of sodium chloride plotted according to equation 60. The numbers at the end of the curves are the molarities of sodium chloride.



From molecular models it can be shown that the DPGH^+ ion can readily assume a conformation in which the phenyl groups are coplanar with one another and with the plane through the sp^2 carbon and the two sp^3 nitrogens, and in which the protonated imino-nitrogen is perpendicular to this plane. Since this conformation would maximize π - π interactions with the phenyl groups of the XAD-2 resin, it is likely that the protonated nitrogen is directed toward the solution phase. Taking the area of a benzene ring as 43 \AA^2 (141) and using tabulated covalent radii of H, N, and C (142), to calculate areas of these atoms, the flat area of a DPGH^+ ion lying on the resin surface is calculated to be $9.0 \times 10^{-15} \text{ cm}^2$. This is close to the experimentally measured area occupied by a DPGH^+ ion noted above. Thus, monolayer coverage is essentially a close-packing of DPGH^+ ions lying flat on the surface. This latter conclusion is also in agreement with the results reported for the adsorption of phenol on XAD-2 (28) and for the adsorption of substituted benzenes on Amberlite XAD-4, a chemically identical adsorbent with a larger specific surface area than XAD-2 (139). The occurrence of Langmuir adsorption isotherms for ionic samples at high concentrations has previously been reported; for example, for tris-3-(2-pyridyl)-5,6-diphenyl-1,2,4-triazine iron (II) on XAD-2 (107) and for the anionic dye Chlorazol Sky Blue FF on graphitized carbon (143), another hydrophobic adsorbent.

In order to relate the distribution isotherm data to the proposed model σ_0 , the surface charge must first be calculated.

σ_0 cannot be directly calculated from Γ_{DPGH} , the experimental surface excess of the potential-determining ion because the value of Γ_{DPGH} is equal to the moles/cm² of DPGH adsorbed on the surface (Γ_{DPGH}^{AD}) minus the moles/cm² of DPGH⁺ that have been expelled by electrostatic repulsion from the diffuse part of the double layer into the bulk solution (Γ_{DPGH}^{DL}).

$$\Gamma_{DPGH} = \Gamma_{DPGH}^{AD} + \Gamma_{DPGH}^{DL} \quad (61)$$

(The quantity Γ_{DPGH}^{DL} has a negative value, because it is a "negative" surface excess.) The surface charge, σ_0 , is thus related to Γ_{DPGH}^{AD} by:

$$\sigma_0 = ZF\Gamma_{DPGH}^{AD} = ZF(\Gamma_{DPGH} - \Gamma_{DPGH}^{DL}) \quad (62)$$

so that it is necessary to correct the experimental surface excess (Γ_{DPGH}) by the negative surface excess of DPGH⁺ in the solution part of the double layer in order to compute σ_0 .

According to Grahame (122), for a flat charge surface in the absence of specific adsorption of counterions, the ratio of the surface excess due to the absence of coions in the solution part of the double layer (negative excess) to that which is due to the positive excess of counterions is given as:

$$\frac{\Gamma_{+}^{DL}}{\Gamma_{-}^{DL}} = \frac{\exp(-Ze\psi_{OHP}/2kT) - 1}{\exp(+Ze\psi_{OHP}/2kT) - 1} \quad (63)$$

where e is the charge of a single univalent ion, ψ_{OHP} is the potential at the outer Helmholtz plane and k is the Boltzmann's constant. At low values of ψ_{OHP} (≤ 0.001 volt) the ratio is near to 1 and for large values of ψ_{OHP} the ratio is close to zero. (Both can be derived from the l'Hopital principle.) For $Z = 1$ and at 25°C , the above equation is written as:

$$\frac{\Gamma_{+}^{DL}}{\Gamma_{-}^{DL}} = \frac{\exp(-19.47\psi_{OHP}) - 1}{\exp(+19.47\psi_{OHP}) - 1} \quad (64)$$

In the presence of an inert electrolyte such as NaCl , there are two types of cations, Na^{+} and DPGH^{+} , so that only part of the negative coion surface excess is due to DPGH^{+} .

$$\begin{aligned} \Gamma_{\text{DPGH}}^{DL} &= \Gamma_{+}^{DL} \cdot \frac{[\text{DPGH}]}{[\text{DPGH}] + [\text{Na}]} \\ &= \Gamma_{+}^{DL} \cdot \alpha \end{aligned} \quad (65)$$

where $[\text{DPGH}]$ and $[\text{Na}]$ are concentrations of these species in the bulk solution at equilibrium and α is the fraction that DPGH^{+} represents of all cations in the bulk solution. The symbol R may be defined:

$$R = \frac{\Gamma_{DPGH}^{DL}}{\Gamma_{-}^{DL}} = \frac{\Gamma_{+}^{DL}}{\Gamma_{-}^{DL}} \cdot \alpha \quad (66)$$

and the following additional relationship noted:

$$\sigma_{DL} = ZF (\Gamma_{-}^{DL} + \Gamma_{+}^{DL}) \quad (67)$$

From equations 42, 61, 62, 65, 66, and 67, it may be shown that:

$$\Gamma_{DPGH}^{DL} = [1 - (\frac{1}{\alpha} + \frac{1}{R})]^{-1} \cdot \Gamma_{DPGH} \quad (68)$$

Substituting this equation into 62 yields:

$$\sigma_0 = ZF \Gamma_{DPGH} \left[\frac{\alpha + R}{\alpha + R(1 - \alpha)} \right] \quad (69)$$

In order to calculate σ_0 from equation 69 it is necessary to know the value of Ψ_{OHP} to be used in equation 64. But Ψ_{OHP} is calculated from equation 51 which requires a knowledge of σ_0 . Thus, equation 51, 64, 66, and 69 must be solved by iteration. A first-approximation to σ_0 is calculated from equation 71 (below). This is then used to calculate a first-approximation value of Ψ_{OHP} from equation 51. First-approximations of $\Gamma_{+}^{DL}/\Gamma_{-}^{DL}$ and R are calculated in turn from equations 64 and 66. This value of R is used in equation 69 to calculate a second-approximation to σ_0 . The process is repeated until Ψ_{OHP} and σ_0 no longer change.

At low values of ψ_{OHP} (i.e. between 0 and 0.001 volt), with no inert electrolyte present, $R = 1$. Equation 69 then becomes:

$$\sigma_0 = ZF \Gamma_{\text{DPGH}}^2 \quad (70)$$

and half of the surface charge is neutralized by a positive excess of Cl^- while the other half is neutralized by a positive excess of DPGH^+ . When the potential is large (i.e. several tenths of a volt) or when the concentration of inert electrolyte in the bulk solution is much larger than that of DPGH^+ then:

$$\sigma_0 = ZF \Gamma_{\text{DPGH}} \quad (71)$$

In the present case the difference in the value of σ_0 calculated by equations 69 and 71 is significant only when a_{DPGH} is large and the concentration of NaCl is small. In the worst case the difference was 12 percent.

Validity of the SGC theory for the adsorption of DPGH^+ on XAD-2 was tested using equation 53 in the following way: Aqueous solution activity coefficients for DPGH^+ (144, 145) were used to convert the abscissa values of $[\text{DPGH}]$ in Figure 25 into activities, a_{DPGH} . For this purpose an ionic parameter of 6×10^{-8} was assumed. Activity coefficients for DPGH^+ at ionic strengths greater than 0.1, were assumed to be equal to those of p-toluene-sulfonic acid which could be looked up in tables (145). Points were then located on each of the five isotherms in Figure 25 at the

same a_{DPGH} (i.e. at the same Ψ_0) and the five corresponding ordinate values were converted to σ_0 , as discussed above. This process was performed at eight different values of a_{DPGH} . Results are given in the Tables 28-35. Column 1 of these tables gives the sodium chloride plus the small amount of HCl concentration; column 2 gives the total electrolyte concentration which includes the chloride from $\text{DPGH}\cdot\text{Cl}$ as well as that from column 1; column 3 gives the activity of DPGH^+ ; column 4 gives the correction factor which equals $(\alpha + R)/(\alpha + R - \alpha R)$; and column 5 gives the reciprocal of the product of the square root of the total chloride concentration and the bracketed term in equation 53 (x represents $ZF\Psi_{\text{OHP}}/2RT$). The quantities in the last two columns are plotted in Figure 27. The lines are linear least squares fits of the experimental points.

The linearity of the curves in Figure 27 is consistent with the predictions of the SGC theory embodied in equation 53. Values of Ψ_0 are calculated from the slopes of each line, that is, Ψ_0 is equal to $(2.28 \times 10^{-4} \cdot \text{slope})^{-1}$. The capacitance of the compact part of the double layer C_1 is equal to $(\Psi_0 \cdot \text{intercept})^{-1}$.

Values of Ψ_0 and C_1 are shown in the second and fourth columns in Table 36, along with their 95 percent confidence intervals.

The uncertainties in the values of C_1 are high because they include the uncertainties in both slopes and intercepts. The grand mean and 95 percent confidence interval of C_1 computed from the eight values in the fourth column of Table 36 are $(1.90 \pm 0.28) \times 10^{-4}$ farad/cm². Within the uncertainty of the measurements, C_1 is a

Figure 27. Adsorption data for diphenylguanidinium ion according to the SGC equation 53 at eight surface potentials. The numbers at the end of the lines are the activities of DPGH^+ at which the calculations were made.

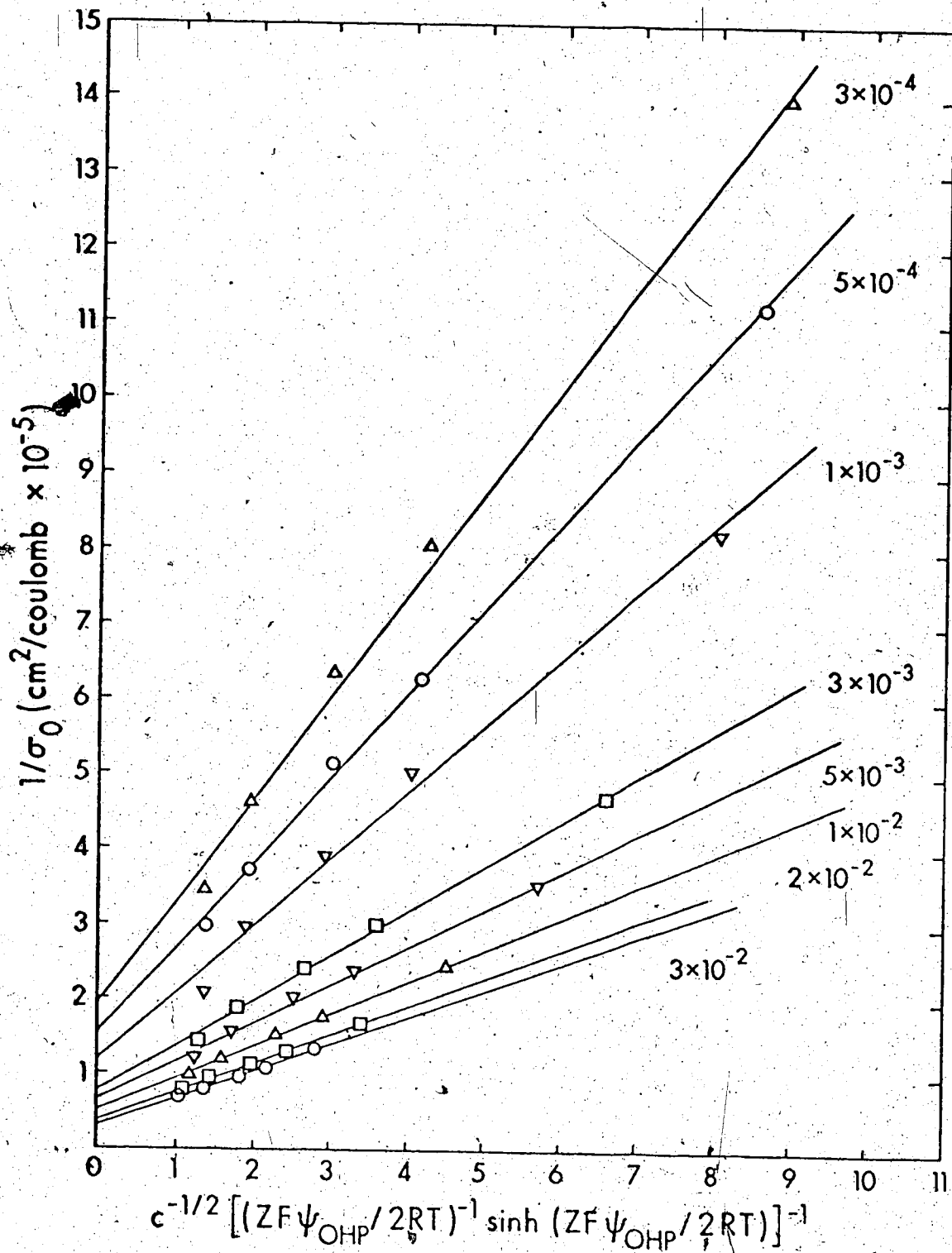


Table 28
 Summary of the quantities used to prepare Figure 27.
 From the distribution isotherms at an activity of
 $\text{DPGH}^+ \text{ of } 3.0 \times 10^{-4}$

$[C^-]$	$[C^+]_T$	τ_{DPGH}	$[\text{DPGH}] \times 10^{+4}$	$\int_{\text{DPGH}} \times 10^{+11}$	$R' (\%) (c^{1/2} \frac{\sinh x^*}{x^*})^{-1} \sigma_0^{-1} \times 10^{-5}$
0.0111	0.0114	0.908	3.30	0.561	8.903
0.0501	0.0515	0.850	3.53	1.288	4.262
0.101	0.102	0.821	3.65	1.630	3.053
0.251	0.251	0.680	4.41	2.239	1.948
0.501	0.501	0.608	4.93	2.872	1.383

$\star x^* = \frac{ZF \psi_{\text{OHP}}}{2RT}$

$R' = (\alpha + R) / (\alpha_0 + R - \alpha R)$

Table 29

Summary of the quantities used to prepare Figure 27.

From the distribution isotherms at an activity of

$DPGH^+$ of 5.0×10^{-4}

$[Cl^-]$	$[Cl^-]_T$	T_{DPGH}	$[DPGH] \times 10^{+4}$	$\int_{DPGH} \times 10^{+11}$	$\sigma_0 \times 10^{+6}$	$R(\%) (c^{1/2} \frac{\sinh x^*}{x^*})^{-1} \sigma_0^{-1} \times 10^{-5}$
0.0111	0.0117	0.907	5.51	0.773	0.892	11.210
0.0511	0.0517	0.850	5.88	1.645	1.595	6.270
0.101	0.102	0.821	6.09	2.012	1.946	5.138
0.251	0.251	0.680	7.35	2.772	2.680	3.731
0.501	0.501	0.608	8.22	2.485	3.364	2.973

$$x^* = \frac{ZF \Psi_{OHP}}{2RT}$$

$$R^1 = (\alpha + R) / (\alpha + R - \alpha R)$$

Table 30

Summary of the quantities used to prepare Figure 27.

From the distribution isotherms at an activity of

DPGH^+ of 1.0×10^{-3}

$[\text{Cl}^-]$	$[\text{Cl}^-]_T$	γ_{DPGH}	$[\text{DPGH}]$ $\times 10^{+4}$	\int_{DPGH} $\times 10^{+11}$	σ_0 $\times 10^{+6}$	$R'(\%)$	$(\frac{1}{2} \frac{\sigma_0}{x^*} \sinh x^*)^{-1} \sigma_0^{-1}$ $\times 10^{-5}$
0.0111	0.0122	0.900	1.11	1.00	1.220	2.81	8.060
0.0511	0.0523	0.848	1.18	2.05	1.994	0.76	5.015
0.101	0.102	0.820	1.22	2.64	2.559	0.42	3.908
0.251	0.253	0.680	1.47	3.50	3.385	0.21	2.954
0.501	0.503	0.608	1.65	5.00	4.832	0.12	2.070

$$*x = \frac{ZF\psi_{\text{OHP}}}{2RT}$$

$$R' = (\alpha + R) / (\alpha + R - \alpha R)$$

Table 31

Summary of the quantities used to prepare Figure 27.

From the distribution isotherms at an activity of

DPGH[†] of 3.0 x 10⁻³

[Cl ⁻] ₀	[Cl ⁻] _T	τ _{DPGH}	[DPGH] ₀ *10 ⁺³	[DPGH] _T x 10 ⁺¹¹	σ ₀ x 10 ⁺⁶	R' (%) (c ^{1/2} sinh(x [*] /x [*])) ⁻¹	σ ₀ ⁻¹ x 10 ⁻⁵
0.0111	0.0144	0.900	3.33	2.10	2.134	5.84	4.686
0.0501	0.0546	0.848	3.54	3.40	3.339	1.74	2.995
0.101	0.105	0.820	3.66	4.24	4.132	0.99	2.420
0.251	0.255	0.680	4.41	5.45	5.288	0.54	1.891
0.501	0.506	0.608	4.93	7.20	6.971	0.31	1.435

$$* x = \frac{ZF\psi_{OHP}}{2RT}$$

$$R' = (\alpha + R) / (\alpha + R - \alpha'R)$$

Table 32

Summary of the quantities used to prepare Figure 27.

From the distribution isotherms at an activity of

DPGH⁺ of 5.0 x 10⁻³

[Cl ⁻]	[Cl ⁻] _T	γ _{DPGH}	[DPGH] x 10 ⁺³	∫ _{DPGH} x 10 ⁺¹¹	σ ₀ x 10 ⁺⁶	R' (%) (c ^{1/2} sinh [*] - 1) σ ₀ ⁻¹ x 10 ⁻⁵
0.0111	0.167	0.897	5.57	2.75	2.842	7.10
0.511	0.570	0.845	5.92	4.24	4.193	2.48
0.101	0.107	0.820	6.10	5.08	4.975	1.47
0.251	0.258	0.676	7.40	6.58	6.403	0.82
0.501	0.509	0.605	8.26	8.53	8.273	0.48

$$*x = \frac{ZF\Psi_{OHP}}{2RT}$$

$$R' = (\alpha + R) / (\alpha + R - \alpha R)$$

Table 33

Summary of the quantities used to prepare Figure 27.

From the distribution isotherms at an activity of

DPGH^\dagger of 1.0×10^{-2}

$[\text{Cl}^-] - [\text{Cl}^-]_T$	\uparrow_{DPGH}	$[\text{DPGH}]$ $\times 10^{+2}$	\int_{DPGH} $\times 10^{+10}$	σ_0 $\times 10^{+6}$	$R^1 (\%) (c^{1/2} \sinh x^*)^{-1} \sigma_0^{-1}$ $\times 10^{-5}$
0.0111	0.888	1.13	0.39	4.116	9.35
0.0511	0.840	1.19	0.57	5.712	4.57
0.101	0.819	1.22	0.67	6.640	2.38
0.251	0.674	1.48	0.85	8.338	1.38
0.501	0.605	1.65	1.05	10.220	0.85
					1.173
					0.979

$$* x = \frac{ZF\psi_{\text{OHP}}}{2RT}$$

$$R^1 = (\alpha + R) / (\alpha + R - \alpha R)$$

Table 34

Summary of the quantities used to prepare Figure 27.

From the distribution isotherms at an activity of DPGH⁺ of 2.0 x 10⁻²

[Cl ⁻]	[Cl ⁻] _T	τ _{DPGH}	[DPGH] x 10 ⁺²	Γ _{DPGH} x 10 ⁺¹⁰	σ ₀ x 10 ⁺⁵	R' (%)	(c ^{1/2} sinhx*) ⁻¹ σ ₀ ⁻¹ x 10 ⁻⁵
0.0111	0.0341	0.871	2.30	0.56	0.597	11.11	3.409
0.0511	0.0752	0.830	2.41	0.76	0.775	6.44	2.438
0.101	0.126	0.813	2.46	0.88	0.881	3.69	1.987
0.251	0.281	0.668	2.99	1.08	1.069	2.30	1.437
0.501	0.534	0.606	3.33	1.30	1.272	1.48	1.093

* x = $\frac{ZF\Psi_{OHP}}{2RT}$

R' = (α + R) / (α + R - αR)

Table 35

Summary of the quantities used to prepare Figure 27.

From the distribution isotherms at an activity of

DPGH^\dagger of 3.0×10^{-2}

$[C]^-$	$[C]^-_T$	γ_{DPGH}	$[\text{DPGH}]$ $\times 10^{+2}$	\int_{DPGH} $\times 10^{+10}$	σ_o $\times 10^{+5}$	$R'(\%)$ $(c^{1/2} \frac{\sinh x^*}{x^*})^{-1} \sigma_o^{-1}$ $\times 10^{-5}$
0.0111	0.0460	0.856	3.51	0.69	0.741	12.13
0.0511	0.0875	0.825	3.64	0.90	0.928	6.78
0.101	0.138	0.810	3.70	1.03	1.040	4.70
0.251	0.296	0.663	4.52	1.25	1.245	3.07
0.501	0.551	0.598	5.02	1.47	1.449	2.01

$$x = \frac{ZF\Psi_{\text{OHP}}}{2RT}$$

$$R' = (\alpha + R) / (\alpha + R - \alpha R)$$

Table 36

Surface potentials and capacitances for the adsorption of DPGH⁺ on Amberlite XAD-2.

a_{DPGH}	ψ_0 (volt) $\times 10^3$		C_1 (farad/cm ²) $\times 10^6$	
	Isotherm ^a	Electrophoresis ^b	Isotherm ^a	Electrophoresis ^b
3.0×10^{-4}	32.0 \pm 4.2		161 \pm 92	
5.0×10^{-4}	39.4 \pm 2.7		161 \pm 47	
$1.0_0 \times 10^{-3}$	49.6 \pm 10.4	27.0 \pm 12.3	168 \pm 149	168 \pm 49
$3.0_0 \times 10^{-3}$	73.2 \pm 9.7		176 \pm 89	
$5.0_0 \times 10^{-3}$	86.9 \pm 12.8	33.2 \pm 35.2	172 \pm 88	283 \pm 196
$1.0_0 \times 10^{-2}$	102.5 \pm 8.4		192 \pm 52	
$2.0_0 \times 10^{-2}$	115.9 \pm 7.9	37.0 \pm 15.6	227 \pm 50	445 \pm 124
$3.0_0 \times 10^{-2}$	121.5 \pm 9.8		262 \pm 91	

a. Calculated from data in Figure 26 via equation 53.

b. Calculated from data in Figure 31 via equation 58.

constant as assumed in equation 53. Constancy of C_1 in the absence of specific adsorption of counterions has been observed for other surfaces including mercury (126) and rutile (146). The thickness of the compact double layer capacitor, δ , may be calculated from the average value of C_1 , assuming the dielectric constant to be that of pure water, by the equation:

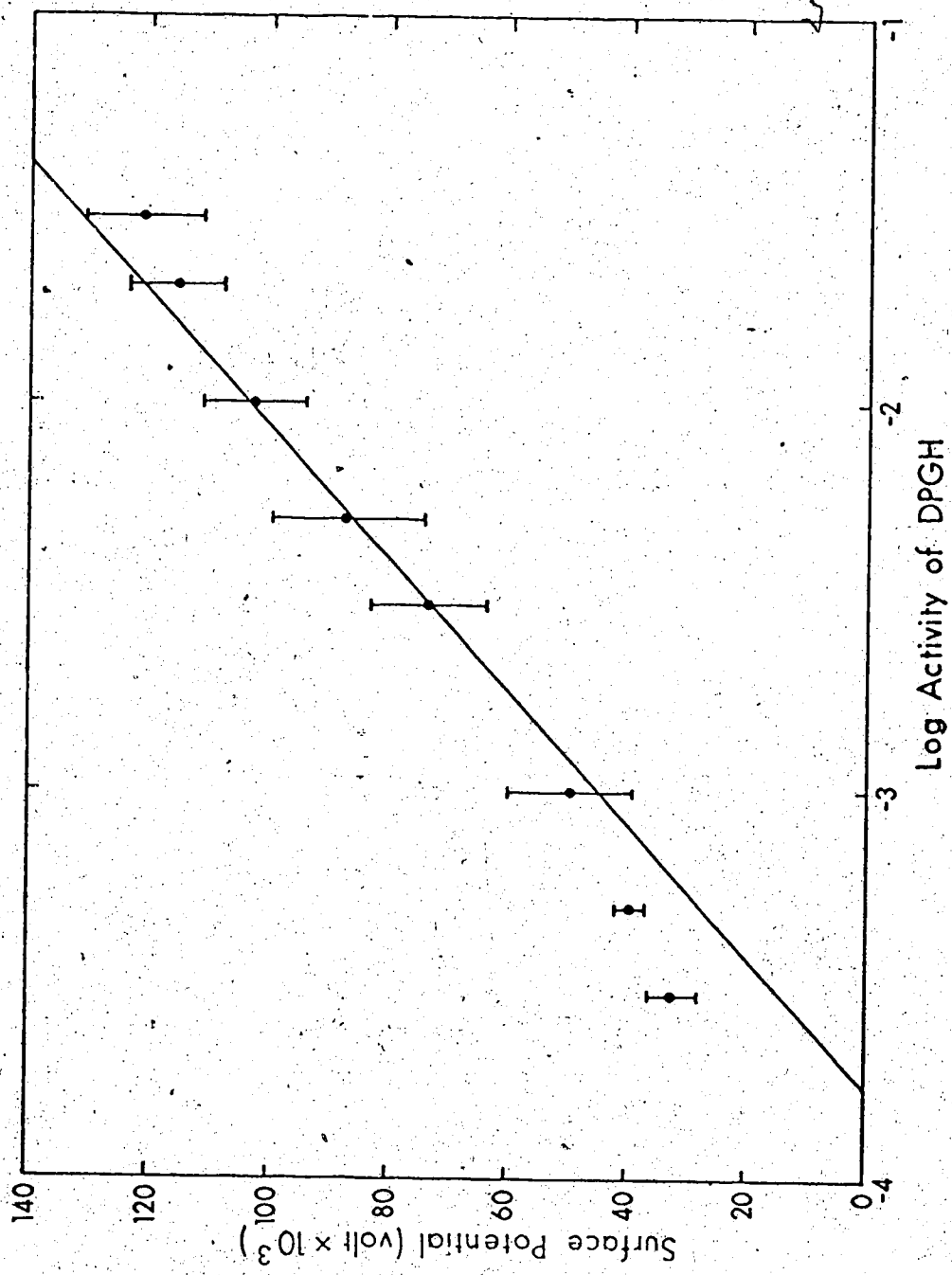
$$\delta = \frac{\epsilon}{4 C_1 \pi} \quad (72)$$

which yields a value of 3.7×10^{-8} cm, or 3.7 \AA . This is approximately equal to the radius of a hydrated chloride counterion (144).

Values of the surface potential obtained from the reciprocal slopes in Figure 27 are plotted against the log of the activity of potential-determining ion in Figure 28. Although it is not necessary that equation 35 apply to the system in order for equation 53 to be valid, it is interesting to note that the slope of the linear portion of the plot in Figure 28 is close to 0.0591 volt (shown as solid line) as predicted by equation 35. Deviations from linearity at low activities of DPGH^+ are probably due to the influence of another potential-determining ion.

Previous studies have shown that XAD-2 does adsorb H^+ and OH^- ions to a slight extent (7). If, in the dilute HCl solutions in which all isotherm measurements were made, the resin surface carries a small residual surface charge because of the adsorption of H^+ , then it will produce curvature in the plot in Figure 28 at low

Figure 28. Dependencies of surface potential (Ψ_0) on log of activity of potential-determining ion (DPGH^+). The line has a slope of 59.1 mv.



values of a_{DPGH} , analogous to the effect of an interfering ion on an ion-selective electrode.

4.2.2 Benzylammonium Ion (BZH^+)

Adsorption isotherms were also measured for benzylammonium ion (BZH^+) in the presence of a large excess of HBr. They were calculated from chromatographic retention volumes. In Figure 29 adjusted retention volumes of BZH^+ are plotted against $[\text{Br}]$ in the mobile phase for six different amounts of BZH^+ injected onto the column. The concentrations of BZH^+ injected vary from 5.04×10^{-3} to 1.08×10^{-1} M. At each fixed concentration of HBr (i.e. $[\text{Br}]$), the concentration of BZH^+ in the aqueous phase and the surface excess of BZH^+ can be calculated. The concentration of BZH^+ in the aqueous phase is taken as the moles of BZH^+ in that phase divided by the column void volume, V_M , in liters and is given by the expression:

$$[\text{BZH}^+] = \frac{T_{\text{BZH}^+}}{V_R} \quad (73)$$

where T_{BZH^+} is the total moles of BZH^+ injected onto the column and V_R is the retention volume of BZH^+ in liters. The surface excess of BZH^+ in moles per cm^2 is given by:

$$\Gamma_{\text{BZH}} = \frac{T_{\text{BZH}^+} \cdot V_N}{3.30 \times 10^9 \cdot W \cdot V_R} \quad (74)$$

where W is the weight of resin in the column in kg; the numerical constant is the specific surface area in cm^2/kg , and V_N is the adjusted retention volume in liters given by:

$$V_N = V_R - V_M \quad (75)$$

Chromatographic peak shapes for BZH^+ all showed some tailing. When the amount of BZH^+ injected was small and the HBr concentration high the tailing was only slight and the peaks nearly symmetrical. The most severe tailing occurred when the amount of BZH^+ injected was large and the HBr concentration was small. In all cases, the retention volume was taken, not at the peak maximum, but at its "centre of gravity" (i.e. the volume of eluate which divides the area of the peak in half). The distribution isotherms, plotted as Γ_{BZH} versus $[\text{BZH}^+]$ (not shown), were more or less slightly curved. Since the sample-loading of the resin in the chromatographic experiments involving BZH^+ was far below that encountered in the batch equilibration studies involving DPGH^+ , such nearly-linear isotherms might be expected for the former (see discussion in Section 4.5, below).

Since the values of $[\text{BZH}^+]$ and Γ_{BZH} cover a very wide range it is more convenient to have Γ_{BZH} and $[\text{BZH}^+]$ in a log-log scale rather than in a linear plot. These distribution isotherms are shown in Figure 30. The isotherm data for BZH^+ are treated in the same manner as that described above for DPGH^+ in order to obtain the plot shown in Figure 31. The lines are fitted by linear least

Figure 129.

Adjusted retention volume for six different concentrations of benzylammonium ion at various total bromide concentrations on a 0.28 x 30-cm. column.

Curve no.	1	2	3	4	5	6
Moles of BZH ⁺ injected	5.04 $\times 10^{-9}$	1.08 $\times 10^{-8}$	5.04 $\times 10^{-8}$	1.08 $\times 10^{-7}$	5.04 $\times 10^{-7}$	1.08 $\times 10^{-6}$

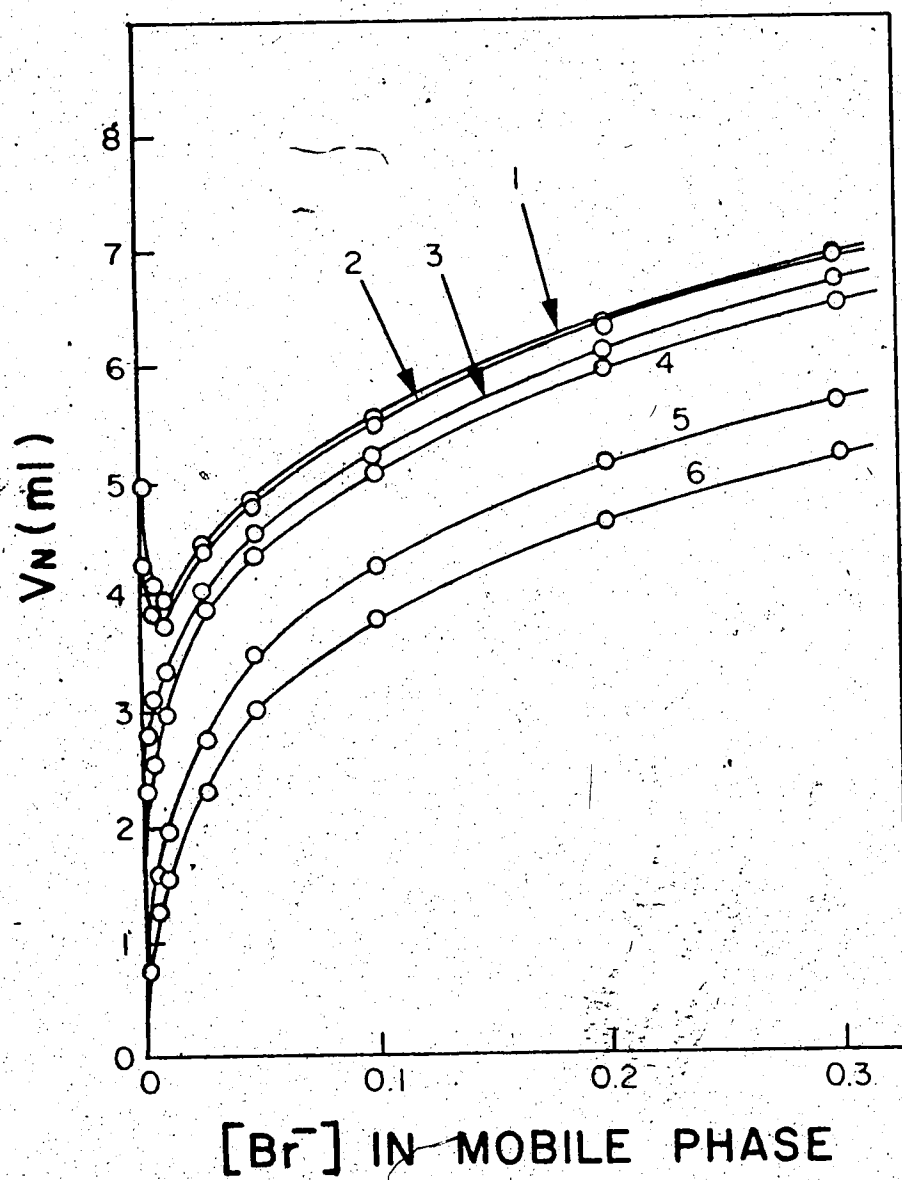
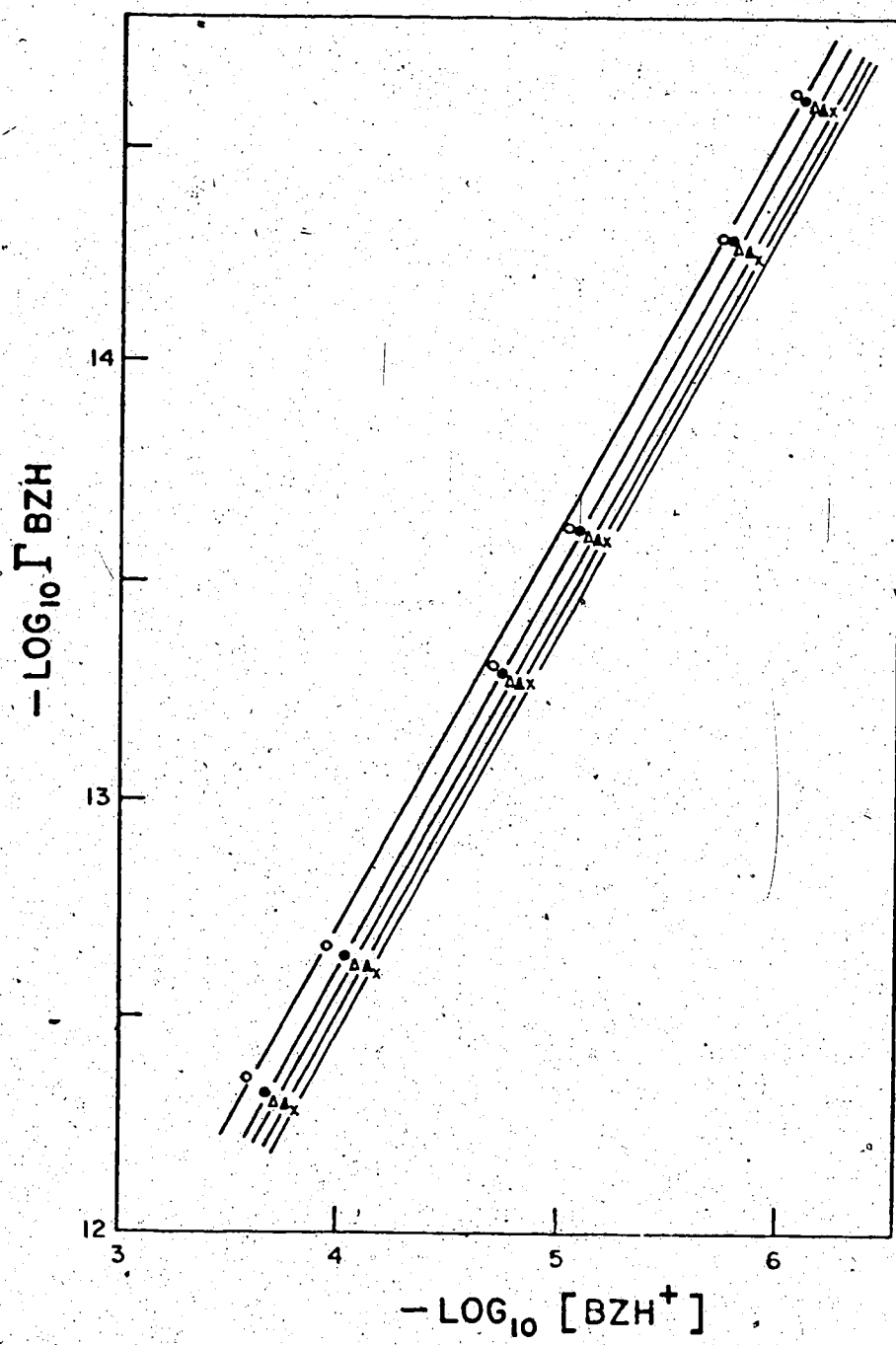


Figure 30. Dependence of the experimental surface charge on the concentration of benzylammonium ion in the aqueous phase at five different total bromide concentrations.

Symbol	Total bromide concentration
o	0.029
•	0.062
Δ	0.098
▲	0.18
x	0.29



squares. In this case the values of Ψ_{OHP} are so low that the bracketed quantity in equation 53 is always equal to 1. Also, the large excess of HBr means that equation 71 can be used in place of equation 69 with negligible error. Table 37 summarizes surface potentials and capacitances along with their 95 percent confidence intervals. As predicted by equation 53, C_1 is essentially constant. The linear relationship between Ψ_0 and $\log(a_{\text{BZH}^+})$ predicted by equation 35 is not observed, which is not surprising since the activities of BZH^+ are very low and the effect of an interfering potential-determining ion would be pronounced. It should be noted that the surface charge, σ_0 , in equation 53 should include the contribution of all adsorbed potential-determining ions. Since only the adsorbed BZH^+ ions are used in the above calculations, the surface potential calculated from equation 53 will be in error if another type of potential-determining ion is also adsorbed. For this reason the absolute values of Ψ_0 in Table 37 will be in error (the same would be true of potentials calculated in the non-Nernstian region of Figure 27 for DPGH^+ adsorption). The fact that values of C_1 observed for BZH^+ are somewhat lower than for DPGH^+ may reflect a difference in the influence of either H^+ , BZH^+ or Br^- on the double layer, compared to Na^+ , DPGH^+ , or Cl^- (see Section 4.4, below).

Figure 31. Adsorption data for benzylammonium ion according to the SGC equation 53 at four surface potentials. The numbers at the end of the lines are the activities of BZH^+ at which the calculations were made.

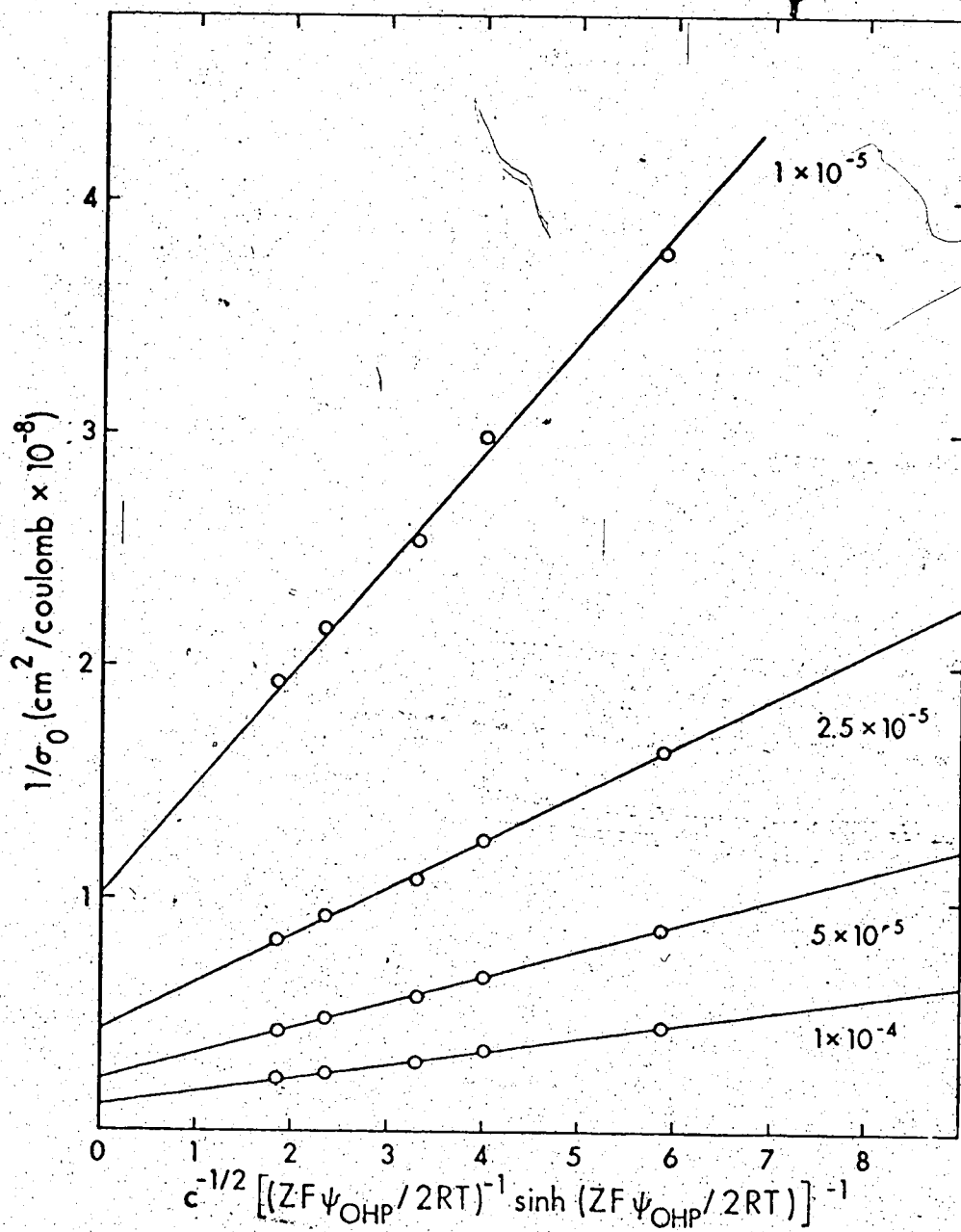


Table 37

Surface potentials and capacitances for the adsorption of BZH^+ on Amberlite XAD-2^a.

a_{BZH}	$-\psi_0(\text{volt}) \times 10^3$	$C_1(\text{farad}/\text{cm}^2) \times 10^6$
1.00×10^{-5}	0.086 ± 0.02	115 ± 76
2.50×10^{-5}	0.21 ± 0.05	106 ± 73
5.00×10^{-5}	0.38 ± 0.09	105 ± 67
1.00×10^{-4}	0.72 ± 0.16	104 ± 63

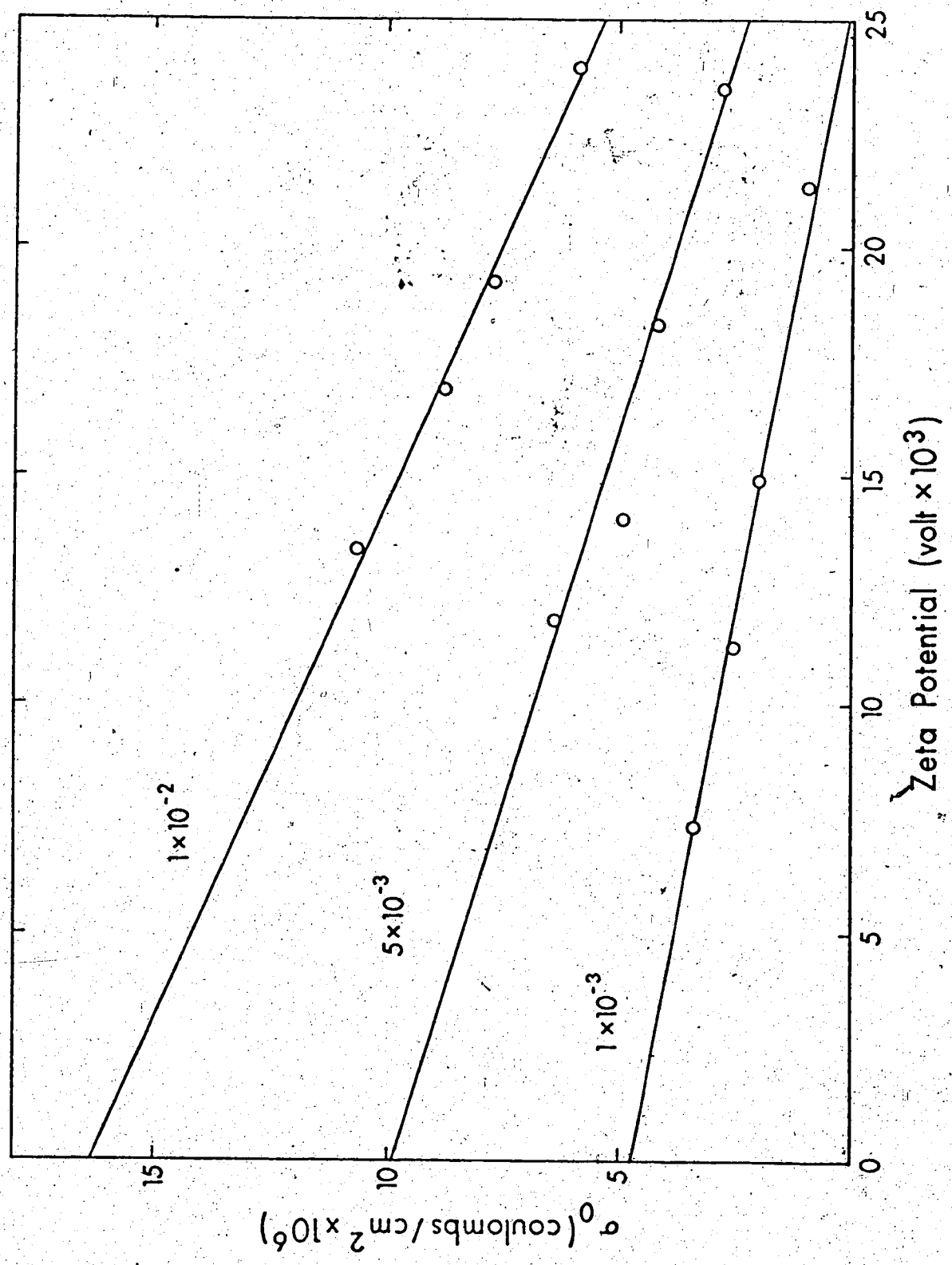
a. Calculated from data in Figure 30 via equation 53.

4.3 Microelectrophoresis

If the behavior of XAD-2 resins can be described by SGC theory, then the resin particle will be charged in the presence of a potential determining ion. This charged particle will migrate in an externally applied electrical potential gradient. The direction of the movement is towards the electrode that is opposite to the charge carried by the resin. Particles of XAD-2 resin will not migrate if there are no potential determining ions present in the solution. This was verified by observing XAD-2 resin in a microelectrophoresis apparatus at several different chloride concentrations in the absence of DPGH^+ .

In order to test equation 58, microelectrophoresis experiments were performed at three different a_{DPGH^+} at various electrolyte concentrations. Values of σ_0 , calculated from the results of the isotherm studies, are plotted in Figure 32 against ζ , obtained from microelectrophoresis measurements. Values of ψ_0 and C_1 calculated from intercepts and slopes of the linear least square lines are given in the third and fifth column of Table 36, along with their 95 percent confidence intervals. Equation 58 predicts parallel straight lines for measurements made at different ψ_0 (i.e. at different a_{DPGH^+}). Although straight lines are obtained, they are not parallel. Uncertainties in ψ_0 values are larger than those for C_1 in this case because C_1 includes only that of the slope, while ψ_0

Figure 32. Dependence of zeta potential of XAD-2 particles on surface charge due to adsorbed diphenylguanidinium ion plotted according to equation 58. The numbers by the lines are the activities of DPGH^+ at which the measurements were made.



uncertainties of both slope and intercept, with the intercept obtained by a long extrapolation. It was impractical to make microelectrophoresis measurements at lower ζ because of the slow electromigration rates of the particles. In general, the surface potentials calculated from the microelectrophoresis measurements are lower than those from the isotherm measurements, and this discrepancy becomes more pronounced at higher surface potentials. Also, the value of C_1 calculated from electrophoresis measurements increases with increasing surface-potential. These deviations from the predictions of equation 58 may be explained in terms of the inaccuracies of the assumptions implicit in that equation:

(i) The assumption that the "plane of shear" coincides with the OHP is inaccurate (124,127). It is more likely that the "plane of shear" lies somewhat farther away from the surface (Figure 24) because water molecules in the primary hydration spheres of counterions lying in the OHP will probably be part of the migrating unit, and the locus of the charge centers of these ions defines the OHP. In addition, the surface of the XAD-2 particle is not smooth, but highly porous (25), so that some of the water beyond the OHP adjacent to surfaces in the "crevasses" may move with the particle and thereby effectively extend the "plane of shear" well beyond the OHP. If the "plane of shear" lies beyond the OHP then potentials will be smaller than the corresponding ψ_{OHP} calculated from the isotherm studies. Consequently, ψ_0 calculated from equation 58 will be too low. (ii) The Helmholtz-Smoluchowski equation neglects local phenomena that may be operative in the

double layer region and therefore, for some systems, the relationship between ζ and electrophoretic mobility given by equation 55 will be in error (123,125,127). Because of these uncertainties in interpreting electrophoretic data, Bier (147) advises caution in identifying potentials obtained from electrophoresis with those derived from adsorption measurements. Errors in ζ are greater at higher ζ and higher σ_0 . This observation is consistent with the results of the present study in which the discrepancies between values obtained from isotherm and electrophoresis measurements are greater for the curves lying at higher σ_0 and ζ .

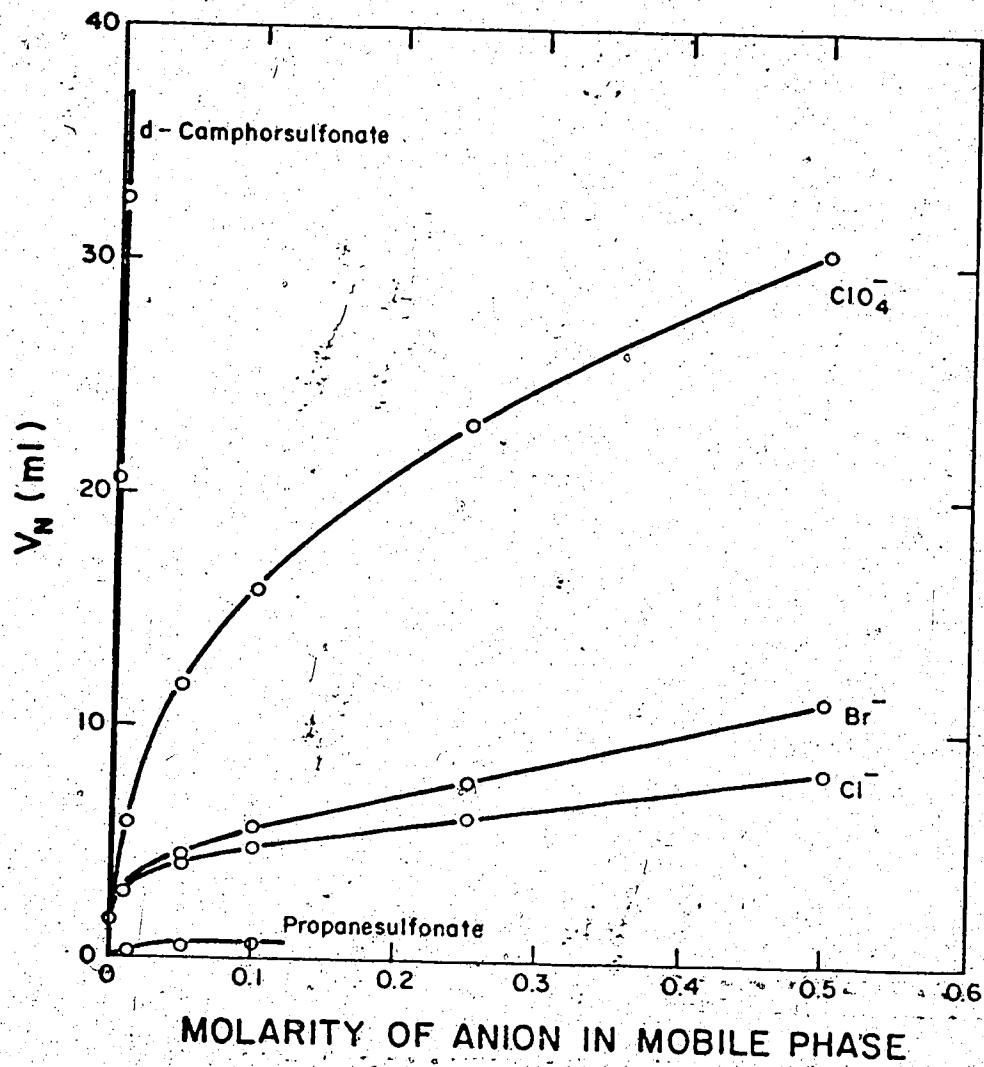
The electrophoretic behavior of XAD-2 in the presence of DPGH^+ provides unequivocal evidence that the resin acquires a charge when it adsorbs DPGH^+ ions and, therefore, rules out an ion pair retention mechanism. This at least semiquantitative corroboration of the results obtained in the isotherm studies by the totally different experimental technique of microelectrophoresis provides strong support for the SGC view of adsorption of ions on XAD-2.

4.4 Effect of the Different Counterions on Chromatographic Behavior

Ionic sample species, identified as potential determining ions, are adsorbed more strongly in the presence of some counterions than others. Thus their chromatographic retention times can be controlled by changing the type as well as the concentration of electrolyte in the mobile phase. Examples of this are shown in Figure 33 where adjusted retention volumes for benzylammonium ion are plotted against anion concentrations in the mobile phase for the anions propane-sulfonate, chloride, bromide, perchlorate and d-camphorsulfonate. At a given anion concentration the adjusted retention volume, and therefore the fraction of BZH^+ adsorbed on the resin, increases with anion type in the order given. The mechanistic interpretation of this dependence of degree of adsorption of potential-determining ion on counterion type has not been experimentally investigated in the present study. However, there are several alternative explanations of the phenomenon which are consistent with the SGC theory and these will be briefly outlined below. The discussion will be restricted to the counterions Cl^- , Br^- and ClO_4^- for which data such as crystal radii are readily available. The possible mode of action of d-camphor-sulfonate will be discussed later.

If the capacitances of the compact and diffuse parts of the double layer are higher in the presence of counterions in the order $Cl^- < Br^- < ClO_4^-$, then σ_0 would be larger for a given value of Ψ_0 (equation 48). The influence of anion type on C_1 can arise from either a decrease in the distance between the charge surface and

Figure 33. Effect of counterion type in the mobile phase on the adjusted retention volume of benzylammonium ion on a 0.28 x 30-cm column of XAD-2. Moles of BZH^+ injected was 1.08×10^{-7} . (A 0.28 x 5 cm column was used for of d-camphorsulfonate.)



OHP or an increase in ϵ . Since the hydrated radius of ClO_4^- is actually slightly larger than that of Br^- and Cl^- (144), a decrease in capacitor thickness might seem an unlikely explanation. On the other hand, anions with larger crystal radii have greater polarizabilities than smaller ones and the shift of the charge centre of an anion situated in the OHP toward the charge surface as a result of polarization would be greater for more polarizable anions. Thus, for counterions with similar hydrated radii (true for Cl^- , Br^- , ClO_4^-) the ones with greater polarizability would have their charge centres, and therefore their OHP, closer to the charge surface on the resin, and would consequently have a larger C_1 . Similar polarizability arguments have been suggested to explain selectivity sequences in synthetic ion exchange resins (148).

In all calculations performed above ϵ was assumed to have the value of pure water, i.e. 8.77×10^{-11} . This may be an oversimplification, since the dielectric constant of water very close to an ion can be significantly lower than that of bulk water, and it is this "local" dielectric constant in the double layer which should be used in SGC calculations. The orientation of water dipoles about an ion can lead to "dielectric saturation" in the primary hydration layer and a resultant low value for the dielectric constant.

Although this effect is generally considered to be slight around anions as compared to cations (122,145), it may not be completely negligible and, if present, would be more pronounced for anions with a smaller crystal radius. Thus the local dielectric constant and the capacitance would increase in the order $\text{Cl}^- < \text{Br}^- < \text{ClO}_4^-$.

Another possible explanation of the specific anion effect is related to the fact that adsorption of a potential-determining ion onto the resin surface must be accompanied by an increased concentration of counterion in the double layer. Therefore counterions whose transfer from the bulk solution into the double layer is accompanied by the greater negative (or smaller positive) free energy change will promote greater adsorption of the potential-determining ion. If one assumes that, because of crowding of ions in the double layer, they will be less hydrated than in the bulk solution, then one might expect that counterions with lower hydration energies would be more readily transferred from the bulk to the double layer solution. A related phenomenon, which has been observed, is the tendency of ions with smaller hydration energies to seek positions at the interface between air and water (122,149,150). The observed sequence is $Cl^- < Br^- < ClO_4^-$, which is the same order as the ionic hydration energies (145).

Adsorption of organic ions onto XAD-2 from water is accompanied by a positive entropy change (28). This suggests a fourth explanation for the specific anion effect. Water adjacent to a hydrophobic surface would be more structured or less random than water in the bulk solution, just as water around dissolved non-polar molecules is more ordered (151). When the adsorbed ions and accompanying counterions are transferred from the bulk solution into the double layer region this water structure is disrupted. The greater the "chaotropic" (151) or "water structure breaking" (145) character of the ions, the more pronounced will

be the disordering effect and the greater will be the positive entropy change. It is well documented that "structure-breaking" character increases in the order $\text{Cl}^- < \text{Br}^- < \text{ClO}_4^-$.

A fifth possible interpretation of the specific anion effect is also suggested by the SGC theory. If specific adsorption of counterions occurs so that an "Inner Helmholtz Plane" is formed, the counterions in the IHP neutralize an equivalent number of potential-determining ions on the surface. This results in a large surface concentration of potential-determining ions for a given ψ_0 and a_j , or in other words, enhanced adsorption of potential-determining ions. Although the present study suggests the absence of specific adsorption of chloride ion, it is possible that the less hydrated and more polarizable bromide and perchlorate ions are adsorbed to some extent. Formally, specific adsorption of counterions is analogous to "ion pair" formation between the potential-determining ion and the counterion, and it is generally observed that the extraction of ion pairs involving organic cations into an organic solvent is greater for counterions in the order $\text{Cl}^- < \text{Br}^- < \text{ClO}_4^-$ (152).

Although the present study does not provide sufficient evidence to distinguish which of the above mechanisms are responsible for the specific anion effects of these small inorganic ions, it is possible to predict from the SGC theory how the adsorption behavior will change with more drastic changes in the nature of cation and anion. In the present case where large organic cations and relatively small inorganic anions are used,

it is seen that the former are adsorbed as potential-determining ions while the latter occupy only the diffuse part of the double layer. If the small inorganic anion were replaced with a somewhat larger organic one, then specific adsorption of the anions into the IHP would occur. Using both a large cation and anion would produce the third situation, in which both ions are adsorbed onto the resin as potential-determining ions. The role of camphorsulfonate might be interpreted in terms of either of these latter two phenomena. Then, reversing the trend, if a large organic anion were used with a smaller organic or inorganic cation, only the anion would be adsorbed as potential-determining ion and the cation would serve as counterion. As an example of this latter case, experiments in this laboratory have shown that the adsorption of organic anions onto XAD-2 is greater the higher the concentration of sodium chloride in the aqueous phase. Also, the adsorption is greater from solutions containing KCl than from those containing an equal concentration of NaCl.

4.5 Chromatographic Behavior and the Effect of TBA⁺ on the Retention of Ionic Species

According to the SGC theory retention of an ionic species is related to the surface potential Ψ_0 of the XAD-2 resin adsorbent. This surface potential is solely determined by the activity of the potential determining ions in the bulk solution. If more than one kind of potential determining ion is present in the bulk solution, then the surface potential will be depend on all the potential determining ions present. The effect of such a situation on the chromatographic retention volume of a sample ion can be understood in terms of the following considerations. The free energy for the adsorption of a sample species onto the resin can be represented as (153,154) :

$$\Delta G = \Delta G_{\text{elec.}} + \Delta G_{\text{spec.}} \quad (76)$$

The first term on the right hand side of the above equation takes into account the electrostatic contribution to the adsorption free energy. This term is equal to zero for a neutral species. The second term includes all the chemical forces such as van der Waal's force. The chromatographic behavior of a neutral species depends solely on this term. At low sample concentrations a symmetrical peak is often obtained. For ionic samples, the retention mechanism depends on both terms. The equilibrium constant, K_s , for adsorption of an ion from solution onto the resin is related to the value of

$\Delta G :$

$$K = \exp \left(- \frac{\Delta G_{\text{elec.}} + \Delta G_{\text{spec.}}}{RT} \right)$$

$$= \exp \left(- ZF\psi_0/RT \right) \cdot \exp \left(- \Delta G_{\text{spec.}}/RT \right) \quad (77)$$

Since ψ_0 varies with the concentration of potential determining ion in bulk solution, it is evident that the equilibrium constant for adsorption would not be constant for an ionic sample adsorbed on the resin and its adsorption isotherm would not be linear.

However, if ψ_0 becomes nearly independent of the concentration (or, activity) of sample ion because of the presence of a second potential determining ion, then ΔG and the equilibrium constant becomes constant and, at low surface coverage of the sample species, a linear isotherm is obtained. A trend toward reduced dependence of ψ_0 on a_{DPGH^+} is evident at low a_{DPGH^+} in Figure 28 and is even more pronounced in the case of BZH^+ . The effect can be greatly amplified by adding to the mobile phase a relatively high concentration of a large cation such as tetra-n-butylammonium ion. Such an ion would be sorbed on the surface as a potential determining ion and, because of its relatively high concentration, would be mainly responsible for establishing ψ_0 , making ψ_0 essentially independent of a_{DPGH^+} . The influence of this quaternary ammonium cation on the adsorption isotherm of DPGH^+ can be seen in Figure 12, Part I of this work where the added quaternary cation reduces the slope of the isotherm and causes it to be linear to higher $[\text{DPGH}^+]$. The reduced slope results from the fact that ψ_0 , though constant because of the relatively high and constant activity of quaternary,

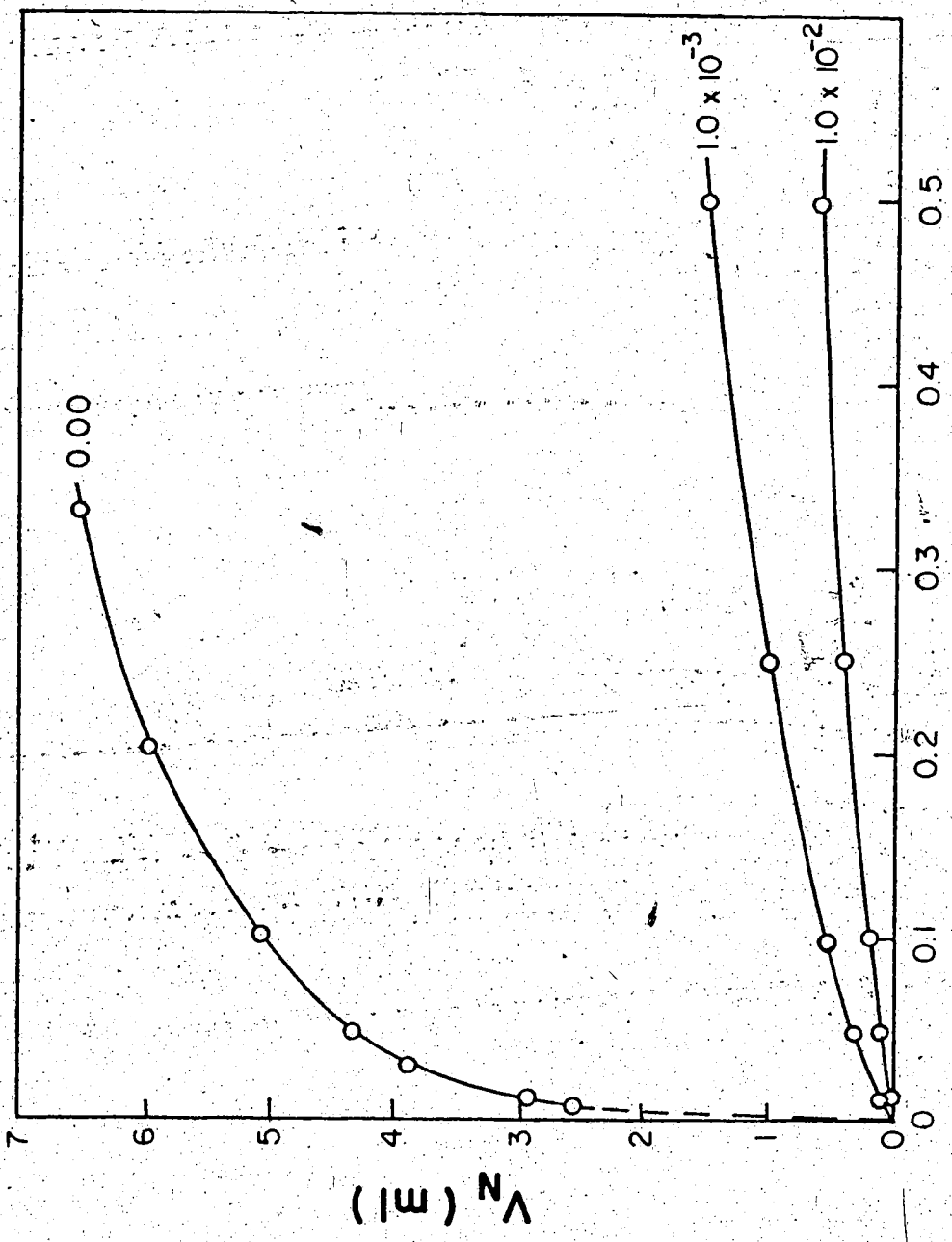
has a larger value than it would in the absence of quaternary, and therefore produces a lower value of K . A still higher concentration of quaternary would reduce K even more.

On the other hand, it was also seen in Part I that the added quaternary has negligible effect on the base. The value of a nonionic species would be independent of surface potential as discussed above (see also Section 4.6, below).

The influence of added TBABr on the chromatographic retention of several organic cations was studied. The behavior of BZH^+ is shown in Figure 34. The adjusted retention volume is plotted against total bromide concentration. Curve A is the result obtained in the absence of TBABr in the mobile phase, while curves B and C correspond to concentrations of 1.01×10^{-3} and 1.01×10^{-2} M TBABr respectively. At a given total bromide concentration the adjusted retention is greatly reduced in the presence of TBABr. Figures 35 and 36 are similar plots for codeinium ion and $DPGH^+$. In the absence of TBABr, the retention times of both of these species are too large to be measured practically.

The data for $DPGH^+$ shown in Figure 36 has been evaluated in more detail as follows: The dependence of log of the adjusted retention volume of $DPGH^+$ on the log of the concentration of quaternary ammonium ion in the mobile phase is given in Figure 37 for five different total concentrations of bromide ion. The bromide concentration was maintained constant for the three points on each curve by the addition of hydrobromic acid. The ionic strength is constant for any given curve, so that a linear relationship could

Figure 34. Adjusted retention volume of benzylammonium ion versus total electrolyte concentration in the mobile phase at three different concentrations of tetra-n-butylammonium bromide, on a 0.28 x 30-cm column of XAD-2. The numbers by the curves are molarity of the quaternary ammonium ion. Moles of BZH^+ injected was 1.08×10^{-7} . Total $[Br^-]$ adjusted with HBr.



MOLARITY OF TOTAL BROMIDE IN MOBILE PHASE

Figure 35. . . Adjusted retention volume of codeinium ion versus total electrolyte concentration in the mobile phase at three different concentrations of tetra-n-butylammonium bromide, on a 0.28 x 30-cm column of XAD-2. The numbers by the curves are molarity of the quaternary ammonium ion. Moles of codeinium injected was 2.61×10^{-8} . Total $[\text{Br}^-]$ adjusted with HBr.

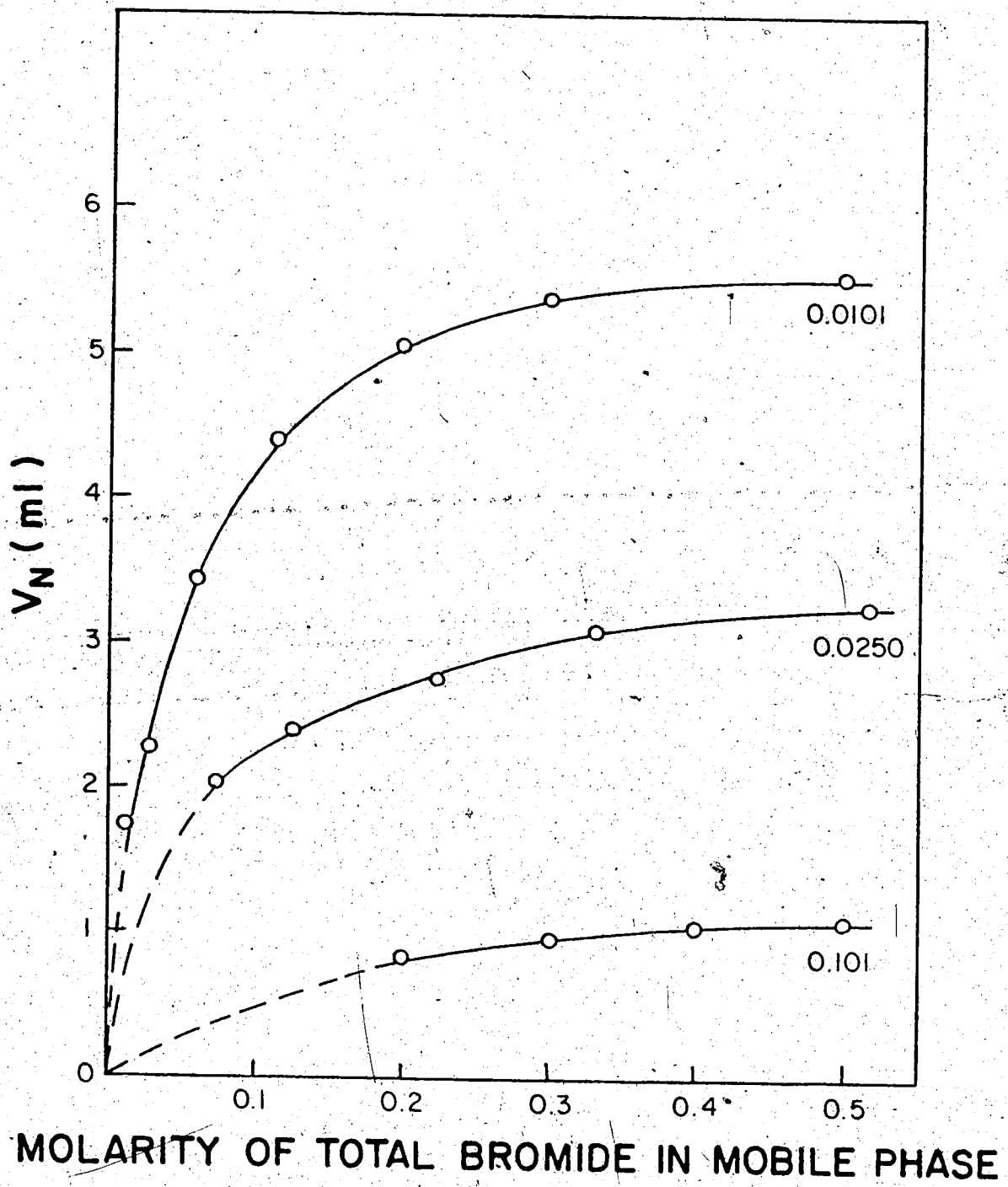


Figure 36. Adjusted retention volume of diphenylguanidinium ion versus total electrolyte concentration in the mobile phase at three different concentrations of tetra-n-butylammonium bromide, on a 0.28 x 30-cm column of XAD-2. The numbers by the curves are molarity of the quaternary ammonium ion. Moles of DPGH^+ injected was 4.3×10^{-8} . Total $[\text{Br}^-]$ adjusted with HBr.

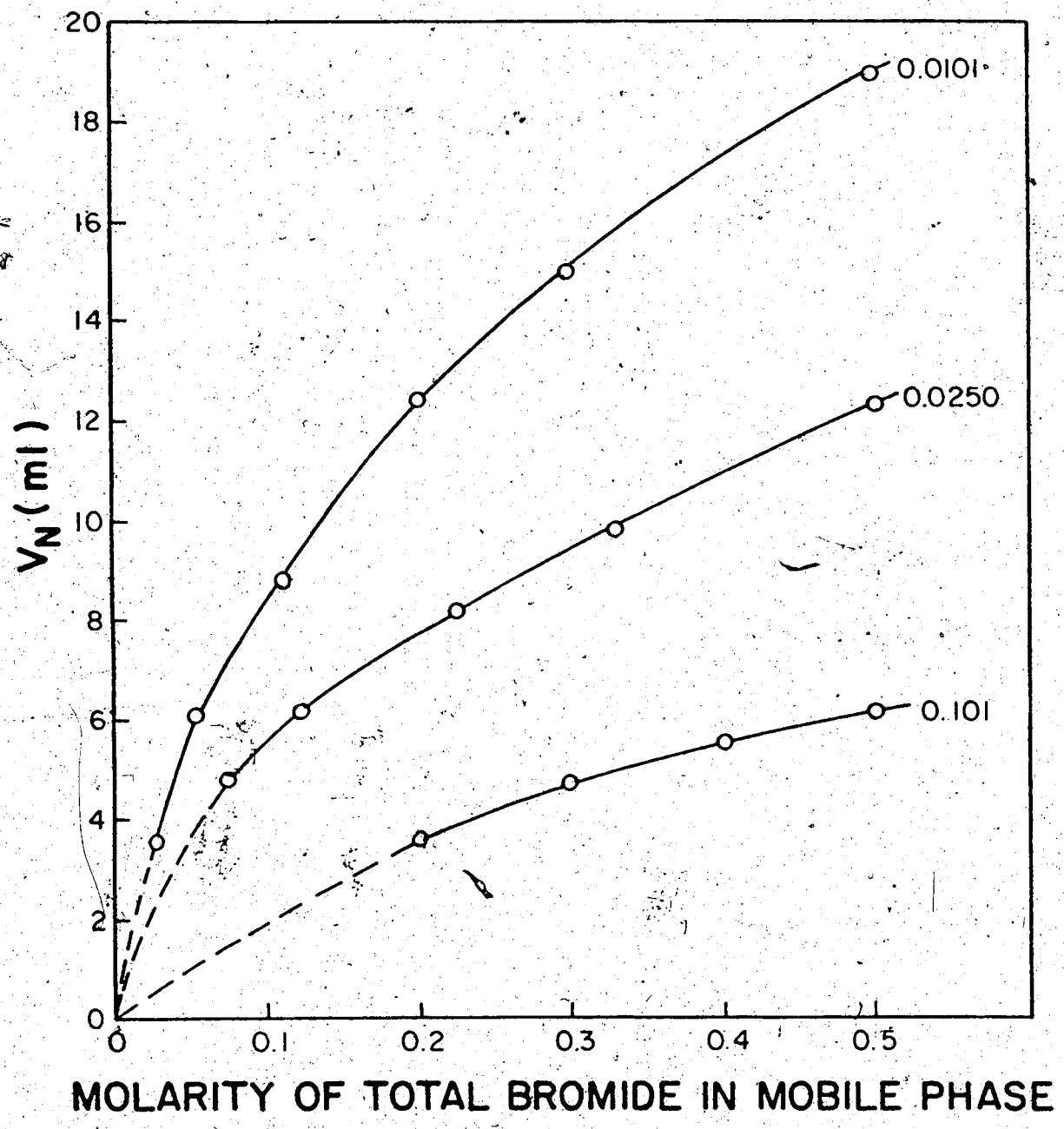
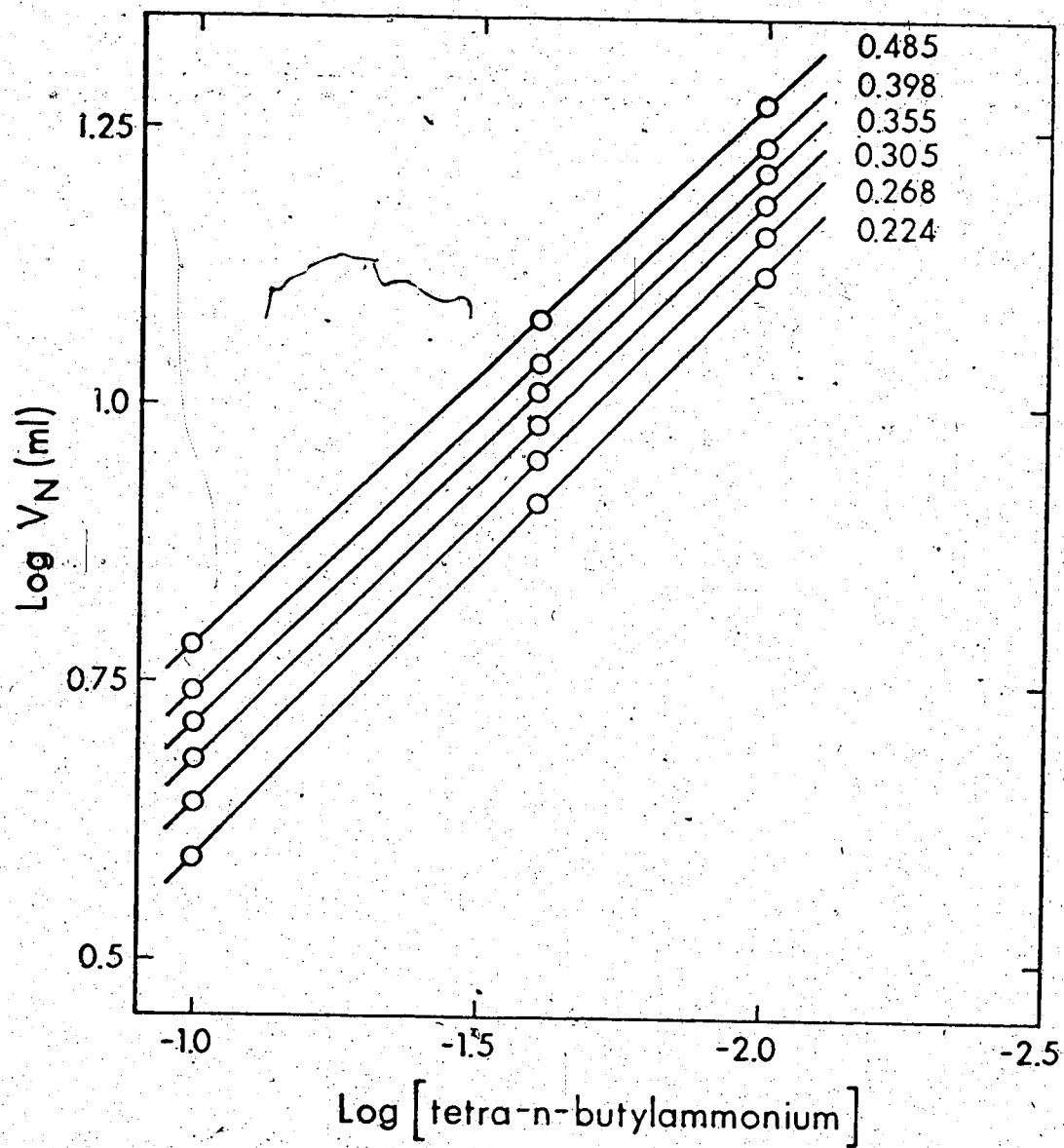


Figure 37. Dependence of adjusted retention volume of diphenylguanidinium ion versus concentration of tetra-n-butylammonium ion in the mobile phase at various total bromide concentrations on a 0.28 x 30-cm column of XAD-2. The numbers at the end of the curves are the total bromide concentrations. Moles of DPGH^+ injected was 4.3×10^{-8} .



be expected if the surface potential were related to activity of quaternary via a Nernst equation, since $\log K$ in equation 77 would vary as the log of the activity of quaternary, and V_N is directly proportional to K . For a constant ionic strength, bulk solution activity coefficients are constant so that a linear relationship is predicted between $\log V_N$ and $\log [TBA^+]$. This is observed in the plots in Figure 37.

The SGC model of the electrical double layer around a particle is analogous to the Debye-Huckel model of the ionic atmosphere around an ion (123), and the role of electrolyte concentration, c , in the two models is also analogous. Thus, the reciprocal square root dependence of σ_0 on c , which is seen in equation 53, may be considered to be analogous to the square root dependence on c of the activity coefficient of an ion in solution. This dependence prevails whether or not the adsorbed ion of interest is the principal potential-determining ion in solution. In chromatography one is interested in the dependence of adjusted retention volume on c . This dependence can be predicted from the SGC model as follows: Rearranging equations 74 and 75 for the case of $DPGH^+$ gives:

$$\frac{1}{V_{N,DPGH}} = \frac{T_{DPGH}}{\Gamma_{DPGH} \cdot 3.30 \times 10^9 \cdot W \cdot V_M} - \frac{1}{V_M} \quad (78)$$

Assuming the presence of a large excess of inert electrolyte and also assuming that Ψ_0 is independent of a_{DPGH} , Γ_{DPGH} is related to σ_0 by equation 71. The bracketed quantity in the denominator

of equation 53 has a value close to one at all but fairly high Ψ_{OHP} and may be taken as equal to one. Thus, equation 53 can be rewritten as:

$$\frac{1}{V_{\text{DPGH}}} = \frac{1}{k_1} + \frac{1}{c^{1/2} \cdot k_2} \quad (79)$$

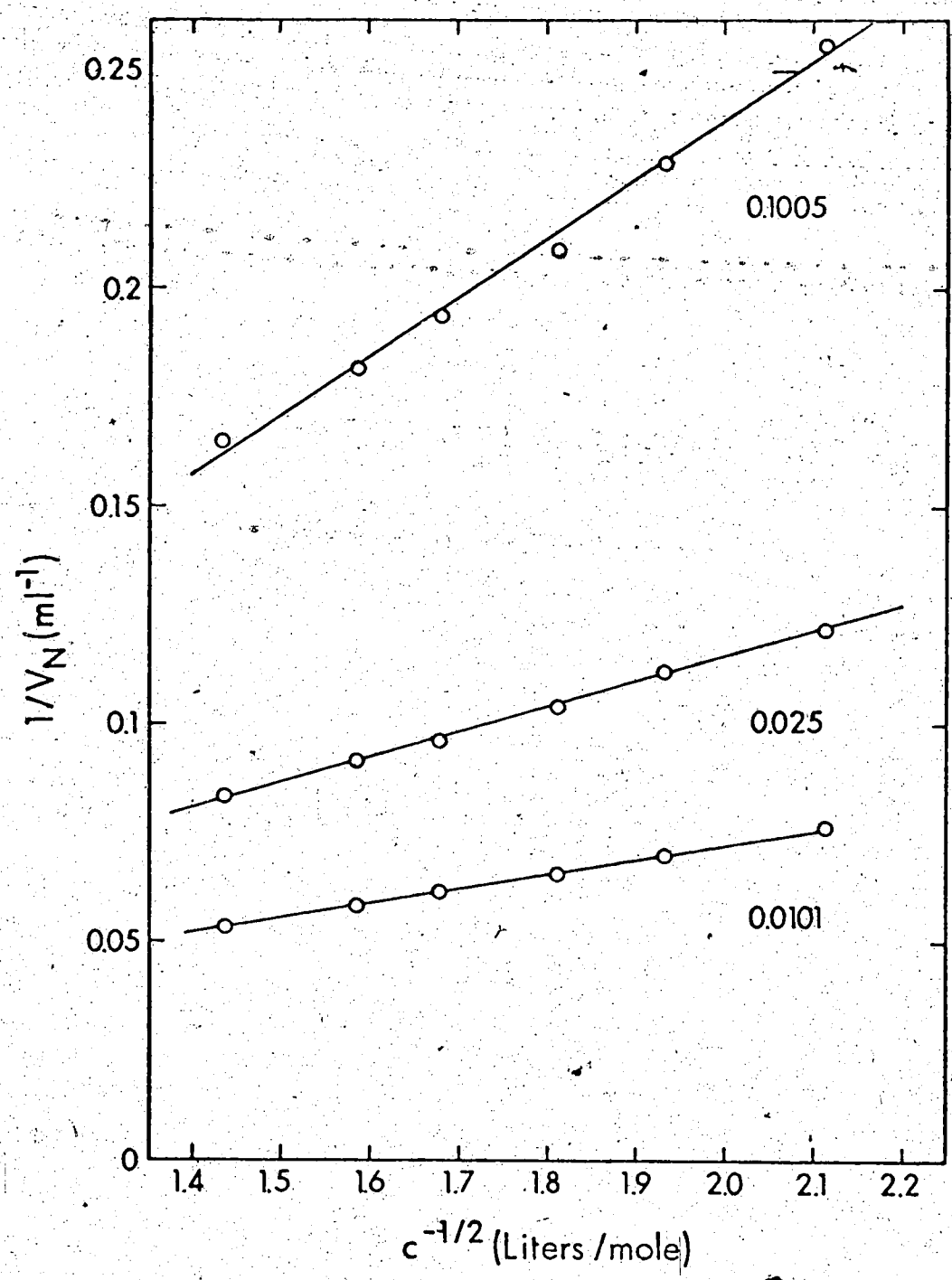
Combining equations 78 and 79 gives:

$$\frac{1}{V_{\text{N,DPGH}}} = \frac{1}{k_5} + \frac{1}{k_4 \cdot c^{1/2}} \quad (80)$$

where k_1 through k_5 are constants. Equation 80 predicts that $V_{\text{N,DPGH}}^{-1}$ will vary linearly with $c^{-1/2}$. Figure 38 shows such linear plots for the chromatography of DPGH^+ on XAD-2 using three sets of mobile phases, each of which contains a different large and constant excess of tetra-n-butylammonium bromide (The data for this figure are calculated from the plots in Figure 35).

It may be noted that if the mobile phase contains an electrolyte with a large anion and small inorganic cation, then the organic anion would be adsorbed on XAD-2 as potential-determining ion and would impart an essentially constant negative surface potential to it. With such a mobile phase the adsorption of a sample cation such as DPGH^+ would be greatly enhanced by virtue of the negative value of Ψ_0 . Chromatography in such a system would be analogous to "so-called" ion pair chromatography that has gained popularity on reversed-phase bonded phases (155).

Figure 38. Dependence of adjusted retention volume of diphenylguanidinium ion on the total electrolyte concentration in the mobile phase at three different concentrations of tetra-n-butylammonium bromide, on a 0.28 x 30-cm column of XAD-2. The numbers by the lines are molarity of the quaternary ammonium ion. Moles of DPGH^+ injected was 4.3×10^{-8} .



4.6 Chromatographic Behavior of a Neutral Species

So far, the discussion has centered mainly on the effect of solvent composition on the adsorption of ionic sample species. It is also of interest to examine the retention behavior of a neutral species. In Part I of this work, the distribution isotherm of diphenylguanidine base was reported. It yielded essentially the same distribution coefficient regardless of whether TBABr or sodium chloride was used as the swamping electrolyte. Acetaminophen is another example of a neutral species given here. This compound was chosen chiefly because its adsorption on XAD-2 is not strong and it can be eluted in a reasonably short retention volume. It is a fairly strong UV absorber. Figure 39 shows the distribution isotherms for acetaminophen obtained in batch equilibration experiments in the presence of various electrolyte concentrations. Despite the fact that NaCl concentration has been increased from 0.01 to 0.5 M it causes relatively little change in the distribution isotherm. This is much different from the result obtained for DPGH^+ shown in Figure 25. This illustrates that the retention mechanism of acetaminophen is not the same as for ionic species which can be described by the SGC model. The slight increase in adsorption at higher NaCl concentration is probably due to the salting out effect (130). That is, the solubility of acetaminophen decreases at higher NaCl concentration which leads to a stronger adsorption and a higher retention on the XAD-2 resin.

Figure 40 shows the chromatographic behavior of acetaminophen

Figure 39. Adsorption isotherms for acetaminophen in the presence of various bulk solution concentrations of sodium chloride.

Symbol	Chloride concentration
o	0.0110
●	0.0515
△	0.101
▲	0.252
x	0.503

4.6 Chromatographic Behavior of a Neutral Species

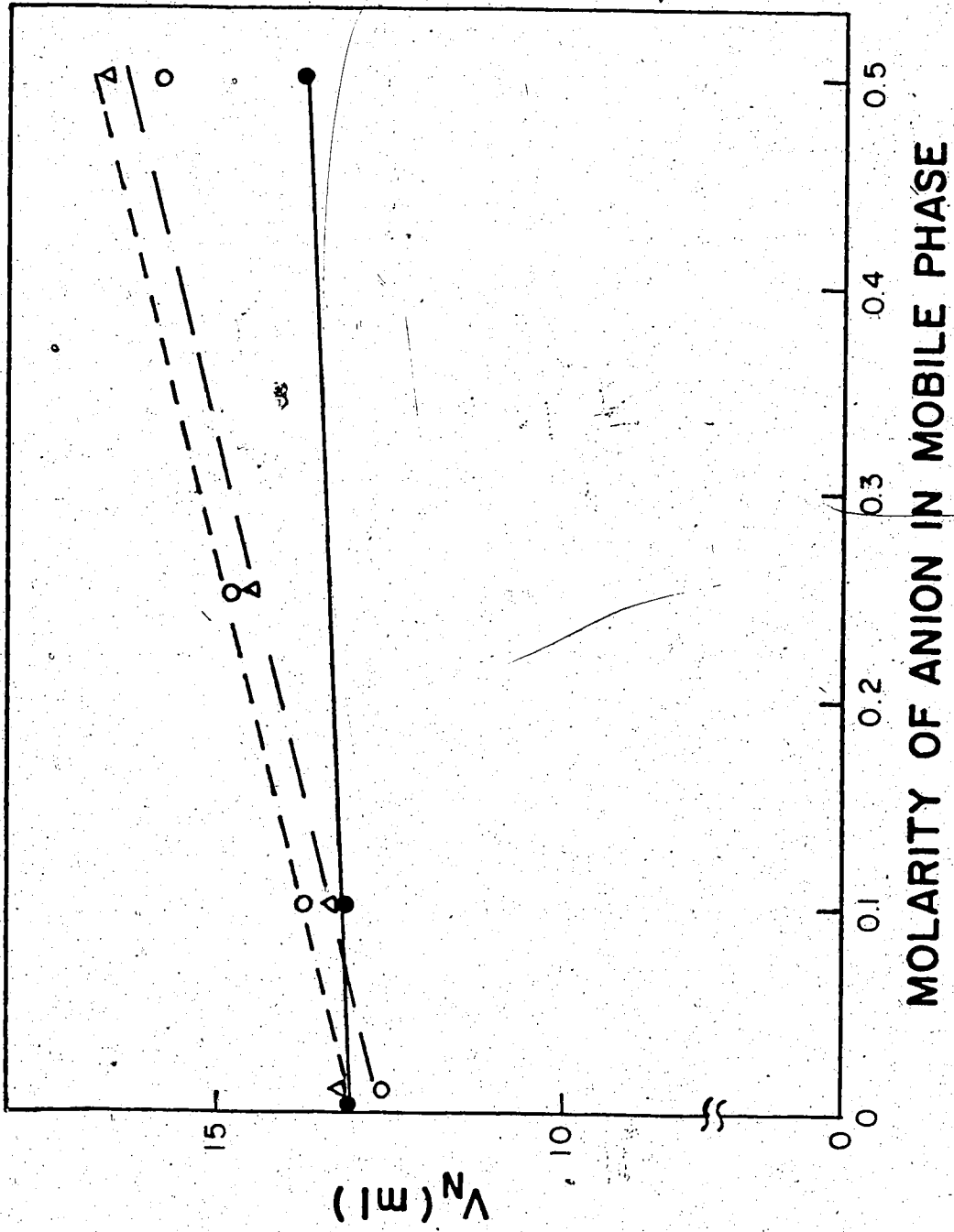
So far, the discussion has centered mainly on the effect of solvent composition on the adsorption of ionic sample species. It is also of interest to examine the retention behavior of a neutral species. In Part I of this work, the distribution isotherm of diphenylguanidine base was reported. It yielded essentially the same distribution coefficient regardless of whether TBABr or sodium chloride was used as the swamping electrolyte. Acetaminophen is another example of a neutral species given here. This compound was chosen chiefly because its adsorption on XAD-2 is not strong and it can be eluted in a reasonably short retention volume. It is a fairly strong UV absorber. Figure 39 shows the distribution isotherms for acetaminophen obtained in batch equilibration experiments in the presence of various electrolyte concentrations. Despite the fact that NaCl concentration has been increased from 0.01 to 0.5 M it causes relatively little change in the distribution isotherm. This is much different from the result obtained for DPGH⁺ shown in Figure 25. This illustrates that the retention mechanism of acetaminophen is not the same as for ionic species which can be described by the SGC model. The slight increase in adsorption at higher NaCl concentration is probably due to the salting out effect (130). That is, the solubility of acetaminophen decreases at higher NaCl concentration which leads to a stronger adsorption and a higher retention on the XAD-2 resin.

Figure 40 shows the chromatographic behavior of acetaminophen

as a function of electrolyte type and concentration. The adjusted retention volume is plotted against the electrolyte concentration. Three different electrolytes, NaCl, NaBr and NaClO₄, were used in this study. When NaClO₄ was used, the adjusted retention volume is almost unchanged over a wide concentration range up to 0.5 M. This agrees with a previous report from this laboratory (18). Sodium chloride and sodium bromide cause a slight increase in adjusted retention volume of acetaminophen which is probably the salting out effect.

Figure 40 Effect of counterion type in the mobile phase on the adjusted retention volume of acetaminophen, on a 0.28 x 30-cm column of XAD-2. Moles of acetaminophen injected was 6.72×10^{-8} .

Symbol	Counterion used
○	Bromide
△	Chloride
●	Perchlorate



5. CONCLUSIONS

The sorption of organic ions on Amberlite XAD-2 has been explained by a modified SGC model. This model shows that the electrical double layer surrounding a charged XAD-2 particle is responsible for the dependence of retention volumes of ions on such factors as electrolyte concentration, amount of sample and the presence of large adsorbable ions in the mobile phase. This electrical double layer model also applies to the adsorption of an ionic sample.

The SGC model will presumably apply to the adsorption of ionic samples on other nonionic adsorbents such as Amberlite XAD-7 and graphitized carbon. The use of mixed aqueous-organic solvents as mobile phase (e.g. water-methanol) would be expected to reduce retention volumes of adsorbed ionic samples by virtue of a reduction of the chemical potential. In addition, a change in dielectric constant would alter the value K in the SGC relationship. Incidentally, a change in solvent viscosity would change the numerical constant used in the microelectrophoresis calculation. It would be expected that the SGC model would be valid in mixed solvents, at least for solvent compositions containing a significant percentage of water.

It is hoped that the experimental approaches employed in this work will find use in studies of retention mechanisms on other nonionic stationary phases.

6. FURTHER WORK

a. The heterogeneous potentiometric method, sorption isotherm studies, and microelectrophoresis can be applied to the study of other nonionic sorbents such as C_{18} bonded phases.

b. The mechanism of the effect of different anions such as Cl^- , Br^- or ClO_4^- on retention volume is an area requiring further study.

c. The use of TBA^+ in the mobile phase provides a way of decreasing long retention times of compounds such as $DPGH^+$ and codeinium⁺. The possibility of using solvent programming by slowly increasing the concentration of TBA^+ might prove practical.

REFERENCES

1. J. S. Fritz, "Acid-Base Titrations in Nonaqueous Solvents", Allyn and Bacon, Boston, Mass. 1973.
2. J. Kucharsky and L. Safarik, "Titrations in Nonaqueous Solvents", Elsevier Publishing Co., New York 1965.
3. R. G. Bates and R. M. Robinson, in B. E. Conway, and R. G. Barrades Eds., "Chemical Physics of Ionic Solutions", Wiley, New York, 1966.
4. F. F. Cantwell, Ph.D. Thesis, University of Iowa, December, 1972.
5. F. F. Cantwell and D. J. Pietrzyk, *Anal. Chem.*, 46, 344 (1974).
6. *Ibid.*, 46, 1450 (1974).
7. S. Puon and F. F. Cantwell, *Anal. Chem.*, 49, 1256 (1977).
8. J. A. Christiansen, *Acta Chem. Scand.*, 16, 2363 (1963).
9. D. Ratajewics and Z. Ratajewics, *Chem. Anal. (Warsaw)*, 16, 1299 (1971).
10. M. D. Komar, *Ind. Lab. (U.S.S.R)*, 34, 617 (1968).
11. F. F. Cantwell and H. Y. Mohammed, in press.
12. H. J. C. Tendeloo, A. E. Mans and G. Dehoogh, *Rec. Trav. Chim. Pays-Bas.*, 67, 395 (1948).
13. *Ibid.*, 68, 253 (1949).
14. A. E. Mans and G. E. Vervelde, *Rec. Trav. Chim. Pays-Bas.*, 71, 977 (1952).
15. Z. Stolkova, *Listy Cukrov.*, 67, 207 (1951).
16. C. F. Hiskey and F. F. Cantwell, *J. Pharm. Sci.*, 57, 2165 (1968).

17. F. F. Cantwell, *Anal. Chem.*, 48, 1854 (1976).
18. H. Y. Mohammed and F. F. Cantwell, *Anal. Chem.*, 50, 491 (1978).
19. L. F. Blackwell, A. Fisher, I. J. Miller, R. D. Topsom and J. Vaughan, *J. Chem. Soc.*, 1964, 3588.
20. M. J. Duffy, Endo Laboratories, Private Communication.
21. T. D. Doyl and J. Levine, *J. Assoc. Offic. Anal. Chem.*, 51, 191 (1968).
22. G. Kortum, W. Vogel and K. Andrussov, "Dissociation Constants of Organic Acids in Aqueous Solution", Butterworths, London, 1961.
23. R. Kunin, E. F. Meitzner and N. Bortnick, *J. Amer. Chem. Soc.*, 84, 305 (1962).
24. R. Kunin, E. F. Meitzner, J. A. Oline, S. Fisher and N. Frisch, *Ind. Eng. Chem. Prod. Res. Develop.*, 1, 140 (1962).
25. K. A. Kun and R. Kunin, *J. Polymer Sci. B*, 2, 389 (1964).
26. *Ibid.*, 2, 587 (1964).
27. *Ibid.*, *J. Polymer Sci. A*, 6, 2689 (1968).
28. R. L. Gustafson, R. L. Albright, J. Heisler, J. A. Lirio and O. T. Reid Jr., *Ind. Eng. Chem., Prod. Res. Develop.*, 7, 107 (1968).
29. R. L. Gustafson and J. A. Lirio, *Ind. Eng. Chem., Prod. Res. Develop.*, 7, 116 (1968).
30. H. L. Bradlow, *Steroids*, 11, 265 (1968).
31. M. Matsui, M. Hakozaiki and Y. Kinuyama, *J. Chromatogr.*, 115, 635 (1975).
32. T. Kamikubo and H. Narahara, *Japan 70*, 38,058.

33. T. Kamikubo and H. Narahara, *Vitamin* 37, 225 (1963); CA 68: 93131f.
34. W. E. Faucette and L. P. Cawley, *Clin. Chem.*, 17, 438 (1971).
35. Y. Ariyoshi and Y. Osawa, *Clin. Chem.*, 22, 232 (1976).
36. J. A. Gustafson and A. Pousette, *Biochim. Biophys. Acta.*, 280, 182 (1972).
37. C. H. L. Shackleton, J. Sjovall and O. Wisen, *Clin. Chim. Acta.*, 27, 354 (1970).
38. Y. Osawa and W. R. Slaunwhite Jr., *Steroids* 15, 73 (1969).
39. F. Y. Leung and J. Griffiths, *Clin. Chim. Acta.*, 37, 423 (1972).
40. M. S. Scandrett, M. Wilson and E. J. Ross, *Clin. Chim. Acta.*, 72, 97 (1976).
41. S. Koontz, D. Bessemer, N. Mackey and R. Philips, *J. Chromatogr.*, 85, 75 (1973).
42. R. I. H. Wang and M. A. Mueller, *J. Pharm. Sci.*, 62, 2047 (1973).
43. N. Weissman, M. L. Lowe, J. M. Beattie and J. A. DeMetriou, *Clin. Chem.*, 17, 875 (1971).
44. S. Y. Yeh and J. L. Lach, *J. Pharm. Sci.*, 60, 793 (1971).
45. S. Y. Yeh and L. A. Woods, *J. Pharmacol. Exptl. Therap.*, 175, 69 (1970).
46. J. M. Fujimoto and V. B. Haarstad, *J. Pharmacol. Exptl. Therap.*, 165, 45 (1969).
47. N. C. Miller, M. P. Kullberg, M. E. Banning, L. D. Brown and B. P. Doctor, *Biochem. Med.*, 7, 145 (1973).
48. S. J. Mule, *J. Chromatogr. Sci.*, 10, 275 (1972).

49. M. L. Bastos, D. Jukofsky and S. J. Mule, *J. Chromatogr.*, 81, 93 (1973).
50. M. L. Bastos, D. Jukofsky, M. Chedelet and C. J. Mule, *J. Chromatogr.*, 71, 549 (1972).
51. P. A. F. Pranitis, J.R. Milzoff and A. Stolman, *J. Forensic Sci.*, 19, 917 (1974).
52. G. Ibrahim, S. Andryauskas and M. L. Bastos, *J. Chromatogr.*, 108, 107 (1975).
53. L. B. Hetland, D. A. Knowlton and D. Couri, *Clin. Chim. Acta.*, 36, 473 (1972).
54. J. L. Rosenbaum, *Ind. Eng. Chem., Prod. Res. Develop.*, 14, 96 (1975).
55. B. Grabensee, H. Goebel, K. Hofmann, E. Schnurr and T. Koenigshausen, *Aktuel Probl. Intensivmed.* 2, 238 (1976). CA 87: 12714v.
56. R. H. Kopp, *Ind. Eng. Chem., Prod. Res. Develop.*, 14, 96 (1975).
57. F. S. Brusse, R. Furst and W. P. VanBennekow, *Pharmaceutische Weekblad*, 109, 921 (1974).
58. J. M. Fujimoto, D. L. Roerig and R. I. H. Wang, *Ind. Eng. Chem., Prod. Res. Develop.*, 14, 90 (1975).
59. A. Stolman and R. A. F. Pranitis, *Clin. Toxicol.*, 10, 49 (1977).
60. G. A. Segar, *Effluent Water Treat.J.* 9, 433 (1969).
61. L. A. Spano, R. A. Chalk, J. A. Walsh and C. Dipietro, *Pollut. Eng. Sci., Solutions, Prac, Int. Meet. Soc. Eng. Sci.*, 1st 288 (1972). Edited by E. S. Barrekette, Plenum, N.Y.
62. D. C. Kennedy, *Ind. Eng. Chem., Prod. Res. Develop.*, 12, 56 (1973).

63. J. J. Richard and J. S. Fritz, *Talanta* 21, 91 (1974).
64. S. Wiktorowski, P. Anielak and M. Kubik, *Przeegl Papier.* 31, 331 (1975). CA 85: 9938z.
65. G. R. Harvey, U.S. Environ. Prot. Agency Off. Res. Dev., [Rep] EPA-R2-73-177, 26 (1973). CA 85: 68028a.
66. R. Dawson, J. P. Riley and R. H. Tennant, *Mar. Chem.*, 4, 83 (1976).
67. J. A. Coburn, I. A. Valdmanis and A. S. Chan, *J. Assoc. Off. Anal. Chem.*, 60, 224 (1977).
68. J. Lawrence and H. M. Tosine, *Environ. Sci., Technol.* 10, 381 (1976).
69. R. Kunin, *Polym. Eng. Sci.*, 17, 58 (1977).
70. B. T. Mori and K. J. Hall, *J. Environ. Sci., Health. Part A*, A12, 341 (1977).
71. J. R. Madia and K. Fruh, *Environ. Sci., Technol.* 10, 1044 (1976).
72. E. R. Johnson, T. C. Yu and M. L. Montgomery, *Bull. Environ. Contam. Toxicol.* 17, 369 (1977).
73. S. O. Farwell, F. W. Bowes and D. F. Adams, *J. Environ. Sci., Health. Part B*, B12, 71 (1977).
74. K. Berkane, G. E. Caissie and V. N. Mallet, *J. Chromatogr.*, 139, 386 (1977).
75. T. F. Walser, *Proc. S. Water Resour. Pollut. Contr. Conf.* 16, 81 (1967). CA 70: 99441z.
76. R. L. Sanks, U.S. Environ. Prot. Agency, Off. Res. Dev., [Rep] EPA-R2-73-255, 149 (1973). CA 84: 140375k.

77. S. Wiktorowski and P. Anielak, *Methody Fizykochem. Oczyszczania Wod Scieknow Ref. Konf. Nauk. Tech.* 2, 69 (1976). CA 86: 110841h.
78. G. A. Junk, C. D. Chriswell, R. C. Chang, L. D. Kissinger, J. J. Richard, J. S. Fritz and H. J. Svec, *Fresenius Z. Anal. Chem.*, 282, 331 (1976).
79. G. Assalini, *Ind. Saccar. Ital.* 61, 69 (1968). CA 69: 78604u.
80. K. J. Parker and J. C. Williams, *Proc. Tech. Sess. Cane Sugar Refining Res.* 117, 1968. (Pub 1969). Edited by F. G. Carpenter, Cane Sugar Refining Res. Project Inc., New Orleans, La. CA 72: 14053t.
81. C. C. Chou and A. E. Rizzuto, U.S., *Agric. Res. Serv., South Reg.*, [Rep] ARS-S-51, 8 (1975). CA 83 :12663v.
82. A. J. Zambito and P. Davis, U.S. 3,987,046 (1977).
83. R. H. Prinz, *Can.* 955,603 (1975).
84. S. Takashi, M. Yoshio, S. Minoru, *Japan* 26,095 (1971).
85. K. Imai, K. Watari and M. Izawa, *J. Radioanal. Chem.*, 316, 125 (1977).
86. A. Jyo, T. Imato, K. Fukamachi and N. Ishibashi, *Chem. Lett.*, 7, 815 (1977).
87. J. R. Parrish, *Anal. Chem.*, 49, 1189 (1977).
88. I. Aoki, E. Konishi and M. Hori, *Bunseki Kagaku* 23, 199 (1974). CA 81: 20612b.
89. A. Warahawskg, *Talanta* 21, 624 (1974).
90. J. S. Fritz and E. M. Moyers, *Talanta* 23, 590 (1976).
91. J. S. Fritz and R. B. Willis, *J. Chromatogr.*, 79, 107 (1973).

92. F. F. Cantwell, H. Y. Mohammed, R. G. Baum and S. Puon, Paper No. 67, Analytical Division, 175th Nat'l. Convention, Amer. Chem. Soc., Anaheim, Calif., March 1978.
93. C. H. Chu and D. J. Pietrzyk, *Anal. Chem.*, 46, 330 (1974).
94. D. J. Pietrzyk and C. H. Chu, *Anal. Chem.*, 49, 757 (1977).
95. *Ibid.*, 49, 860 (1977).
96. *Industrial Research/Development*, June 1978, P. C1.
97. D. J. Pietrzyk, E. P. Kroeff and T. D. Rotsch, *Anal. Chem.*, 50, 497 (1978).
98. E. P. Kroeff and D. J. Pietrzyk, *Anal. Chem.*, 50, 502 (1978).
99. J. Seidl and F. Krska, *Chem. Prum.*, 25, 597 (1975).
100. J. S. Fritz, *Ind. Eng. Chem., Prod. Res. Develop.*, 14, 94 (1975).
101. R. F. Mantouri and J. P. Riley, *Anal. Chim. Acta.*, 76, 97 (1975).
102. S. C. O'Conner, *Methods Enzymol.*, 43, 296 (1975).
103. R. L. Gustafson and J. Paleos, Chapter 10 in "Organic Compounds in Aquatic Environments", Dekker, N.Y. 1971.
104. M. D. Grieser, Ph.D. Thesis, University of Iowa, 1972.
105. M. W. Scoggins and J. W. Miller, *Anal. Chem.*, 40, 1155 (1968).
106. M. W. Scoggins, *Anal. Chem.*, 44, 1285 (1972).
107. J. L. Lundgren and A. A. Schilt, *Anal. Chem.*, 49, 974 (1977).
108. S. Eksborg and G. Schill, *Anal. Chem.*, 45, 2095 (1973).
109. B. A. Persson and B. L. Karger, *J. Chromatogr. Sci.*, 12, 521 (1974).

110. W. Santi, J. M. Huen and R. W. Frei, *J. Chromatogr.*, 115, 423 (1975).
111. D. P. Wittmer, M. O. Nüssle and W. G. Haney, Jr., *Anal. Chem.*, 47, 1422 (1975).
112. J. H. Knox and G. R. Laird, *J. Chromatogr.*, 122, 17 (1976).
113. J. H. Knox and J. Jurand, *J. Chromatogr.*, 125, 89 (1976).
114. P. T. Kissinger, *Anal. Chem.*, 49, 883 (1977).
115. I. Molnar and C. Horvath, *Clin. Chem.*, 22, 1497 (1976).
116. C. Horvath, W. Melander and I. Molnar, *Anal. Chem.*, 49, 142 (1977).
117. C. Horvath, W. Melander, I. Molnar and P. Molnar, *Anal. Chem.*, 49, 2295 (1977).
118. C. Tanford, "The Hydrophobic Effect", Wiley-Interscience, New York, N. Y. 1973.
119. G. Gouy, *J. Phys.*, 9, 457 (1910); *Ann. Phys.*, 7, 129 (1917).
120. D. L. Chapman, *Phil. Mag.*, 25, 475 (1913).
121. O. Stern, *Z. Elektrochem.*, 30, 508 (1924).
122. D. C. Grahame, *Chem. Revs.*, 41, 441 (1947).
123. J. Th. Overbeek, Chapters 4 and 5 in H. R. Kruyt, ed., "Colloid Science", Vol. I, Elsevier, N.Y., 1952.
124. K. J. Mysels, "Introduction to Colloid Chemistry", Chapter 15, Interscience, N.Y., 1967.
125. A. W. Adamson, "Physical Chemistry of Surfaces", 2nd ed., Chapter 4, Interscience, N.Y., 1967.

126. J. O'M. Brockris and A. K. N. Reddy, "Modern Electrochemistry", Vol 2, Plenum, N. Y., 1970.
127. D. J. Shaw, "Electrophoresis", Academic Press, London, 1969.
128. K. M. Van Dolsen and M. J. Vold, Chapter 12 in W. J. Webber and E. Matijevic, "Adsorption from Aqueous Solutions", Amer. Chem. Soc., Washington, D.C., 1968.
129. R. C. Weast, ed., "Handbook of Chemistry and Physics", 51st Edition, The Chemical Rubber Co., Cleveland, Ohio, 1970.
130. H. A. Laitinen and W. E. Harris, "Chemical Analysis", 2nd ed., McGraw-Hill Book Co., 1975.
131. C. D. Scott, Anal. Biochem., 24, 292 (1968).
132. H. J. Creighton, "Principles and Applications of Electrochemistry", Vol. I. John Wiley & Sons, Inc., N. Y., 1943.
133. H. A. Abramson, "Electrokinetic Phenomena and Their Application to Biology and Medicine", Amer. Chem. Soc., N. Y., 1934.
134. A. D. Wilks and D. J. Pietrzyk, Anal. Chem., 44, 676 (1972).
135. A. V. Kiselev, in F. M. Fowkes ed., "Hydrophobic Surfaces", Academic Press, N. Y., 1969.
136. W. Hertl and M. G. Neuman, J. Chromatogr., 60, 319 (1971).
137. O. L. Hollis, J. Chromatogr. Sci., 11, 335 (1973).
138. A. C. Zettlemoyer, in F. M. Fowkes, ed., "Hydrophobic Surfaces", Academic Press, N. Y., 1969.
139. J. Paleos, J. Colloid and Interfac. Sci., 31, 7 (1969).
140. Amberlite XAD-2, Technical Bulletin, Rohm and Haas Co., Philadelphia, Pa., 1972.

141. A. L. McClellan and H. F. Harnsberger, *J. Colloid and Interfac. Sci.*, 23, 577 (1967).
142. L. Pauling, "The Nature of the Chemical Bond", 3rd ed., Cornell Univ. Press, 1960.
143. S. R. Sivaraja Iyer, A. S. Chanekar and G. Srinivason, Chapter 6 in K. L. Mittal, ed., "Adsorption at Interfaces", Amer. Chem. Soc., Washington, D. C., 1975.
144. J. Kielland, *J. Amer. Chem. Soc.*, 59, 1675 (1937).
145. R. A. Robinson and R. H. Stokes, "Electrolyte Solutions", Butterworths, London, 1959.
146. Y. G. Berube and P. L. DeBruyn, *J. Colloid and Interfac. Sci.*, 28, 92 (1968).
147. M. Bier, "Electrophoresis", Academic Press, N. Y., 1959.
148. F. Helfferich, "Ion Exchange", McGraw-Hill, N. Y., 1962. p. 162.
149. A. Frumkin, *Z. Physik. Chem.*, 109, 34 (1924). CA 18: 1934.
150. A. Frumkin, S. Reichstein and R. Kulvarskaja, *Kolloid Z.*, 40, 9 (1926). CA 21: 1042.
151. W. B. Dandliker and V. A. de Saussure, Chapter 1 in M. L. Hair, "The Chemistry of Biosurfaces", Vol 1, Dekker, N. Y., 1971.
152. G. Schill, Chapter in J. A. Marinsky and Y. Marcus ed., "Ion Exchange and Solvent Extraction", Vol. 6, Dekker, N. Y., 1974.
153. D. W. Fuerstenau, Chapter 4 in M. L. Hair "The Chemistry of Biosurfaces", Vol. 1, Dekker, N. Y., 1971.

154. J. Th. Overbeek, Chapter 6 in H. R. Kruyt, ed., "Colloid Science", Vol. 1, Elsevier, N. Y., 1952.

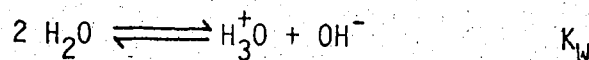
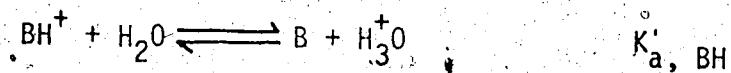
155. R. Gloor and E. L. Johnson, J. Chromatogr. Sci., 15, 413 (1977).

Appendix I

Theoretical derivation of the titration curve of BH^+ type acid in the absence of XAD-2 resin.

Case I. No precipitation during the course of the titration.

There are two equilibria that can be written:



where equilibrium constants of the above equilibria are written as:

$$K'_{a, BH} = \frac{[B] \cdot a_H}{[BH^+]} \quad (1)$$

$$K_W = a_H \cdot a_{OH} \quad (2)$$

Besides the equilibrium equations, there are charge and mass balance equations:

$$[BH^+] + [H^+] + [M^+] = [OH^-] + [X^-] \quad (3)$$

$$n_{BH} = V ([B] + [BH^+]) \quad (4)$$

In the above equation, n_{BH} is the total number of moles of B that is present in the system. The main purpose of the above equations is to express n_{OH} , the number of moles of the titrant added as a function of pH (a_H). Rearranging equations 1 and 2 will lead to:

$$[OH^-] = a_{OH}/\gamma_{OH} = K_W/a_H \cdot \gamma_{OH} \quad (5)$$

$$[B] = [BH^+] K'_{a,BH}/a_H \quad (6)$$

Substituting equation 6 into 4 will yield:

$$[BH^+] = n_{BH} - [BH^+] \cdot V \cdot K'_{a,BH}/a_H \quad (7)$$

After rearranging the above equation, $[BH^+]$ is expressed as a function of n_{BH} only:

$$[BH^+] = n_{BH} / [V \cdot (1 + K'_{a,BH}/a_H)] \quad (8)$$

Substituting equations 5, 6 and 8 into 3 :

$$n_{OH} = K_W \cdot V/a_H \cdot \gamma_{OH} - a_H \cdot V/\gamma_H + n_{BH} K'_{a,BH}/(K'_{a,BH} + a_H) \quad (9)$$

A computer program for the above equation for the titration of BH^+ acid is enclosed on the next page. All of the computer programs in the Appendices are in Fortran IV language.

```
1 C   COMPUTER PROGRAM FOR THE TITRATION OF
2 C   AN HYPOTHETICAL BH+ TYPE ACID IN THE
3 C   ABSENCE OF RESIN.
4     ROH=0.76
5     RH=0.83
6     VAQ=0.05
7     CKW=1.0E-14
8     CKA=1.0E-10
9     TNE=5.0E-4
10    PRINT 300
11    300 FORMAT('1')
12    PRINT 100
13    100 FORMAT (10X, 'AH', 10X, 'PH', 10X, 'NNADH')
14    STEP=6.5
15    6 AH=10.**(-STEP)
16    PH=-ALOG10(AH)
17    A=(CKW*VAQ)/(AH*ROH)
18    B=(TNE*CKA)/(CKA+AH)
19    C=(AH*VAQ)/RH
20    PNNADH=A+B-C
21    IF (PNNADH .LE. 0.0 ) GO TO 10
22    PRINT 200, AH, PH, PNNADH
23    200 FORMAT (4X, E10.4, 4X, F6.2, 4X, E10.4)
24    STEP=STEP+0.5
25    IF (STEP-12.) 6,6,56
26    10 CONTINUE
27    56 CONTINUE
28    PRINT 300
29    STOP
30    END
```


Case II. Precipitation occurs during titration.

The solving of this system is similar to the Case I described above; if S is the solubility of B , then there is a third equilibrium present as:



$$S = [B]_{\text{Sat.}} \quad (10)$$

Equation 6 can be rewritten as:

$$[BH^+] = S \cdot a_H / K'_{a,BH} \quad (11)$$

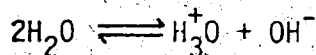
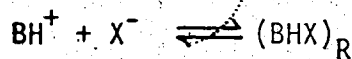
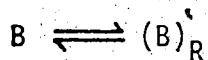
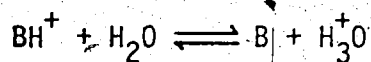
Substituting equations 10, 11 and 5 into 3:

$$n_{OH} = n_{BH} + K_w \cdot V / a_H \cdot \gamma_{OH} - a_H \cdot V / \gamma_H - S \cdot a_H \cdot V / K'_{a,BH} \quad (12)$$

Appendix II

Theoretical derivation of the titration curve of BH^+ type acid in the presence of XAD-2 resin.

Four equilibria can be written for the titration of BH^+ ; they are as follows:



Subscript R in the above equilibria indicates the resin phase and the rest without R means the aqueous phase. There are four equilibrium constants associated to the four equilibria above:

$$K'_{a,BH} = \frac{[B] \cdot a_H}{[BH^+]} \quad (1)$$

$$K_B = \frac{[B]_R}{[B]} \quad (2)$$

$$K_{BH} = \frac{[BHX]_R}{[BH^+]} = K_{eq,BH} \cdot [X^-] \quad (3)$$

$$K_W = a_H \cdot a_{OH} \quad (4)$$

Besides the above equations, mass balance and electroneutrality equations are necessary to describe the whole system. They are listed as follows:

$$[BH^+] + [H_3O^+] + [M^+] = [OH^-] + [X^-] \quad (5)$$

$$n_{BH} = V \cdot ([B] + [BH^+]) + W \cdot ([B]_R + [BHX]_R) \quad (6)$$

Subscript R in equation 6 means the resin phase. Equations 1-3 can be rearranged, that all the variables can be expressed as a function of $[B]$:

$$[BH^+] = [B] \cdot a_H / K'_{a,BH} \quad (7)$$

$$[B]_R = K_B \cdot [B] \quad (8)$$

$$[BHX]_R = K_{BH} \cdot [BH^+] = K_{BH} \cdot a_H \cdot [B] / K'_{a,BH} \quad (9)$$

By substituting equations 7, 8 and 9 into 6, $[B]$ then can be solved:

$$n_{BH} = [B] \cdot (V + a_H \cdot V / K'_{a,BH} + K_B \cdot W + a_H \cdot K_{BH} \cdot W / K'_{a,BH}) \quad (10)$$

$$\text{Or, } [B] = n_{BH} \cdot (V + a_H \cdot V / K'_{a,BH} + K_B \cdot W + a_H \cdot K_{BH} \cdot W / K'_{a,BH})^{-1} \quad (11)$$

Before equation 11 can be substituted into equation 5, mass balance for $[X^-]$ in the aqueous phase is necessary:

$$[X^-] = [BH^+] + [B] + W \cdot [B]_R / V \quad (12)$$

Now, the whole system can be described by substituting equations 11 and 12 into equation 5:

$$\begin{aligned} [M^+] &= [OH^-] - [H_3O^+] + [X^-] - [BH^+] \\ &= [OH^-] - [H_3O^+] + (1 + W/V) \cdot n_{BH} \cdot (V + a_H \cdot V / K'_{a,BH} + \\ &\quad K_{BH} \cdot a_H \cdot W / K'_{a,BH})^{-1} \quad (13) \end{aligned}$$

Since $[M^+]$ is the concentration of the base added in the titration, it can be rewritten as $[M^+] = n_{OH} / V$. So the final equation has form of:

$$\begin{aligned} n_{OH} &= K_W \cdot V / a_H \cdot \gamma_{OH} - a_H \cdot V / \gamma_H + (1 + W/V) \cdot n_{BH} \cdot (1 + a_H / K'_{a,BH} + \\ &\quad K_B \cdot W / V + K_{BH} \cdot W \cdot a_H / K'_{a,BH} \cdot V)^{-1} \quad (14) \end{aligned}$$

A computer program for the above equation for the titration of BH^+ acid in the presence of resin is enclosed on the next page.

```

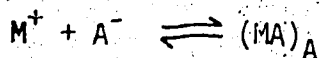
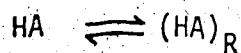
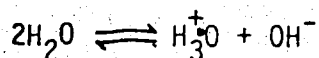
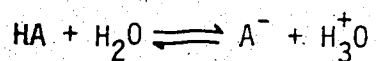
1      C      COMPUTER PROGRAM FOR THE TITRATION OF
2      C      HYPOTHETICAL BH+ TYPE ACID IN THE
3      C      PRESENCE OF RESIN.
4      ROH = 0.76
5      RH = 0.83
6      VAQ = 0.05
7      CKW = 1.0E-14
8      CKA = 1.0E-10
9      WR = 0.005
10     TNB = 5.0E-4
11     CKBH=0.
12     DO 10 I = 1, 6
13     K = I-2
14     CKB=10.**K
15     IF (K.LT.0) CKB=0.
16     PRINT 400
17     400 FORMAT('1')
18     PRINT 100, CKBH,CKB
19     100 FORMAT (1X, 'KBH=', F3.1,5X, 'KB=', F8.1)
20     PRINT 500
21     500 FORMAT('0')
22     PRINT 200
23     200 FORMAT (5X, 'PH', 5X, 'NNAOH')
24     STEPJ=4.5
25     DO 20 J=1,15
26     STEPJ=STEPJ+0.5
27     AH=10**(-STEPJ)
28     PH=-ALOG10(AH)
29     A=(CKW*VAQ)/(AH*ROH)
30     B=AH*VAQ/RH
31     C=1. + (CKB*WR/VAQ)
32     D=1. + (AH/CKA) + (CKB*WR/VAQ)
33     1+(CKBH*AH*WR/(CKA*VAQ))
34     FNNADH=A-B+TNB*(C/D)
35     IF (FNNADH.LE. 0.0) GO TO 20
36     PRINT 300, PH, FNNADH
37     300 FORMAT (4X, F4.1, 4X, E10.4)
38     20 CONTINUE
39     10 CONTINUE
40     PRINT 400
41     STOP
42     END

```

Appendix III

Theoretical derivation of titration of type HA acid in the presence of XAD-2 resin.

There are four equilibria as follows:



There are four equilibrium constants and distribution coefficients that correspond to the above four equilibria:

$$K'_{a,HA} = \frac{[\text{A}^-] \cdot a_{\text{H}}}{[\text{HA}]} \quad (1)$$

$$K_W = a_{\text{H}} \cdot a_{\text{OH}} \quad (2)$$

$$K_{HA} = \frac{[\text{HA}]_R}{[\text{HA}]} \quad (3)$$

$$K_A = [MA]_R/[A^-] \quad (4)$$

In order to derive the entire titration curve, mass balance and charge balance are required. Mass balances for three species are:

$$n_{HA} = V \cdot ([HA] + [A^-]) + W \cdot ([HA]_R + [MA]_R) \quad (5)$$

$$[M^+] = [MX] + n_{OH}/V - W \cdot [MA]_R/V \quad (6)$$

$$[X^-] = [MX] \quad (7)$$

The charge balance in the aqueous phase can be expressed as:

$$[H_3O^+] + [M^+] = [OH^-] + [A^-] + [X^-] \quad (8)$$

Rearranging equations 1, 3 and 4 in such a way that all the variables can be expressed in terms of [HA] only:

$$[A^-] = K'_{a,HA} \cdot [HA]/a_H \quad (9)$$

$$[HA]_R = K_{HA} \cdot [HA] \quad (10)$$

$$[MA]_R = K_A \cdot [A^-] = K_A \cdot K'_{a,HA} \cdot [HA]/a_H \quad (11)$$

In equation 5, n_{HA} is a known value, the rest are variables. However, they can be solved by substituting equations 9, 10 and 11 into 5; then $[HA]$ can be expressed in terms of n_{HA} :

$$[HA] = n_{HA} \cdot a_H \cdot \gamma_{OH} / [a_H(V + WK_{HA}) + K'_{a,HA}(V + WK_A)] \quad (12)$$

Substituting equations 6 and 12 into 8 and rearranging:

$$n_{OH} = K_w \cdot V / a_H \cdot \gamma_{OH} - a_H \cdot V / \gamma_H + n_{HA} \cdot K'_{a,HA} \cdot (V + WK_A) \cdot [a_H \cdot (V + WK_{HA}) + K'_{a,HA} \cdot (V + WK_A)]^{-1}$$

This is the titration equation which relates n_{OH} , the titrant added, to pH (a_H).

Appendix IV

Derivation of the pH difference at half equivalent point in the titration of BH^+ and HA acids, with and without the presence of XAD-2 resin.

Derivation of equation 13, page 12, which is the pH difference at the half equivalent point, is shown here. As previously indicated, there are two equations derived for the BH^+ titration. The first one is the titration without the resin and can be given as:

$$n_{OH} = \frac{K_w \cdot V}{a_H \gamma_{OH}} - \frac{a_H}{\gamma_H} + \frac{n_{BH} K'_{a,BH}}{K'_{a,BH} + a_H}$$

Between the range of pH 4 and 10, the first two terms are negligible compared with the last one. So the above equation can be rewritten as:

$$n_{OH} \approx n_{BH} \cdot K'_{a,BH} / (a_H + K'_{a,BH})$$

Or, after rearrangement,

$$a_H \approx (n_{BH}/n_{OH} - 1) \cdot K'_{a,BH} \quad (a)$$

By taking logarithms and changing signs on both sides, the above equation takes the form:

$$\text{pH} = -\log K'_{a,BH} - \log(n_{BH}/n_{OH} - 1)$$

The second equation, which is the titration curve in the presence of XAD-2 resin, is presented as:

$$n_{OH} = \frac{K_W \cdot V}{a_H n_{OH}} - \frac{a_H \cdot V}{T_H} + \left(1 + K_B \frac{W}{V}\right) n_{BH} \left(1 + \frac{a_H}{K'_{a,BH}} + K_B \frac{W}{V} + \frac{K_{BH}}{K'_{a,BH}} a_H \frac{W}{V}\right)^{-1}$$

In the same manner as before, between pH 4 to 10, the first two terms can be neglected, and after rearrangement, the above equation is simplified as:

$$(V + K_{BH} \cdot W) \cdot a_H / K'_{a,BH} \approx (n_{BH}/n_{OH} - 1) \cdot (V + K_B W)$$

By taking logarithms and changing signs on both sides, the above equation has the form:

$$\text{pH} \approx \log(V + K_{BH} \cdot W) - \log(V + K_B W) - \log K'_{a,BH} - \log(n_{BH}/n_{OH} - 1) \quad (b)$$

Then the difference in pH at the point where n_{BH} equals twice the n_{OH} is equation (a) minus (b):

$$\Delta \text{pH} = \text{pH}(\text{NR}) - \text{pH}(\text{R})$$

$$\Delta \text{pH} \approx \log(V + K_B W) - \log(V + K_{BH} W)$$

$$\approx \log \frac{V + K_B W}{V + K_{BH} W}$$

The expressions for the titration of acid HA are treated in a similar way and yield:

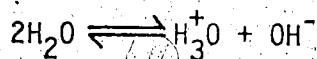
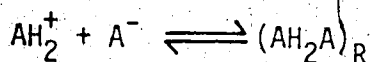
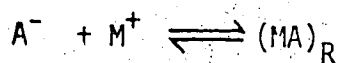
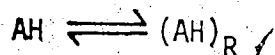
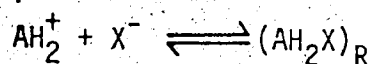
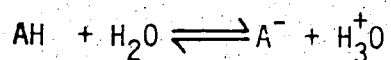
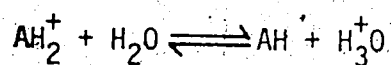
$$\Delta \text{pH} = \text{pH}(\text{NR}) - \text{pH}(\text{R})$$

$$\approx \log \frac{V + K_A W}{V + K_{HA} W}$$

APPENDIX V

A detailed derivation of the theoretical titration curve for an AH_2^+ type acid with NaOH in the presence of resin is presented here.

The complete equilibria that describe the system are given below:



Subscript R indicates the resin phase, while the rest of the terms are aqueous phase. There is an equilibrium constant that corresponds to each of the equilibrium equations. They are listed below:

$$K'_{a, AH_2} = [AH] \cdot a_H / [AH_2^+] \quad (1)$$

$$K'_{a, AH} = [A^-] \cdot a_H / [AH] \quad (2)$$

$$K_{AH_2} = [AH_2X]_R / [AH_2^+] \quad (3)$$

$$K_{AH} = [AH]_R / [AH] \quad (4)$$

$$K_A = [MA]_R / [A^-] \quad (5)$$

$$K_{AH_2A} = [AH_2A]_R / [AH_2^+] \cdot [A^-] \quad (6)$$

$$K_W = a_H \cdot a_{OH} \quad (7)$$

Besides the equations given above, there are mass balance and electroneutrality equations that are required to give a complete description of the system. Electroneutrality of the aqueous phase in this system is:

$$[H_3O^+] + [M^+] + [AH_2^+] = [OH^-] + [X^-] + [A^-] \quad (8)$$

Mass balance for species $[M^+]$, $[X^-]$ and $[AH_2^+]$ are given as:

$$n_{\text{AH}_2} = V \cdot ([\text{AH}_2^+] + [\text{AH}] + [\text{A}^-]) + W \cdot ([\text{AH}_2\text{X}]_{\text{R}} + [\text{AH}]_{\text{R}} + [\text{MA}]_{\text{R}} + 2 \cdot [\text{AH}_2\text{A}]_{\text{R}}) \quad (9)$$

$$[\text{X}^-] = [\text{MX}] + [\text{AH}_2^+] + [\text{AH}] + [\text{A}^-] + ([\text{AH}]_{\text{R}} + [\text{MA}]_{\text{R}} + 2 \cdot [\text{AH}_2\text{A}]_{\text{R}}) \cdot W/V \quad (10)$$

$$[\text{M}^+] = [\text{MX}] - [\text{MA}] \cdot W/V + n_{\text{OH}^-}/V \quad (11)$$

For simplicity, equations 1 to 6 can be rearranged in such a way that all the different variables can be expressed as a function of [AH]:

$$[\text{AH}_2^+] = [\text{AH}] \cdot a_{\text{H}} / K'_{\text{a}, \text{AH}_2} \quad (12)$$

$$[\text{A}^-] = K'_{\text{a}, \text{AH}} \cdot [\text{AH}] / a_{\text{H}} \quad (13)$$

$$[\text{AH}_2\text{X}]_{\text{R}} = K_{\text{AH}_2} \cdot [\text{AH}_2^+] = K_{\text{AH}_2} \cdot a_{\text{H}} \cdot [\text{AH}] / K'_{\text{a}, \text{AH}_2} \quad (14)$$

$$[\text{AH}]_{\text{R}} = K_{\text{AH}} \cdot [\text{AH}] \quad (15)$$

$$[\text{MA}]_{\text{R}} = K_{\text{A}} \cdot [\text{A}^-] = K_{\text{A}} \cdot K'_{\text{a}, \text{AH}} \cdot [\text{AH}] / a_{\text{H}} \quad (16)$$

$$[\text{AH}_2\text{A}]_{\text{R}} = K_{\text{AH}_2\text{A}} \cdot [\text{AH}_2^+] \cdot [\text{A}^-] = K_{\text{AH}_2\text{A}} \cdot K'_{\text{a}, \text{AH}} \cdot [\text{AH}]^2 / K'_{\text{a}, \text{AH}_2} \quad (17)$$

[AH] can be solved by substituting equations 12 to 17 into 9:

$$\begin{aligned}
 n_{\text{AH}_2} = & V \cdot ([\text{AH}] a_{\text{H}} / K'_{\text{a, AH}_2} + [\text{AH}] + K'_{\text{a, AH}} [\text{AH}] / a_{\text{H}}) \\
 & + W \cdot ([\text{AH}] a_{\text{H}} K_{\text{AH}_2} / K'_{\text{a, AH}_2} + K_{\text{AH}} [\text{AH}] + K_{\text{A}} K'_{\text{a, AH}} [\text{AH}] / \\
 & a_{\text{H}} + 2 K_{\text{AH}_2} K'_{\text{a, AH}} \cdot [\text{AH}]^2 / K'_{\text{a, AH}_2}) \quad (18)
 \end{aligned}$$

Equation 18 can be rearranged so that it will be a quadratic equation. The $[\text{AH}]$ can be put into the form $ax^2 + bx + c = 0$:

$$\begin{aligned}
 & 2 W K_{\text{AH}_2} K'_{\text{a, AH}} \cdot [\text{AH}]^2 + [W(K_{\text{AH}} + K_{\text{AH}_2} a_{\text{H}} / K'_{\text{a, AH}_2} + \\
 & K_{\text{A}} K'_{\text{a, AH}} / a_{\text{H}}) + V(1 + a_{\text{H}} / K'_{\text{a, AH}_2} + K'_{\text{a, AH}} / a_{\text{H}})] \cdot [\text{AH}] \\
 & - n_{\text{AH}_2} = 0 \quad (19)
 \end{aligned}$$

a, b, c have been defined as:

$$a = 2(W/V) K_{\text{AH}_2} K'_{\text{a, AH}} / K'_{\text{a, AH}_2} \quad (20)$$

$$\begin{aligned}
 b = & [1 + (W/V) K_{\text{AH}}] + [1 + (W/V) K_{\text{A}}] K'_{\text{a, AH}} / a_{\text{H}} + \\
 & [1 + (W/V) K_{\text{AH}_2}] \cdot a_{\text{H}} / K'_{\text{a, AH}_2} \quad (21)
 \end{aligned}$$

$$c = - n_{\text{AH}_2} / V \quad (22)$$

$$\text{and } [\text{AH}] = [(b^2 + 4 \cdot a \cdot c)^{1/2} - b] / 2 \cdot a \quad (23)$$

Only the positive solution will be taken since $[\text{AH}]$ can not be negative.

Equations 10 and 11 are also used to relate the amount of titrant added and the pH changes. By substituting equations 12 to 17 into 10 one gets:

$$\begin{aligned}
 [X^-] = & [MX] + a_H[AH]/K'_{a,AH_2} + [AH] + K'_{a,AH}[AH]/a_H \\
 & + (W/V) \cdot K_{AH}[AH] + (W/V) \cdot K_A K'_{a,AH}[AH]/a_H + \\
 & 2 \cdot (W/V) \cdot K_{AH_2} \cdot K'_{a,AH}[AH]^2/K'_{a,AH_2} \quad (24)
 \end{aligned}$$

Equation 11 is treated a similar way:

$$[M^+] = [MX] + n_{OH}/V - (W/V) \cdot K_A K'_{a,AH}[AH]/a_H \quad (25)$$

Substituting equations 25 and 26 into the electroneutrality equation 8:

$$\begin{aligned}
 [H_3O^+] + [MX] + n_{OH}/V = & (W/V) \cdot K_A K'_{a,AH}[AH]/a_H + \\
 a_H[AH]/K'_{a,AH_2} = & [OH^-] + K'_{a,AH}[AH]/a_H + [MX] + [AH] + \\
 a_H[AH]/K'_{a,AH_2} + & K'_{a,AH}[AH]/a_H + (W/V)K_{AH}[AH] + \\
 (W/V) K_A K'_{a,AH}[AH]/a_H + & 2(W/V) \cdot K_{AH_2} K'_{a,AH}[AH]^2/K'_{a,AH_2} \quad (26)
 \end{aligned}$$

After rearranging the above equation:

$$\begin{aligned}
 n_{OH} = & K_W \cdot V/a_H \cdot \tau_{OH} - a_H \cdot V/\tau_H + [(V + WK_{AH}) + 2(V + \\
 & WK_A)K'_{a,AH}/a_H] \cdot [AH] + 2 \cdot W \cdot K_{AH_2} K'_{a,AH}[AH]^2/K'_{a,AH_2} \quad (27)
 \end{aligned}$$

The above equation can be simplified by using equation 19:

$$n_{OH} = K_w \cdot V / a_H \cdot \tau_{OH} - a_H V / \tau_H + n_{AH_2} - (V + WK_{AH_2}) \cdot [AH] / \left(a_H / K'_{a,AH_2} + (V + WK_A) \cdot [AH] \cdot K'_{a,AH} / a_H \right) \quad (28)$$

[AH] has to be solved from equation 22 in order to evaluate the relationship between n_{OH} and pH. On the next page is the computer program used to calculate the titration curve for a diprotic acid AH_2^+ .

```

1      C   THIS IS THE COMPUTER PROGRAM FOR THE THEO-
2      C   RETICAL TITRATION CURVE OF AH2+ TYPE ACID.
3      COMPLEX ZSM, ZLG
4      RH=0.83
5      ROH=0.76
6      VAQ=0.05
7      CKW=1.0E-14
8      TNAH2=5.0E-4
9      WR=0.000
10     CKAH=5.0E-10
11     CKAH2=1.0E-8
12     CKMA=10.0
13     CKAH2X=10.0
14     CKAH=1.0E3
15     CKAH2A=1.0E12
16     PRINT 300
17     300 FORMAT('1')
18     PRINT 703,WR,VAQ
19     703 FORMAT(4X,'WT. OF RESIN=',F5.3,5X,'AQ. VOL =',
20     1,F5.3)
21     PRINT 573 ,TNAH2
22     573 FORMAT(4X,'NO. OF MOLES=',E10.4)
23     PRINT 401, CKAH2X,CKMA
24     401 FORMAT(4X,'KAH2X=',F7.1,5X,'KMA=',F4.1)
25     PRINT 600, CKAH2,CKAAH
26     600 FORMAT(4X,'KAH2=',E10.4,5X,'KAAH=',E10.4)
27     PRINT 800, CKAH2A ,CKAH
28     800 FORMAT(4X,'KAH2A=',E10.4 ,5X,'KAH=',E10.4)
29     PRINT 205
30     205 FORMAT('0')
31     PRINT 100
32     100 FORMAT (10X, 'AH', 10X, 'PH', 8X, 'NNAOH',
33     1,8X, 'AH+2',8X, 'A-',12X, 'AH',8X, 'AH2AR')
34     STEP=0.0
35     6 AH=10.**(-STEP)
36     PH=-ALOG10(AH)
37     P=WR/VAQ

```

```

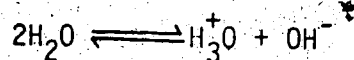
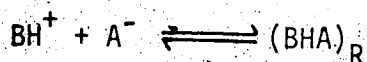
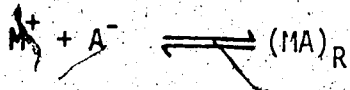
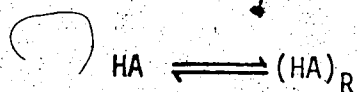
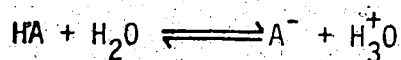
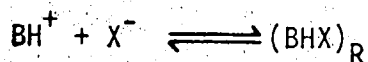
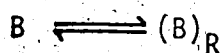
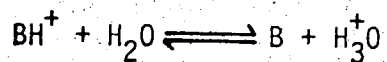
38      A=2.*P*CKAH2A*CKAAH/CKAAH2
39      B11=1.+(AH/CKAAH2)+(CKAAH/AH)
40      B12=P*(CKAH+(CKAH2X*AH/CKAAH2)+(CKMA*CKAAH/AH))
41      B=B11+B12
42      C=-TNAH2/VAQ
43      IF(P.EQ.0.0) GO TO 121
44      IF(CKAH2A.EQ.0.0) GO TO 121
45      CALL ZQABR(A,B,C,ZSM,ZLG,IER)
46      AHO=ZSM
47      GO TO 17
48      121 AHO=-C/B
49      17  A1=CKW*VAQ*(AH*ROH)
50      AH2=AHO*AH/CKAAH2
51      AO=AHO*CKAAH/AH
52      AH2AR=CKAH2A*AH2*AO
53      B1=AH*VAQ/RH
54      C1=TNAH2
55      D1=VAQ*(AH/CKAAH2)*(1.+(WR/VAQ)*CKAH2X)
56      E1=(VAQ*CKAAH/AH)*(1.0+P*CKMA)
57      FNNAOH=A1-B1+C1+(E1-D1)*AHO
58      IF(FNNAOH.LT.0.0) GO TO 10
59      PRINT200,AH,PH,FNNAOH,AH2,AO,AHO,AH2AR
60      200 FORMAT(4X,E10.4,4X,F6.2,5E13.4)
61      10  STEP=STEP+0.25
62      IF (STEP-12.) 6,6,56
63      56  CONTINUE
64      PRINT 300
65      STOP
66      END

```

APPENDIX VI

Theoretical derivation of the titration curve for the mixed type acids BH^+ and HA in the presence of XAD-2 resin.

The complete equilibrium equations are presented as follows:



Subscripts indicate the resin phase, while the rest of the terms are the aqueous phase. For each of the equilibrium equations there is an equilibrium constant. There are eight different constants

given below in the order of the equilibria above:

$$K'_{a,BH} = \frac{[B] \cdot a_H}{[BH^+]} \quad (1)$$

$$K_B = \frac{[B]_R}{[B]} \quad (2)$$

$$K_{BH} = \frac{[BHX]_R}{[BH^+]} \quad (3)$$

$$K'_{a,HA} = \frac{[A^-] \cdot a_H}{[HA]} \quad (4)$$

$$K_{HA} = \frac{[HA]_R}{[HA]} \quad (5)$$

$$K_A = \frac{[MA]_R}{[A^-]} \quad (6)$$

$$K_{BHA} = \frac{[BHA]_R}{[BH^+] \cdot [A^-]} \quad (7)$$

$$K_W = a_H \cdot a_{OH} \quad (8)$$

In order to solve the complete equations, electroneutrality as well as mass balance equations are required. The electroneutrality equation of the aqueous phase is given in equation 9:

$$[BH^+] + [H_3O^+] + [M^+] = [A^-] + [OH^-] + [X^-] \quad (9)$$

The mass balances of the different species are given as follows:

$$n_{HA} = V \cdot ([HA] + [A^-]) + W \cdot ([HA]_R + [MA]_R + [BHA]_R) \quad (10)$$

$$n_{BH} = V \cdot ([BH^+] + [B]) + W \cdot ([B]_R + [BHX]_R + [BHA]_R) \quad (11)$$

$$[M^+] = [MX] + n_{OH}/V - (W/V) \cdot [MA]_R \quad (12)$$

$$[X^-] = [MX] + [B] + (W/V) \cdot ([B]_R + [BHX]_R + [BHA]_R) \quad (13)$$

Equations 1-8 can be rearranged in such a way that all the variables can be expressed either in terms of [B] or [HA]:

$$[BH^+] = [B] \cdot a_H / K'_{a,BH} \quad (14)$$

$$[B]_R = [B] \cdot K_B \quad (15)$$

$$[BHX]_R = K_{BH} \cdot [BH^+] = K_{BH} \cdot [B] \cdot a_H / K'_{a,BH} \quad (16)$$

$$[A^-] = K'_{a,HA} \cdot [HA] / a_H \quad (17)$$

$$[HA]_R = K_{HA} \cdot [HA] \quad (18)$$

$$[MA]_R = K_A \cdot [A^-] = K_A \cdot K'_{a,HA} \cdot [HA] / a_H \quad (19)$$

$$[BHA]_R = K_{BHA} \cdot [BH^+] \cdot [A^-] = K_{BHA} \cdot K'_{a,HA} \cdot [B] \cdot [HA] / K'_{a,BH} \quad (20)$$

$$[OH^-] = K_w / a_H \cdot \gamma_{OH} \quad (21)$$

Substituting equations 16-20 into 10 and 11 and rearranging:

$$n_{HA} = [HA] \cdot V \cdot (1 + K'_{a,HA}/a_H + W \cdot K_{HA}/V + WK_A \cdot K'_{a,HA}/V \cdot a_H + W \cdot K_{BHA} \cdot K'_{a,HA} \cdot [B]/V \cdot K'_{a,BH}) \quad (22)$$

$$n_{BH} = [B] \cdot V \cdot (1 + a_H/K'_{a,BH} + W \cdot K_B/V + W \cdot K_{BH} \cdot a_H/V \cdot K'_{a,BH} + W \cdot K_{BHA} \cdot K'_{a,BH} \cdot [HA]/V \cdot K'_{a,BH}) \quad (23)$$

For simplicity, different symbols are used for equations 22 and 23:

$$a = K'_{a,HA}/a_H$$

$$b = (W/V) \cdot K_{HA}$$

$$c = (W/V) \cdot K_A \cdot (K'_{a,HA}/a_H)$$

$$d = a_H/K'_{a,BH}$$

$$e = (W/V) \cdot K_B$$

$$f = (W/V) \cdot K_{BH} \cdot (a_H/K'_{a,BH})$$

$$q = (W/V) \cdot K_{BHA} \cdot (K'_{a,HA}/K'_{a,BH})$$

So equations 22 and 23 can be rewritten as:

$$n_{HA} = [HA] \cdot V \cdot (1 + a + b + c + q \cdot [B]) \quad (24)$$

$$n_{BH} = [B] \cdot V \cdot (1 + d + e + f + q \cdot [HA]) \quad (25)$$

The two variables $[HA]$ and $[B]$ can be solved from the above equations.

$[HA]$ can be expressed as a function of $[B]$ from 24. Then substituting into 25 and solving for $[B]$:

$$[HA] = n_{HA} \cdot V^{-1} \cdot (1 + a + b + c + q \cdot [B])^{-1} \quad (26)$$

Substituting 26 into 25:

$$n_{BH} = [B] \cdot V \cdot (1 + d + e + f + n_{HA} \cdot q) / V(1 + a + b + c + q[B]) \quad (27)$$

Equation 27 can be rearranged as:

$$n_{BH} (1 + a + b + c) + n_{BH} \cdot q \cdot [B] - q \cdot [B]^2 \cdot V \cdot (1 + d + e + f) \\ [B] \cdot V \cdot (1 + a + b + c) \cdot (1 + d + e + f) = n_{HA} \cdot q \cdot [B]$$

After rearranging, it becomes a quadratic equation:

$$[B]^2 + [B] [n_{HA} \cdot q - n_{BH} \cdot q + V \cdot (1 + a + b + c) \cdot (1 + d + e + f)] / \\ q \cdot V \cdot (1 + d + e + f) - n_{BH} \cdot (1 + a + b + c) / qV(1 + d + e + f) = 0$$

Let
$$2s = [q(n_{HA} - n_{BH}) + V(1 + a + b + c) \cdot (1 + d + e + f)] \cdot [q V (1 + d + e + f)]^{-1}$$

and
$$t = n_{BH} \cdot (1 + a + b + c) / q \cdot V \cdot (1 + d + e + f)$$

So the quadratic equation takes the form:

$$[B]^2 + 2s [B] - t = 0 \quad (28)$$

$$[B] = -s + (s^2 + t)^{1/2} \quad (29)$$

Or,
$$[B] = -s - (s^2 + t)^{1/2} \quad (30)$$

Since $[B]$ cannot have a negative value, only equation 29 is taken as the solution. Substituting equation 30 into 26, $[HA]$ is solved for, giving:

$$[HA] = n_{HA} \cdot V^{-1} \cdot [1 + a + b + c + q \cdot (-s + (s^2 + t)^{1/2})]^{-1} \quad (31)$$

Since $[HA]$ and $[B]$ are the only two variables that have been solved for, others also have to be defined or solved for to interpret the entire titration curve. Equations 12 and 13 can be changed to:

$$[M^+] = [MX] + n_{OH}/V - W \cdot K_A \cdot [A]/V \quad (32)$$

$$[X^-] = [MX] + [B] + a_H \cdot [B]/K'_{a,BH} + W \cdot K_B \cdot [B]/V + (W/V) \cdot K_{BHA} \cdot K'_{a,HA} [B] \cdot [HA]/K'_{a,BH} \quad (33)$$

Substituting equations 32 and 33 into equation 9:

$$[BH^+] + [H_3O^+] + [MX] + n_{OH}/V - WK_A [A^-]/V = [A^-] + [OH^-] + [MX] + [B] + a_H \cdot [B]/K'_{a,BH} + W \cdot K_B \cdot [B]/V + (W/V) \cdot K_{BHA} \cdot [B] \cdot [HA] \cdot K'_{a,HA}/K'_{a,BH} \quad (34)$$

After rearranging, the final equation can be rewritten as:

$$n_{OH} = K_W \cdot V/a_H \cdot r_{OH} - a_H \cdot V/r_H + K'_{a,HA} (V + WK_A) \cdot [HA] \cdot V/a_H + (V + W \cdot K_B) \cdot V \cdot [B] + W \cdot K_{BHA} [B] \cdot [HA] \cdot K'_{a,HA}/K'_{a,BH} \quad (35)$$

Substituting equations 29 and 31 into 35 a complete solution is obtained:

$$n_{OH} = K_W \cdot V/a_H \cdot r_{OH} - a_H \cdot V/r_H + K'_{a,HA} \cdot (1 + WK_A/V) \cdot n_{HA}/a_H \cdot \left\{ 1 + K'_{a,HA}/a_H + (W/V)K_{HA} + (W/V)K_A \cdot (K'_{a,HA}/a_H) + (W/V) \cdot K_{BHA} \cdot (K'_{a,HA}/K'_{a,BH}) \cdot [(s^2 + t)^{1/2} - s] \right\}^{-1} + (1 + WK_B/V) \cdot V \cdot [(s^2 + t)^{1/2} - s]^{-1} \quad (36)$$

where $s = \left\{ (W/V) \cdot K_{BHA} \cdot (n_{HA} - n_{BH}) \cdot (K'_{a,HA}/K'_{a,BH}) + V[1 + K'_{a,HA}/a_H] \right.$
 $+ (W/V) \cdot K_{HA} + (W/V) \cdot K_A \cdot (K'_{a,HA}/a_H) \cdot [1 + a_H/K'_{a,BH}] +$
 $\left. (W/V) \cdot K_B + (W/V) \cdot K_{BH} \cdot (a_H/K'_{a,BH}) \right\} \cdot \left\{ 2 \cdot V \cdot (W/V) \cdot K_{BHA} \cdot (K'_{a,HA}/K'_{a,BH}) \cdot [1 + a_H/K'_{a,BH}] + (W/V) \cdot K_B + (W/V) \cdot K_{BH} \cdot (a_H/K'_{a,BH}) \right\}^{-1}$

and $t = n_{BH} \cdot \left\{ 1 + K'_{a,HA}/a_H + (W/V)K_{HA} + (W/V)K_A(K'_{a,HA}/a_H) \right\} \cdot$
 $\left\{ V \cdot (W/V) \cdot K_{BHA} \cdot (K'_{a,HA}/K'_{a,BH}) \cdot (1 + a_H/K'_{a,BH} + (W/V)K_B + (W/V) \cdot K_{BH} \cdot (a_H/K'_{a,BH})) \right\}^{-1}$

In the special case of $K_{BHA} = 0$, then, $q = 0$, and $[B]$ and $[HA]$ are not dependent. $[B]$ and $[HA]$ can be solved from equations 24 and 25:

$$[HA] = n_{HA} \cdot V^{-1} \cdot (1 + a + b + c)^{-1} \quad (26a)$$

$$[B] = n_{BH} \cdot V^{-1} \cdot (1 + d + e + f)^{-1} \quad (27a)$$

and equation 30 can be simplified to :

$$n_{OH} = K_W \cdot V/a_H \cdot \gamma_{OH} - a_H \cdot V/\gamma_H + (K'_{a,HA}/a_H) \cdot (2 + WK_A/V) \cdot n_{HA} \cdot$$

$$\cdot [1 + K'_{a,HA}/a_H + (W/V)K_{HA} + (W/V) \cdot K_A \cdot (K'_{a,HA}/a_H)]^{-1}$$

$$+ (1 + WK_B/V) \cdot n_{BH} \cdot [1 + a_H/K'_{a,BH} + (W/V)K_B + (W/V) \cdot K_{BH} \cdot (a_H/K'_{a,BH})]^{-1} \quad (35a)$$

Equation 35a actually is the sum of individual titrations of acid types, BH^{+} and HA.

On the next page is a program for this calculation.

```

1  C THIS IS THE COMPUTER PROGRAM FOR THE THEO-
2  C RETICAL TITRATION OF MIXED ACIDS BH+ AND HA .
3  COMPLEX ZSM, ZLG
4  ROH=0.76
5  RH=0.83
6  VAQ=0.05
7  CKW=1.0E-14
8  TNHA=3.60E-4
9  TNB=1.80E-4
10 CKAHA=1.0E-7
11 CKABH=1.0E-7
12 CKHA=430.0
13 CKMA=4.8
14 CKBHx=10.0
15 CKB=2.90E4
16 WR=0.005
17 KBHA=0.0
18 PRINT 300
19 300 FORMAT('1')
20 PRINT 703,WR,VAQ
21 703 FORMAT(4X,'WT. OF RESIN=',F5.3,5X,'AQ. VOL ='
22 1, F5.3)
23 PRINT 298,TNHA, TNB
24 298 FORMAT(4X,'TNHA=',E10.4,5X,'TNB=',E10.4)
25 PRINT 299,CKAHA,CKABH
26 299 FORMAT(4X,'KAHA=',E10.4,5X,'KABH=',E10.4)
27 PRINT 401,CKHA,CKMA
28 401 FORMAT(4X,'KHA=',F7.1,5X,'KMA=',F4.1)
29 PRINT 600,CKB,CKBHx
30 600 FORMAT(4X,'KB=',F7.1,5X,'KBHx=',F4.1)
31 PRINT 800,CKBHA
32 800 FORMAT(4X,'KBHA=',E10.4)
33 PRINT 205
34 205 FORMAT('0')
35 PRINT 100
36 100 FORMAT('PH',10X,'NNAOH',10X,'BHAQ',8X,'BAQ',
37 110X,'AAQ',10X,'HAAQ',8X,'BHAR')
38 STEP=0.0
39 6 AH=10.*( -STEP)
40 PH=-ALOG10(AH)

```

```

41      F=WR/VAQ
42      Q=P*CKBHA*(CKAHA/CKABH)
43      QQ=Q/P
44      AF=CKAHA/AH
45      BF=P*CKHA
46      CF=P*CKMA*CKAHA/AH
47      D=AH/CKABH
48      E=P*CKB
49      F=F*CKBH*AH/CKABH
50      CON1=1.+AF+BF+CF
51      CON2=1.+D+E+F
52      S1=Q*(TNHA-TNB)+VAQ*CON1*CON2
53      S2=Q*VAQ*CON2
54      IF(S2.EQ.0) GO TO 11
55      T1=TNB*CON1
56      A=S2
57      B=S1
58      C=-T1
59      CALL ZQADR (A,B,C,ZSM,ZLG,IER)
60      BAQ=ZSM
61      GO TO 13
62      11 BAQ=TNB/(CON2*VAQ)
63      13 HAAQ=TNHA/(VAQ*(CON1+Q*BAQ))
64      BHAQ=BAQ*D
65      AAQ=HAAQ*AF
66      BHAR=QQ*BAQ*HAAQ
67      A1=CKW*VAQ/(AH*ROH)
68      B1=AH*VAQ/RH
69      C1=AF*(1.+P*CKMA)*VAQ*HAAQ
70      D1=BAQ*(1.+E)*VAQ
71      FNNAOH=A1-B1+C1+D1+BHAR*WR
72      IF(FNNAOH.LE.0.0) GO TO 10
73      PRINT 200, PH, FNNAOH, BHAQ, BAQ, AAQ, HAAQ, BHAR
74      200 FORMAT(F6.2,6E13.4)
75      10 STEP=STEP+0.25
76      IF(STEP-12.) 6,6,56
77      56 CONTINUE
78      PRINT 300
79      STOP
80      END

```

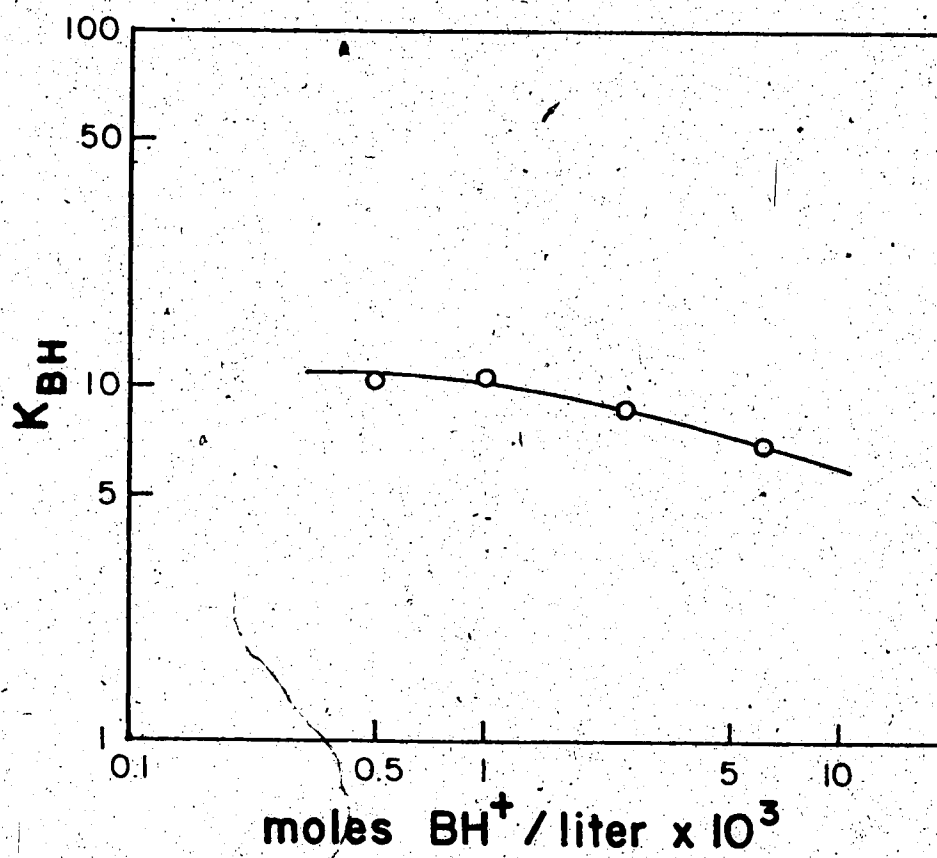
Calculation of the Curve C, Figure 11.

Theoretically, the titration curve of diphenylguanidine hydrochloride in the presence of resin can be calculated from equation 11 (Section 2, Part I). However, the nonlinearity of K_{BH} (Figure 12) impedes the direct use of this titration equation. Indirectly, equation 11 can be solved by relating a_H (pH) to K_{BH} and $[BH^+]$. a_H can be expressed as a function of K_{BH} and $[BH^+]$:

$$a_H = \frac{(K_B W + V) [BH^+] K'_{a,BH}}{n_{BH} - [BH^+](V + K_{BH} W)} \quad (1)$$

In the above equation, K_{BH} is not a constant, but varies with $[BH^+]$. From the experiment results (Table 16) K_{BH} is plotted against $[BH^+]$ on a log-log scale (Figure A). The log scale is necessary since a much wider range can be covered. The procedure of calculating equation 1 is as follows: Fixed a $[BH^+]$ (starting from a higher value), then K_{BH} is fixed from Figure A. In turn, a_H is known from equation 1; and then n_{OH} can be calculated after knowing a_H and K_{BH} by using equation 11. Repeat this process until the entire titration curve is calculated. This method cannot be used in a computer since it involves a plot reading process. Instead, K_{BH} is expressed as a linear function of $[BH^+]$ at different sections. A computer program which was used to solve the titration curve of $DPGH^+$ is enclosed on the next page.

Figure A. Plot of K_{BH} with $[BH^+]$. Data taken from Table 6.



```
1 C COMPUTER PROGRAM FOR THE TITRATION OF
2 C DIPHENYLGUANIDINE HYDROCHLORIDE, USED TO
3 C CALCULATE CURVE C, FIGURE 11.
4 ROH = 0.76
5 RH = 0.83
6 VAR = 0.050
7 CKW = 1.0E-14
8 CKA = 1.0E-10
9 WR = 0.0055
10 PH=0.0
11 TNB = 4.97E-4
12 CKB=2.90E4
13 PRINT 400
14 400 FORMAT('1')
15 PRINT 100
16 100 FORMAT(10X, 'BHAQ', 10X, 'CKBH', 5X, 'PH', 10X
17 1, 'NNAOH')
18 STEPJ=0.5
19 DO 20 J=1,20
20 IF(PH.LE.7.5) XC=0.1
21 IF(PH.GT.7.5) XC=0.25
22 13 STEPJ=STEPJ+XC
23 BHAQ=10**(-STEPJ)
24 IF (BHAQ - 5.80E-3) 7,8,8
25 7 IF(BHAQ-2.7E-3) 99,10,10
26 99 IF (BHAQ - 1.4E-3) 77, 88, 88
27 77 IF (BHAQ - 7.0E-4) 101, 111, 111
28 101 IF (BHAQ - 5.0E-4) 4, 9, 9
29 4 CKBH = 11.0
30 GO TO 11
31 9 CKBH= 11.75 - 1.5E3*BHAQ
32 GO TO 11
33 111 CKBH = 11.40 -1.0E3*BHAQ
34 GO TO 11
```

```
35      88 CKBH = 11.51 - 1.08E3*BHAQ
36      GO TO 11
37      10 CKBH=9.82 - 4.52E2*BHAQ
38      GO TO 11
39      8 CKBH =9.70- 4.26E2*BHAQ
40      IF (CKBH .LE. 0.0) GO TO 13
41      11 Q=(TNR/VAQ)-BHAQ*(1.+CKBH*(WR/VAQ))
42      IF(Q.LE.0.) GO TO 13
43      C=1. +(CKB*WR/VAQ)
44      AH=C*BHAQ*CKA/Q
45      PH=-ALOG10(AH)
46      A=(CKW*VAQ)/(AH*ROH)
47      B=AH*VAQ/RH
48      D=1. + (AH/CKA) + (CKE*WR/VAQ) +(CKBH*AH*
49      1WR/(CKA*VAQ))
50      PNNAQH=A-B+TNR*(C/D)
51      PRINT 300,BHAQ,CKBH,PH,PNNAQH
52      300 FORMAT '(4X,E10.4,4X,E10.4,4X,F5.2,4X,E10.4)
53      20 CONTINUE
54      STOP
55      END
```